PHYSICAL REVIEW D **85,** 072004 (2012)

Measurement of the inclusive $W^{\pm}$ and $Z/\gamma*$ cross sections in the e and μ decay channels in pp collisions at $\sqrt{s} = 7$ TeV with the ATLAS detector

G. Aad *et al.**
(ATLAS Collaboration)

(Received 26 September 2011; published 23 April 2012)

The production cross sections of the inclusive Drell-Yan processes $W^{\pm} \to \ell\nu$ and $Z/\gamma^* \to \ell\ell$ ($\ell = e$, μ) are measured in proton-proton collisions at $\sqrt{s} = 7$ TeV with the ATLAS detector. The cross sections are reported integrated over a fiducial kinematic range, extrapolated to the full range, and also evaluated differentially as a function of the W decay lepton pseudorapidity and the Z boson rapidity, respectively. Based on an integrated luminosity of about 35 pb^{-1} collected in 2010, the precision of these measurements reaches a few percent. The integrated and the differential $W^{\pm}$ and Z/γ^* cross sections in the e and μ channels are combined, and compared with perturbative QCD calculations, based on a number of different parton distribution sets available at next-to-next-to-leading order.

DOI: 10.1103/PhysRevD.85.072004 PACS numbers: 12.38.Qk, 13.38.Be, 13.38.Dg, 13.85.Qk

I. INTRODUCTION

The inclusive Drell-Yan [1] production cross sections of W and Z bosons have been an important testing ground for QCD. Theoretical calculations of this process extend to next-to-leading order (NLO) [2–4] and next-to-next-to-leading order (NNLO) [5–9] perturbation theory. Crucial ingredients of the resulting QCD cross section calculations are the parametrizations of the momentum distribution functions of partons in the proton (PDFs). These have been determined recently in a variety of phenomenological analyses to NLO QCD by the CTEQ [10,11] group and to NNLO by the MSTW [12], ABKM [13,14], HERAPDF [15,16], JR [17], and NNPDF [18,19] groups.

The present measurement determines the cross sections times leptonic branching ratios, $\sigma_{W^{\pm}} \cdot \mathrm{BR}(W \to \ell\nu)$ and $\sigma_{Z/\gamma^*} \cdot \mathrm{BR}(Z/\gamma^* \to \ell\ell)$, of inclusive W and Z production for electron and muon final states, where $\ell = e$, μ. Compared to the initial measurement by the ATLAS Collaboration [20], the data set is enlarged by 100 and the luminosity uncertainty significantly reduced [21] from 11% to 3.4%. The CMS Collaboration has updated their initial measurement of total W and Z cross sections [22] to include data corresponding to an integrated luminosity similar to that used here [23]. Similar measurements have been performed at the $p\bar{p}$ collider Tevatron by the CDF and D0 collaborations [24,25].

The presented cross section values are integrated over the fiducial region of the analysis and also extrapolated to the full kinematic range. The data are also reported differentially, as functions of the lepton pseudorapidity,[3] η_l, for the $W^{\pm}$ cross sections, and of the boson rapidity, y_Z, for the Z/γ^* cross section. For the "Z/γ^*" case, which will subsequently often be denoted simply as "Z," all values refer to the dilepton mass window from 66 to 116 GeV. The Z cross section measurement in the electron channel is significantly extended by the inclusion of the forward detector region, which allows the upper limit of the pseudorapidity range for one of the electrons to be increased from 2.47 [20] to 4.9.

The electron and muon $W^{\pm}$ and Z cross sections are combined to form a single joint measurement taking into account the systematic error correlations between the various data sets. This also leads to an update of the initial differential measurement of the W charge asymmetry published by ATLAS [26]. Normalized cross sections as a function of the Z boson rapidity and W boson and lepton charge asymmetry measurements have been performed also by the CMS [27,28] and the CDF and D0 collaborations [29–34].

The combined $W^{\pm}$ and Z cross sections, integrated and differential, are compared with QCD predictions based on recent determinations of the parton distribution functions of the proton. In view of the percent level precision of the measurements, such comparisons are restricted to PDFs obtained to NNLO.

*Full author list given at the end of the article.

[3] ATLAS uses a right-handed coordinate system with its origin at the nominal interaction point (IP) in the center of the detector and the z axis along the beam pipe. The x axis points from the IP to the center of the LHC ring, and the y axis points upward. Cylindrical coordinates (r, ϕ) are used in the transverse plane, ϕ being the azimuthal angle around the beam pipe. The pseudorapidity is defined in terms of the polar angle θ as $\eta = -\ln\tan(\theta/2)$. Distances are measured as $\Delta R = \sqrt{\Delta\eta^2 + \Delta\phi^2}$.

A brief overview of the ATLAS detector, trigger, simulation, and the analysis procedure are presented in Sec. II. The acceptance corrections and their uncertainties are discussed in Sec. III, while Sec. IV presents the selection, the efficiencies, and the backgrounds for both electron and muon channels. The cross section results are first given, in Sec. V, separately for each lepton flavor. In Sec. VI the e and μ data sets are combined and the results are compared to theoretical predictions. The paper is concluded with a brief summary of the results.

II. DATA AND SIMULATION

A. ATLAS detector

The ATLAS detector [35] comprises a superconducting solenoid surrounding the inner detector (ID) and a large superconducting toroid magnet system enclosing the calorimeters. The ID system is immersed in a 2 T axial magnetic field and provides tracking information for charged particles in a pseudorapidity range matched by the precision measurements of the electromagnetic calorimeter. The silicon pixel and strip (SCT) tracking detectors cover the pseudorapidity range $|\eta| < 2.5$. The transition radiation tracker (TRT), which surrounds the silicon detectors, enables tracking up to $|\eta| = 2.0$ and contributes to electron identification.

The liquid argon (LAr) electromagnetic (EM) calorimeter is divided into one barrel ($|\eta| < 1.475$) and two end-cap components ($1.375 < |\eta| < 3.2$, EMEC). It uses an accordion geometry to ensure fast and uniform response and fine segmentation for optimum reconstruction and identification of electrons and photons. The hadronic scintillator tile calorimeter consists of a barrel covering the region $|\eta| < 1.0$, and two extended barrels in the range $0.8 < |\eta| < 1.7$. The LAr hadronic end-cap calorimeter (HEC) ($1.5 < |\eta| < 3.2$) is located behind the end-cap electromagnetic calorimeter. The forward calorimeter (FCal) covers the range $3.2 < |\eta| < 4.9$ and also uses LAr as the active material.

The muon spectrometer (MS) is based on three large superconducting toroids with coils arranged in an eightfold symmetry around the calorimeters, covering a range of $|\eta| < 2.7$. Over most of the η range, precision measurements of the track coordinates in the principal bending direction of the magnetic field are provided by monitored drift tubes (MDTs). At large pseudorapidities ($2.0 < |\eta| < 2.7$), cathode strip chambers (CSCs) with higher granularity are used in the innermost station. The muon trigger detectors consist of resistive plate chambers (RPCs) in the barrel ($|\eta| < 1.05$) and thin gap chambers (TGCs) in the end-cap regions ($1.05 < |\eta| < 2.4$), with a small overlap in the $|\eta| \simeq 1.05$ region.

The ATLAS detector has a three-level trigger system consisting of level-1 (L1), level-2 (L2), and the event filter (EF). The L1 trigger rate at design luminosity is approximately 75 kHz. The L2 and EF triggers reduce the event rate to approximately 200 Hz before data transfer to mass storage.

B. Triggers

The analysis uses data taken in the year 2010 with proton beam energies of 3.5 TeV. For the electron channels the luminosity is 36.2 pb^{-1}. For the muon channels the luminosity is smaller, 32.6 pb^{-1}, as a fraction of the available data, where the muon trigger conditions varied too rapidly, is not included.

Electrons are triggered in the pseudorapidity range $|\eta_e| < 2.5$, where the electromagnetic calorimeter is finely segmented. A single electron trigger with thresholds in transverse energy of 10 GeV at L1 and 15 GeV at the higher trigger levels is used for the main analysis. Compact electromagnetic energy depositions triggered at L1 are used as the seed for the higher level trigger algorithms, which are designed for identifying electrons based on calorimeter and fast track reconstruction.

The electron trigger efficiency is determined from $W \to e\nu$ and $Z \to ee$ events as the fraction of triggered electrons with respect to the offline reconstructed signal [36]. The efficiency is found to be close to 100%, being constant in both the transverse energy E_T and the pseudorapidity η_e, with a small reduction by about 2% towards the limits of the fiducial region ($E_T = 20$ GeV and $|\eta_e| = 2.5$, see Sec. II D). A systematic uncertainty of 0.4% is assigned to the efficiency determination.

The muon trigger is based at L1 on a coincidence of layers of RPCs in the barrel region and TGCs in the end caps. The parameters of muon candidate tracks are then derived by fast reconstruction algorithms in both the inner detector and muon spectrometer. Events are triggered with a single muon trigger with an EF threshold of transverse momentum $p_T = 13$ GeV.

The muon trigger efficiency is determined from a study of $Z \to \mu\mu$ events. The average efficiency is measured to be 85.1% with a total uncertainty of 0.3%. The lower efficiency of the muon trigger system is due to the reduced geometrical acceptance in the barrel region.

C. Simulation

The properties of both signal and background processes, including acceptances and efficiencies, are modeled using the MC@NLO [37], POWHEG [38–41], PYTHIA [42], and HERWIG [43] Monte Carlo (MC) programs. All generators are interfaced to PHOTOS [44] to simulate the effect of final state QED radiation. The response of the ATLAS detector to the generated particles is modeled using GEANT4 [45,46]. The CTEQ 6.6 PDF set [10] is used for the MC@NLO and POWHEG samples. For the PYTHIA and HERWIG samples the MRSTLO* [47] parton distribution functions are used. MC parameters describing the properties of minimum bias events and the underlying event are tuned to the first ATLAS measurements [48]. Furthermore, the simulated events are

TABLE I. Signal and background Monte Carlo samples as well as the generators used in the simulation. For each sample the production cross section, multiplied by the relevant branching ratios (BR), to which the samples are normalized, is given. The electroweak W and Z cross sections are calculated at NNLO in QCD, $t\bar{t}$ at approximate NNLO, and dibosons at NLO in QCD. The inclusive jet and heavy-quark cross sections are given at LO. These samples are generated with requirements on the transverse momentum of the partons involved in the hard-scattering process, $\hat{p}_T$. No systematic uncertainties are assigned for the jet and heavy-quark cross sections, since methods are used to extract their normalization and their systematic uncertainties from data (see text).

Physics process	Generator	$\sigma \cdot$ BR (nb)	
$W^+ \to \ell^+ \nu$ ($\ell = e, \mu$)	MC@NLO	6.16 ± 0.31	NNLO
$W^- \to \ell^- \bar{\nu}$ ($\ell = e, \mu$)	MC@NLO	4.30 ± 0.21	NNLO
$Z/\gamma^* \to \ell\ell$ ($m_{\ell\ell} > 60$ GeV, $\ell = e, \mu$)	MC@NLO	0.99 ± 0.05	NNLO
$W \to \tau\nu$	PYTHIA	10.46 ± 0.52	NNLO
$Z/\gamma^* \to \tau\tau$ ($m_{\tau\tau} > 60$ GeV)	PYTHIA	0.99 ± 0.05	NNLO
$t\bar{t}$	MC@NLO	$0.165 + 0.011 - 0.016$	$\approx$ NNLO
WW	HERWIG	0.045 ± 0.003	NLO
WZ	HERWIG	0.0185 ± 0.0009	NLO
ZZ	HERWIG	0.0060 ± 0.0003	NLO
Dijet (e channel, $\hat{p}_T > 15$ GeV)	PYTHIA	1.2×10^6	LO
Dijet (μ channel, $\hat{p}_T > 8$ GeV)	PYTHIA	10.6×10^6	LO
$b\bar{b}$ (μ channel, $\hat{p}_T > 18$ GeV, $p_T(\mu) > 15$ GeV)	PYTHIA	73.9	LO
$c\bar{c}$ (μ channel, $\hat{p}_T > 18$ GeV, $p_T(\mu) > 15$ GeV)	PYTHIA	28.4	LO

reweighted so that the resulting transverse momentum distributions of the W and Z bosons match the data [49,50].

The effect of multiple pp interactions per bunch crossing ("pile-up") is modeled by overlaying simulated minimum bias events over the original hard-scattering event. MC events are then reweighted so that the reconstructed vertex distribution agrees with the data.

The Monte Carlo simulation is also corrected with respect to the data in the lepton reconstruction and identification efficiencies as well as in the energy (momentum) scale and resolution.

Table I summarizes the information on the simulated event samples used for the measurement, including the cross sections used for normalization. The W and Z samples are normalized to the NNLO cross sections from the FEWZ program [20,51]. The uncertainties on those cross sections arise from the choice of PDF, from factorization and renormalization scale dependence, and from the α_s uncertainty. An uncertainty of $(+7, -10)\%$ is taken for the $t\bar{t}$ cross section [52–54].

D. Analysis procedure

The integrated and differential W and Z production cross sections are measured in the fiducial volume of the ATLAS detector using the equation

$$\sigma_{\text{fid}} = \frac{N - B}{C_{W/Z} \cdot L_{\text{int}}}, \tag{1}$$

where N is the number of candidate events observed in data, B the number of background events, determined using data and simulation, and L_{int} the integrated luminosity corresponding to the run selections and trigger employed. The correction by the efficiency factor $C_{W/Z}$ determines the cross sections σ_{fid} within the fiducial regions of the measurement. These regions are defined as

$W \to e\nu$: $p_{T,e} > 20\,\text{GeV}$, $|\eta_e| < 2.47$, excluding $1.37 < |\eta_e| < 1.52$, $p_{T,\nu} > 25\,\text{GeV}$, $m_T > 40\,\text{GeV}$;

$W \to \mu\nu$: $p_{T,\mu} > 20\,\text{GeV}$, $|\eta_\mu| < 2.4$, $p_{T,\nu} > 25\,\text{GeV}$, $m_T > 40\,\text{GeV}$;

$Z \to ee$: $p_{T,e} > 20\,\text{GeV}$, both $|\eta_e| < 2.47$, excluding $1.37 < |\eta_e| < 1.52$, $66 < m_{ee} < 116\,\text{GeV}$;

Forward $Z \to ee$: $p_{T,e} > 20\,\text{GeV}$, one $|\eta_e| > 2.47$, excluding $1.37 < |\eta_e| < 1.52$, other $2.5 < |\eta_e| < 4.9$, $66 < m_{ee} < 116\,\text{GeV}$;

$Z \to \mu\mu$: $p_{T,\mu} > 20\,\text{GeV}$, both $|\eta_\mu| < 2.4$, $66 < m_{\mu\mu} < 116\,\text{GeV}$.

For the W channels the transverse mass m_T is defined as $m_T = \sqrt{2 p_{T,\ell} p_{T,\nu} \cdot (1 - \cos\Delta\phi_{\ell,\nu})}$, where $\Delta\phi_{\ell,\nu}$ is the azimuthal separation between the directions of the charged lepton and the neutrino.

The main analysis, used to determine the integrated cross sections, is performed for the W and Z electron and muon decay channels for leptons in the central region of the detector of $|\eta_e| < 2.47$ and $|\eta_\mu| < 2.4$, respectively. A complementary analysis of the $Z \to ee$ channel is used in

addition to measure the differential cross section at larger rapidity. Here the allowed pseudorapidity range is chosen from $|\eta_e| = 2.5$ to 4.9 for one of the electrons.

The differential cross sections are measured, as a function of the absolute values of the W decay lepton pseudorapidity and Z boson rapidity, in bins with boundaries at

$$\eta_\ell = [0.00, 0.21, 0.42, 0.63, 0.84, 1.05, 1.37, 1.52, 1.74, 1.95, 2.18, 2.47(e) \quad \text{or} \quad 2.40(\mu)];$$
$$y_Z = [0.0, 0.4, 0.8, 1.2, 1.6, 2.0, 2.4, 2.8, 3.6],$$

where the notation for absolute η and y is omitted.

The combined efficiency factor $C_{W/Z}$ is calculated from simulation and corrected for differences in reconstruction, identification, and trigger efficiencies between data and simulation (see Sec. IV). Where possible, efficiencies in data and MC are derived from $Z \to \ell\ell$ and, in the case of the electron channel, $W \to e\nu$ events [36,55]. The efficiency estimation is performed by triggering and selecting such events with good purity using only one of the two leptons in the $Z \to \ell\ell$ case and a significant missing transverse energy in the $W \to e\nu$ case, a procedure often referred to as ''tagging.'' Then the other very loosely identified lepton can be used as a probe to estimate various efficiencies after appropriate background subtraction. The method is therefore often referred to as the ''tag-and-probe'' method.

The total integrated cross sections are measured using the equation

$$\sigma_{\text{tot}} = \sigma_{W/Z} \times \text{BR}(W/Z \to \ell\nu/\ell\ell) = \frac{\sigma_{\text{fid}}}{A_{W/Z}}, \quad (2)$$

where the acceptance $A_{W/Z}$ is used to extrapolate the cross section measured in the fiducial volume σ_{fid} to the full kinematic region. The acceptance is derived from MC, and the uncertainties on the simulation modeling and on parton distribution functions constitute an additional uncertainty on the total cross section measurement. The total and fiducial cross sections are corrected for QED radiation effects in the final state.

The correction factors $C_{W/Z}$ and $A_{W/Z}$ are obtained as follows:

$$C_{W/Z} = \frac{N_{\text{MC,rec}}}{N_{\text{MC,gen,cut}}} \quad \text{and} \quad A_{W/Z} = \frac{N_{\text{MC,gen,cut}}}{N_{\text{MC,gen,all}}}, \quad (3)$$

where $N_{\text{MC,rec}}$ are sums of weights of events after simulation, reconstruction, and selection; $N_{\text{MC,gen,cut}}$ are taken at generator level after fiducial cuts; and $N_{\text{MC,gen,all}}$ are sums of weights of all generated MC events (for the Z/γ^* channels within $66 < m_{\ell\ell} < 116$ GeV).

For the measurement of charge-separated $W^\pm$ cross sections, the C_W factor is suitably modified to incorporate a correction for event migration between the W^+ and W^- samples as

$$C_{W+} = \frac{N_{\text{MC,rec}+}}{N_{\text{MC,gen}+,\text{cut}}} \quad \text{and} \quad C_{W-} = \frac{N_{\text{MC,rec}-}}{N_{\text{MC,gen}-,\text{cut}}}, \quad (4)$$

where $N_{\text{MC,rec}\pm}$ and $N_{\text{MC,gen}\pm,\text{cut}}$ are sums of weights of events reconstructed or generated as $W^\pm$, respectively, without any further charge selection. For example, $N_{\text{MC,rec}+}$ includes a small component of charge misidentified events generated as W^-, while $N_{\text{MC,gen}+,\text{cut}}$ contains only events generated as W^+ without requirements on the reconstructed charge. This charge misidentification effect is only relevant for the electron channels, and is negligible in the muon channels.

Electron and muon integrated measurements are combined after extrapolation to the full phase space available for W and Z production and decay and also to a common fiducial region, chosen to minimize the extrapolation needed to adjust the electron and muon cross sections to a common basis. This kinematic region is defined by extrapolating both channels to $|\eta_\ell| < 2.5$ and interpolating the electron measurement over the region $1.37 < |\eta_e| < 1.52$. The differential cross sections are combined by extrapolating all Z measurements to full phase space in lepton pseudorapidity accessible in Z production and decay and extending the range of the most forward bin of W measurements to $2.18 < |\eta_\ell| < 2.5$. The experimental selections on the transverse momenta of the leptons and on the transverse or invariant mass are retained for the differential cross sections.

III. ACCEPTANCES AND UNCERTAINTIES

The acceptances $A_{W/Z}$ are determined using the MC@NLO Monte Carlo program and the CTEQ 6.6 PDF set. The central values and their systematic uncertainties are listed in Table II, separately for W^+, W^-, $W^\pm$, and Z/γ^* production. The uncertainties due to the finite

TABLE II. Acceptance values (A) and their relative uncertainties (δA) in percent for W and Z production in electron and muon channels. The various components of the uncertainty are defined in the text. The total uncertainty (δA_{tot}) is obtained as the quadratic sum of the four parts.

	A	$\delta A^{\text{pdf}}_{\text{err}}$	$\delta A^{\text{pdf}}_{\text{sets}}$	δA_{hs}	δA_{ps}	δA_{tot}
Electron channels						
W^+	0.478	1.0	0.7	0.9	0.8	1.7
W^-	0.452	1.5	1.1	0.2	0.8	2.0
$W^\pm$	0.467	1.0	0.5	0.6	0.8	1.5
Z	0.447	1.7	0.6	0.2	0.7	2.0
Muon channels						
W^+	0.495	1.0	0.8	0.6	0.8	1.6
W^-	0.470	1.5	1.1	0.3	0.8	2.1
$W^\pm$	0.485	1.0	0.5	0.4	0.8	1.5
Z	0.487	1.8	0.6	0.2	0.7	2.0

statistics of the Monte Carlo samples are negligible. The systematic uncertainties are obtained by combining four different components:

(i) The uncertainties within one PDF set ($\delta A^{\rm pdf}_{\rm err}$). They are derived from the CTEQ 6.6 PDF [10] eigenvector error sets at 90% C.L.

(ii) The uncertainties due to differences between PDF sets ($\delta A^{\rm pdf}_{\rm sets}$). They are estimated as the maximum difference between the CTEQ 6.6, ABKM095fl [13,14], HERAPDF 1.0 [15], MSTW2008 [12], CT10, CT10W [11], and NNPDF2.1 [18] sets, where samples generated with CTEQ 6.6 are reweighted event by event to other PDFs [56].

(iii) The uncertainties due to the modeling of the hard-scattering processes of W and Z production ($\delta A_{\rm hs}$). These are derived from comparisons of MC@NLO and POWHEG simulations, using the CTEQ 6.6 PDF set and the parton shower and hadronization models based on the HERWIG simulation.

(iv) The uncertainties due to the parton shower and hadronization description ($\delta A_{\rm ps}$). These are derived as the difference in the acceptances calculated with POWHEG Monte Carlo, using the CTEQ 6.6 PDF set but different models for parton shower and hadronization descriptions, namely, the HERWIG or PYTHIA programs.

In addition, to compute the total cross section ratios (see Sec. VI E), the correlation coefficients between the full W and Z acceptance uncertainties are used. They are 0.80 for $W^{\pm} - Z$, 0.83 for $W^{-} - Z$, 0.78 for $W^{+} - Z$, and 0.67 for $W^{+} - W^{-}$.

The corrections, and their uncertainties, to extrapolate the electron and the muon measurements from each lepton fiducial region to the common fiducial region, where they are combined, are calculated with the same approach as described for the acceptances. The extrapolations contribute $\sim$3% to the $W \to \mu\nu$ and $\sim$7% to the $W \to e\nu$ cross sections. Similarly, the fiducial measurement of the Z cross section is enhanced by $\sim$5% in the muon channel and by $\sim$12% in the electron channel. The uncertainties on these corrections are found to be on the 0.1% level. The combined fiducial measurements are therefore characterized by negligible theoretical uncertainty due to the extrapolation to the unmeasured phase space.

The differential cross sections for the electron and the muon channels are also combined after extrapolating each measurement to the common fiducial kinematic region. In the case of the W measurements the applied correction is effective only in the highest η_ℓ bin and is about 30% in the muon channel and about 9% in the electron channel. The extrapolation factors needed to combine the Z electron and muon measurements, and their systematic uncertainties, are listed in Table III. The uncertainty is of the order of 0.1% in most of the rapidity intervals and increases to 1%–2% near the boundary of the fiducial regions.

TABLE III. Central values and absolute uncertainties (in parentheses) of extrapolation correction factors from fiducial regions to full lepton pseudorapidity η phase space. The factors are provided in bins of Z boson rapidity for $Z \to \mu\mu$ and for central and forward $Z \to ee$ measurements.

$y_Z^{\rm min}$	$y_Z^{\rm max}$	$Z \to \mu\mu$	Central $Z \to ee$	Forward $Z \to ee$
0.0	0.4	1.000(0)	0.954(1)	...
0.4	0.8	1.000(0)	0.903(1)	...
0.8	1.2	0.984(1)	0.855(2)	...
1.2	1.6	0.849(2)	0.746(3)	0.103(1)
1.6	2.0	0.578(5)	0.512(4)	0.327(3)
2.0	2.4	0.207(5)	0.273(5)	0.590(7)
2.4	2.8	...	...	0.797(1)
2.8	3.6	...	...	0.404(4)

IV. EVENT SELECTION, EFFICIENCIES, AND BACKGROUND DETERMINATION

A. Electron channels

1. Event selection: Events are required to have at least one primary vertex formed by at least three tracks. To select W boson events in the electron channel, exactly one well reconstructed electron is required with $E_T > 20$ GeV and $|\eta| < 2.47$. Electrons in the transition region between the barrel and end-cap calorimeter, $1.37 < |\eta| < 1.52$, are excluded, as the reconstruction quality is significantly reduced compared to the rest of the pseudorapidity range. The transverse energy is calculated from calorimeter and tracker information. The electron is required to pass ''medium'' identification criteria [36]. To efficiently reject the QCD background, the electron track must, in addition, have a hit in the innermost layer of the tracking system, the ''pixel b-layer.'' The additional calorimeter energy deposited in a cone of size $\Delta R \leq 0.3$ around the electron cluster is required to be small, where the actual selection is optimized as a function of the electron η and p_T to have a flat 98% efficiency in the simulation for isolated electrons from the decay of a W or Z boson. The missing transverse energy, $E_T^{\rm miss}$, is determined from all measured and identified physics objects, as well as remaining energy deposits in the calorimeter and tracking information [57]. It is required to be larger than 25 GeV. Further, the transverse mass m_T has to be larger than 40 GeV.

The selection as described is also used for the Z boson case with the following modifications: instead of one, two electrons are required to be reconstructed and pass the medium criteria without the additional pixel b-layer and isolation cuts; their charges have to be opposite, and their invariant mass has to be within the interval 66 to 116 GeV.

For the selection of Z events at larger rapidities, a central electron passing ''tight'' [36] criteria, as well as the calorimeter isolation requirement described above for the W channel, is required. A second electron candidate with $E_T > 20$ GeV has to be reconstructed in the forward

region, $2.5 \leq |\eta| \leq 4.9$, and has to pass "forward loose" identification requirements [36]. Its transverse energy is determined from the calorimeter cluster energy and position. As the forward region is not covered by the tracking system, no charge can be measured and the electron identification has to rely on calorimeter cluster shapes only. The invariant mass of the selected pair is required to be between 66 and 116 GeV.

2. Calibration and efficiencies: Comprehensive studies of the electron performance are described in [36]. Energy scale and resolution corrections are determined from data as a function of η in the central and forward regions, by comparing the measured $Z \rightarrow ee$ line shape to the one predicted by the simulation. For the central region, the linearity and resolution are, in addition, cross-checked using $J/\psi \rightarrow ee$ and single electron E/p measurements in $W \rightarrow e\nu$ events.

The electron efficiencies are evaluated in two steps called reconstruction and identification. The reconstruction step consists of the loose matching of a good quality track to a high p_T calorimeter cluster. Identification summarizes all the further requirements to reduce the background contamination.

The electron reconstruction efficiency in the central region is obtained from the Z tag-and-probe method. The efficiency in data is found to be slightly higher by 1.3% than in MC, and the simulation is adjusted accordingly with an absolute systematic uncertainty of 0.8%.

The identification efficiency for electrons from W or Z decay in the central region is determined using two different tag-and-probe methods, which are performed on selected W and Z data samples, respectively. The W-based determination employs the significant missing transverse energy in those events to obtain an unbiased electron sample. The method benefits from larger statistics but needs more involved procedures for background subtraction, as compared to the Z-related determination. Consistent correction factors to be applied to the simulation are derived from the two methods as a function of the electron rapidity. For the medium identification criteria, the Monte Carlo efficiency is adjusted by about -2.5% on average, with a resulting absolute uncertainty of typically less than 1% on this correction. The quality of the data to MC agreement in the tight identification criteria efficiency is found to depend significantly on electron η, and an adjustment by, on average, $+2\%$ with an absolute uncertainty of about 1% is performed. The additional requirements on b-layer hits and calorimeter isolation are found to be very efficient and rather well described in the simulation, resulting in small adjustments and small systematic uncertainties only.

To distinguish W^+ from W^- events, the charge of the decay electron has to be known. The charge misidentification probability as a function of η is determined from a sample of $Z \rightarrow ee$ events where both electrons are reconstructed with the same sign. It depends on the identification criteria and, in general, increases at large $|\eta|$. For electrons passing the medium criteria, about 1% of all electrons are assigned the wrong charge, while for tight electrons this figure is about half. From these measurements, additional uncertainties are derived from the opposite charge requirement on the Z cross section (0.6%) and from migration and charge dependent effects on the W^+ and W^- cross sections (0.1%).

In the forward region ($|\eta| > 2.5$), the electron reconstruction is nearly 100% efficient and taken from MC. The identification efficiency is determined using the Z tag-and-probe method in two forward electron rapidity bins, which correspond to the inner part of the EMEC ($2.5 < |\eta| < 3.2$) and the FCal ($3.2 < |\eta| < 4.9$), respectively. The simulation overestimates the efficiency by 8.4% and 1.7% in these two bins and is adjusted accordingly, with absolute uncertainties of 5.8% and 8.8%, respectively.

3. Background determination: The largest electroweak background in the $W \rightarrow e\nu$ channel is given by the $W \rightarrow \tau\nu$ production, mainly from decays involving true electrons, $\tau \rightarrow e\bar{\nu}_e\nu_\tau$. Relative to the number of all $W^\pm$ candidate events, this contribution is estimated to be 2.6%. The background from $t\bar{t}$ events is determined to be 0.4% and further contributions on the 0.1–0.2% level arise from $Z \rightarrow \tau\tau$, $Z \rightarrow ee$, and diboson production. The sum of electroweak and $t\bar{t}$ backgrounds are found to be 3.7% in the W^- and 3.2% in the W^+ channel of the respective numbers of events.

A further significant source of background in the $W \rightarrow e\nu$ channel, termed "QCD background," is given by jet production faking electron plus missing transverse energy final states. The QCD background is derived from the data using a template fit of the E_T^{miss} distribution in a control sample selected without the E_T^{miss} requirement and inverting a subset of the electron identification criteria. The E_T^{miss} templates for the signal and the other electroweak and $t\bar{t}$ backgrounds are taken from the simulation. The QCD background in the signal region is determined to be 3.4% and 4.8% for the W^+ and W^- channels, respectively. The statistical uncertainty of this fit is negligible. The background as well as the signal templates are varied to assess the systematic uncertainty on the fraction of QCD background. The relative uncertainty is estimated to be 12% for W^+ and 8% for W^-, corresponding to a fraction of about 0.5% of the W^+ or W^- candidates. The fit is performed in each bin of electron pseudorapidity separately to obtain the background for the differential analysis.

The relative background contributions in the central $Z \rightarrow ee$ analysis due to electroweak processes, $W \rightarrow e\nu$, $Z \rightarrow \tau\tau$, and $W \rightarrow \tau\nu$, and to $t\bar{t}$ production are estimated using the corresponding MC samples to be 0.3% in total. The fraction of candidate events due to diboson decays is 0.2%.

The QCD background in the central $Z \to ee$ analysis is estimated from data by fitting the invariant mass distribution using a background template selected with inverted electron identification cuts and the signal template from MC. This procedure yields a fraction of QCD background of 1.6%. The relative systematic uncertainty on this fraction is dominant and evaluated to be 40% using different background templates and fit ranges, as well as an alternative method based on fitting a sample selected with looser identification criteria. For the differential analysis, the sum of the backgrounds is determined from the global fit, and the relative contributions of each bin are taken from the background template. Differences between templates lead to further relative 25% bin-to-bin uncorrelated uncertainties on the QCD background fraction.

In the forward $Z \to ee$ analysis the main electroweak background comes from $W \to e\nu$ events with an associated jet faking an electron in the forward region. It is estimated to be 1.9%. The QCD background is estimated by fitting the m_{ee} distribution in a similar manner as for the central analysis. Because of the larger level of background the fit can be performed directly in all boson rapidity y_Z bins. In total the QCD background is estimated to be 9.4% with relative statistical and systematic uncertainties of 8% and 17%. Differentially, the QCD background fraction varies from 7% to 20% with typical relative total uncertainties of 20% to 40%.

B. Muon channels

1. Event selection: Collision events are selected with the same vertex requirement as for the electron channels. In addition, the vertex with the highest squared transverse momentum sum of associated tracks is selected as the primary vertex for further cuts. To reduce fake collision candidates from cosmic-ray or beam-halo events, the position of the primary vertex along the beam axis is required to be within 20 cm of the nominal position. The efficiency of this requirement is larger than 99.9% in both data and simulation.

Muon track candidates are formed from pairs of standalone tracks in the inner detector and the muon spectrometer, combined using a chi-square matching procedure [58]. W and Z events are selected by requiring at least one or two combined track muons with $p_T > 20$ GeV and $|\eta| < 2.4$, respectively. The z position of the muon track extrapolated to the beam line has to match the z coordinate of the primary vertex within ± 1 cm. A set of ID hit requirements [55] is applied to select high quality tracks also demanding at least one hit in the pixel b-layer.

A track-based isolation criterion is defined by requiring the sum of transverse momenta, $\sum p_T^{\mathrm{ID}}$, of ID tracks with $p_T > 1$ GeV within a cone $\Delta R < 0.2$ around the muon direction, divided by the muon transverse momentum p_T, to be less than 0.1. When analyzed after all other selection cuts, this requirement has a high QCD background rejection power, while keeping more than 99% of the signal events in both the W and Z channels.

$W \to \mu\nu$ events are further selected by requiring the missing transverse energy, defined as in the electron analysis, to be larger than 25 GeV and the transverse mass to be larger than 40 GeV. In the $Z \to \mu\mu$ analysis, the two decay muons are required to be of opposite charge, and the invariant mass of the $\mu^+\mu^-$ pair to be within the interval 66 to 116 GeV.

2. Calibration and efficiencies: Muon transverse momentum resolution corrections are determined by comparing data and MC as a function of η in the barrel and end-cap regions [59]. They are derived by fitting the invariant mass distribution from $Z \to \mu\mu$ events and the curvature difference between inner detector and muon spectrometer tracks weighted by the muon electric charge in $Z \to \mu\mu$ and $W \to \mu\nu$ events. Muon transverse momentum scale corrections are measured by comparing the peak position of the $Z \to \mu\mu$ invariant mass distribution between data and MC and fitting the muon transverse momentum distributions in $Z \to \mu\mu$ events [26,59]. Scale corrections are well below 1% in the central pseudorapidity region, and they increase to about 1% in the high-η regions due to residual misalignment effects in the ID and MS.

Muon trigger and identification efficiencies are measured in a sample of $Z \to \mu\mu$ events selected with looser requirements on the second muon and with tighter cuts on the invariant mass window and on the angular correlation between the two muons than in the main analysis in order to reduce the contamination from background events [55]. The efficiencies are measured using a factorized approach: the efficiency of the combined reconstruction is derived with respect to the ID tracks, and the isolation cut is tested relative to combined tracks; finally, the trigger efficiency is measured relative to isolated combined muons. The residual background contamination is measured from data, by fitting the invariant mass spectrum with a signal template plus a background template describing the shape of multijet events measured from a control sample of nonisolated muons. The total background contamination, subtracted from the signal sample, is estimated to be 1.0% in the measurement of the reconstruction efficiency and negligible for other selections. The data-to-Monte Carlo correction factors are all measured to be very close to 1, i.e. $0.993 \pm 0.002(\mathrm{sta.}) \pm 0.002(\mathrm{sys.})$ for the combined reconstruction, $0.9995 \pm 0.0006(\mathrm{sta.}) \pm 0.0013(\mathrm{sys.})$ for the isolation, and $1.020 \pm 0.003(\mathrm{sta.}) \pm 0.002(\mathrm{sys.})$ for the trigger efficiencies. Systematic uncertainties are evaluated by varying the relevant selection cuts within their resolution and the amount of subtracted background within its uncertainty. For the ID reconstruction efficiency, no correction has to be applied.

3. Background determination: The electroweak background in the $W \to \mu\nu$ channel is dominated by the

$Z \to \mu\mu$ and the $W \to \tau\nu$ channels. Relative to the number of $W^{\pm}$ candidate events, these contributions are determined to be 3.3% and 2.8%, respectively. The contribution from $Z \to \tau\tau$ decay is 0.1% while the $t\bar{t}$ contribution is estimated to be 0.4%. Diboson decays contribute 0.1%. Overall, these backgrounds are found to be 6.1% in the W^+ and 7.6% in the W^- channel, respectively.

The QCD background in the $W \to \mu\nu$ channel is primarily composed of heavy-quark decays, with smaller contributions from pion and kaon decays in flight and hadrons faking muons. Given the uncertainty in the dijet cross section prediction and the difficulty of simulating fake prompt muons, the QCD background is derived from data. The number of expected events is determined by extrapolating from control regions defined by reversing the isolation and missing transverse energy requirements. This analysis yields a fraction of background events of 1.7% in the W^+ and of 2.8% in the W^- channel, respectively. The systematic uncertainty is dominated by the uncertainty on the extrapolation of the isolation efficiency for QCD events from the control to the signal sample, which is estimated to be about 23% relative to the number of background events.

The relative background contributions in the $Z \to \mu\mu$ channel due to $t\bar{t}$ events, $Z \to \tau\tau$ and diboson decays are estimated to be 0.1%, 0.07%, and 0.2%, respectively. The background contaminations from $W \to \tau\nu$ and $W \to \mu\nu$ are found to be negligible.

The QCD background in the $Z \to \mu\mu$ channel is also estimated from data. The number of events is measured in control samples, selected using inverted isolation and $m_{\mu\mu}$ requirements, corrected for the signal and electroweak background contamination, and extrapolated to the signal region. The measured fraction of background events is 0.4%. The systematic uncertainty is evaluated by testing a different isolation definition for the control region, propagating the uncertainties in the electroweak background subtraction, and checking the stability of the method against boundary variations of the control regions. Additional cross-checks of the background estimation are done by comparing with the result of a closure test on simulated events and of an analysis of the invariant mass spectrum based on fit templates, derived from the data and the Monte Carlo. The relative systematic uncertainty amounts to 56% while the relative statistical uncertainty is 40%.

Cosmic-ray muons overlapping in time with a collision event are another potential source of background. From a study of noncolliding bunches this background contribution is found to be negligible.

V. CROSS SECTION MEASUREMENTS

A. Electron cross sections

1. Control distributions: The understanding of the W and Z measurements can be illustrated by comparing the measured with the simulated distributions. A total of 77 885 W^+ and 52 856 W^- events are selected in the electron channel. A crucial quantity in the W measurement is the missing transverse energy $E_T^{\rm miss}$, for which the distributions for the two charges are shown in Fig. 1. The requirement $E_T^{\rm miss} > 25$ GeV is seen to suppress a large fraction of the QCD background. Figure 2 shows the distributions of the electron transverse energy E_T and the transverse mass m_T of the $W \to e\nu$ candidates. The observed agreement between data and MC is good.

A total of 9725 and 3376 candidates are selected by the central and forward $Z \to ee$ analyses, respectively. The invariant mass and boson rapidity distributions are compared to the simulation in Figs. 3 and 4 for the two analyses. The complementarity in the rapidity region covered is easily visible. For the forward $Z \to ee$ analysis the lepton rapidity distributions for the two electrons are shown in Fig. 5. The forward electron reaches

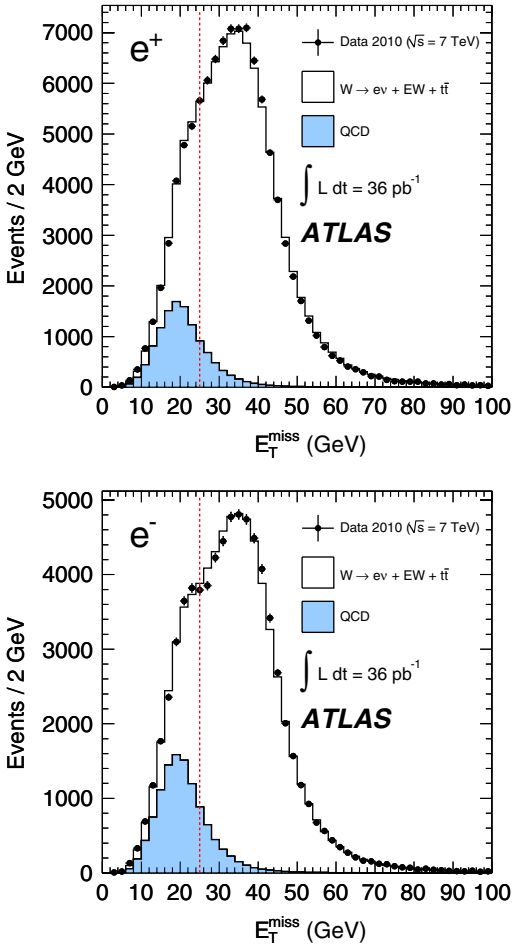

FIG. 1 (color online). Distributions of $E_T^{\rm miss}$ in the selected $W \to e\nu$ candidate events for positive (top panel) and negative (bottom panel) charge. The QCD background is represented by a background template taken from data (see text). The analysis uses the requirement $E_T^{\rm miss} > 25$ GeV, indicated by the vertical line.

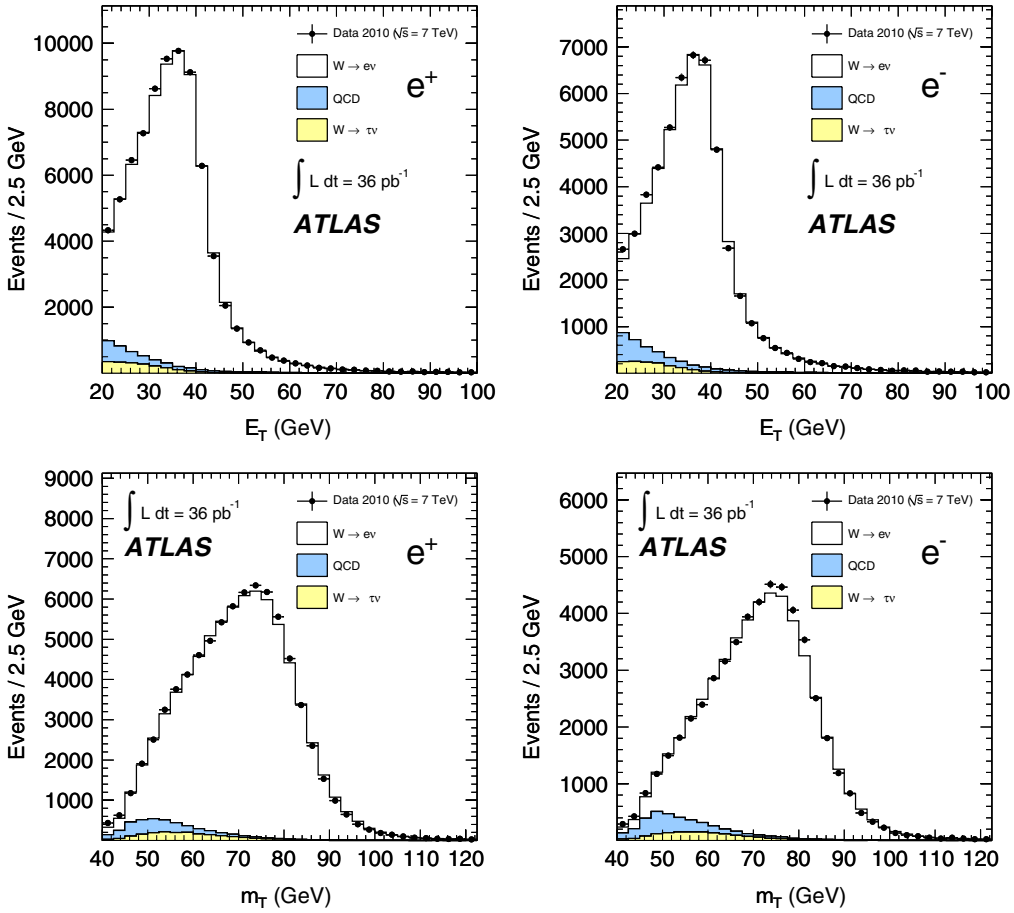

FIG. 2 (color online). Top panel: Distribution of the electron transverse energy E_T in the selected $W \rightarrow e\nu$ candidate events after all cuts for positive (left panel) and negative (right panel) charge. Bottom panel: Transverse mass distributions for W^+ (left panel) and W^- (right panel) candidates. The simulation is normalized to the data. The QCD background shapes are taken from background control samples (top panels) or MC simulation with relaxed electron identification criteria (bottom panel) and are normalized to the total number of QCD events as described in the text.

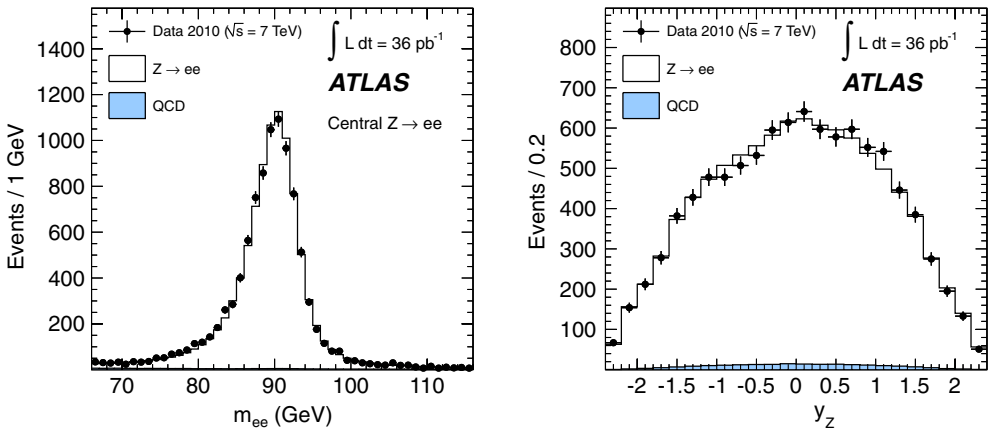

FIG. 3 (color online). Dielectron invariant mass m_{ee} (left panel) and rapidity y_Z distribution (right panel) for the central $Z \rightarrow ee$ analysis. The simulation is normalized to the data. The QCD background shapes are taken from a background control sample and normalized to the result of the QCD background fit.

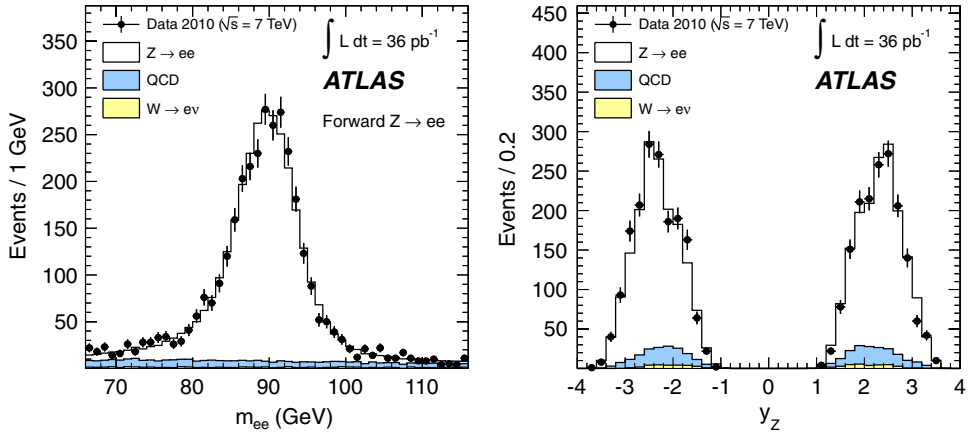

FIG. 4 (color online). Dielectron invariant mass m_{ee} (left panel) and rapidity y_Z distribution (right panel) for the forward $Z \to ee$ analysis. The simulation is normalized to the data. The QCD background shapes are taken from a background control sample and normalized to the result of the QCD background fit.

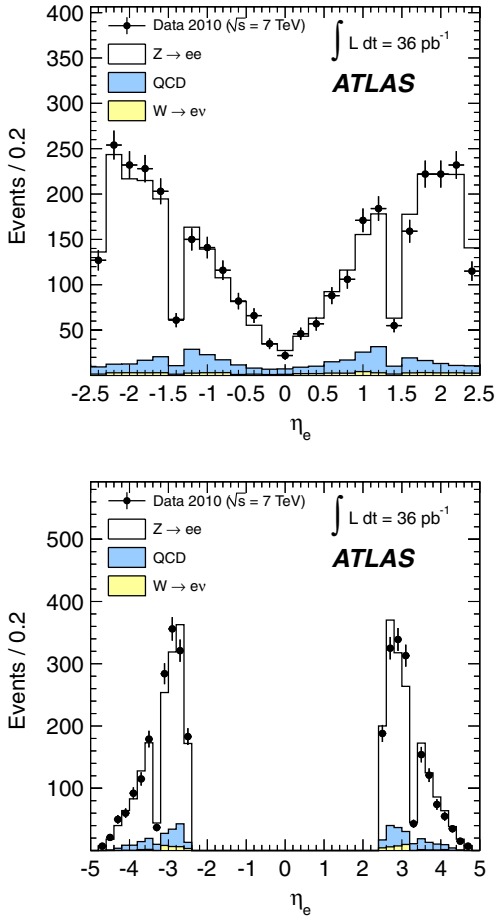

FIG. 5 (color online). Pseudorapidity for the central (top panel) and the forward (bottom panel) electron in the forward $Z \to ee$ analysis. The simulation is normalized to the data. The QCD background shapes are taken from a background control sample and normalized to the result of the QCD background fit.

pseudorapidities up to $|\eta| = 4.9$. The agreement between data and Monte Carlo is good in all cases. Because of a small number of nonoperational LAr readout channels, the rapidity distributions show an asymmetry, which is well described by the simulation. The overlaps between different calorimeter parts are visible as regions with significantly lower efficiency.

2. Results: Table IV reports the number of candidates, estimated background events, and the $C_{W/Z}$ and $A_{W/Z}$ correction factors used, where the uncertainties on $A_{W/Z}$ are obtained from Table II. The cross sections for all channels are reported in Table V with fiducial and total values and the uncertainties due to data statistics, luminosity, further experimental systematic uncertainties, and the acceptance extrapolation in the case of the total cross sections.

Table VI presents the sources of systematic uncertainties in all channels. Excluding the luminosity contribution of 3.4%, the W cross sections are measured with an experimental uncertainty of 1.8% to 2.1%, where the main contributions are due to electron reconstruction and identification as well as missing transverse energy performance related to the hadronic recoil [57].

TABLE IV. Number of observed candidates N and expected background events B, efficiency and acceptance correction factors for the W and Z electron channels. Efficiency scale factors used to correct the simulation for differences between data and MC are included in the reported $C_{W/Z}$ factors. The given uncertainties are the quadratic sum of statistical and systematic components. The statistical uncertainties on the $C_{W/Z}$ and $A_{W/Z}$ factors are negligible.

	N	B	$C_{W/Z}$	$A_{W/Z}$
W^+	77 885	5130 ± 350	0.693 ± 0.012	0.478 ± 0.008
W^-	52 856	4500 ± 240	0.706 ± 0.014	0.452 ± 0.009
$W^\pm$	130 741	9610 ± 590	0.698 ± 0.012	0.467 ± 0.007
Z	9725	206 ± 64	0.618 ± 0.016	0.447 ± 0.009

TABLE V. Fiducial and total cross sections times branching ratios for W^+, W^-, $W^{\pm}$, and Z/γ^* production in the electron decay channel. The electron fiducial regions are defined in Sec. II D. The uncertainties denote the statistical (sta), the experimental systematic (sys), the luminosity (lum), and the extrapolation (acc) uncertainties.

	$\sigma_W^{\mathrm{fid}} \cdot \mathrm{BR}(W \to e\nu)$ (nb)			
	sta	sys	lum	
W^+	$2.898 \pm 0.011 \pm 0.052 \pm 0.099$			
W^-	$1.893 \pm 0.009 \pm 0.038 \pm 0.064$			
$W^{\pm}$	$4.791 \pm 0.014 \pm 0.089 \pm 0.163$			
	$\sigma_W^{\mathrm{tot}} \cdot \mathrm{BR}(W \to e\nu)$ (nb)			
	sta	sys	lum	acc
W^+	$6.063 \pm 0.023 \pm 0.108 \pm 0.206 \pm 0.104$			
W^-	$4.191 \pm 0.020 \pm 0.085 \pm 0.142 \pm 0.084$			
$W^{\pm}$	$10.255 \pm 0.031 \pm 0.190 \pm 0.349 \pm 0.156$			
	$\sigma_{Z/\gamma^*}^{\mathrm{fid}} \cdot \mathrm{BR}(Z/\gamma^* \to ee)$ (nb)			
	sta	sys	lum	
Z/γ^*	$0.426 \pm 0.004 \pm 0.012 \pm 0.014$			
	$\sigma_{Z/\gamma^*}^{\mathrm{tot}} \cdot \mathrm{BR}(Z/\gamma^* \to ee)$ (nb)			
	sta	sys	lum	acc
Z/γ^*	$0.952 \pm 0.010 \pm 0.026 \pm 0.032 \pm 0.019$			

TABLE VI. Summary of relative systematic uncertainties on the measured integrated cross sections in the electron channels in percent. The theoretical uncertainty of $A_{W/Z}$ applies only to the total cross section.

	$\delta\sigma_{W^{\pm}}$	$\delta\sigma_{W+}$	$\delta\sigma_{W-}$	$\delta\sigma_Z$
Trigger	0.4	0.4	0.4	<0.1
Electron reconstruction	0.8	0.8	0.8	1.6
Electron identification	0.9	0.8	1.1	1.8
Electron isolation	0.3	0.3	0.3	...
Electron energy scale and resolution	0.5	0.5	0.5	0.2
Nonoperational LAr channels	0.4	0.4	0.4	0.8
Charge misidentification	0.0	0.1	0.1	0.6
QCD background	0.4	0.4	0.4	0.7
Electroweak + $t\bar{t}$ background	0.2	0.2	0.2	<0.1
E_T^{miss} scale and resolution	0.8	0.7	1.0	...
Pile-up modeling	0.3	0.3	0.3	0.3
Vertex position	0.1	0.1	0.1	0.1
$C_{W/Z}$ theoretical uncertainty	0.6	0.6	0.6	0.3
Total experimental uncertainty	1.8	1.8	2.0	2.7
$A_{W/Z}$ theoretical uncertainty	1.5	1.7	2.0	2.0
Total excluding luminosity	2.3	2.4	2.8	3.3
Luminosity	3.4			

The Z cross section is measured, apart from the luminosity contribution, with an experimental precision of 2.7%. This is dominated by the uncertainty on the electron reconstruction and identification efficiency.

The theoretical uncertainties on $C_{W/Z}$ are evaluated by comparisons of MC@NLO and POWHEG Monte Carlo simulations and by testing the effect of different PDF sets, as described in Sec. III for the acceptances. The total theoretical uncertainty is found to be 0.6% for C_W and 0.3% for C_Z.

The theoretical uncertainty on the extrapolation from the fiducial region to the total phase space for W and Z production is between 1.5% and 2.0%, as mentioned above.

The cross sections measured as a function of the W electron pseudorapidity, for separated charges, and of the Z rapidity are presented in Tables XVI, XVII, XVIII, and XIX. The statistical, bin-correlated, and uncorrelated systematic and total uncertainties are provided. The overall luminosity uncertainty is not included. The statistical uncertainty in each bin is about 1%–2% for the W differential

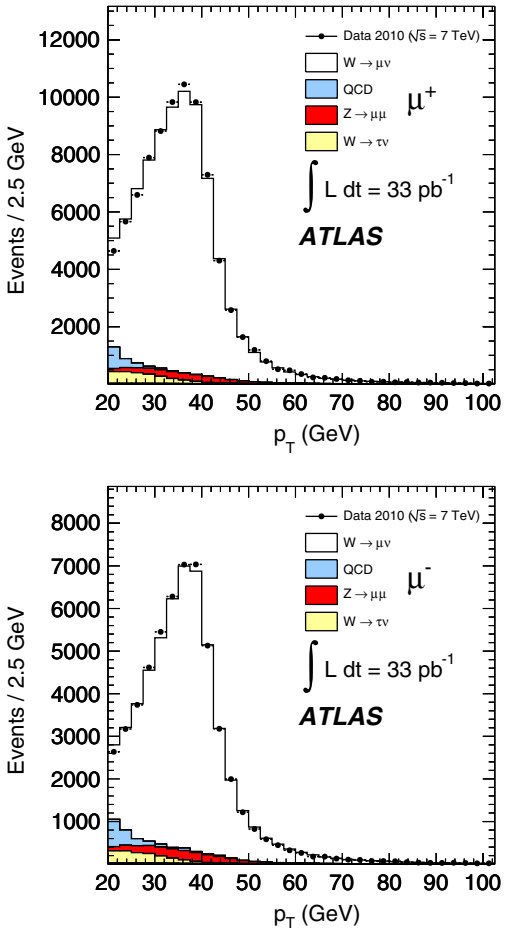

FIG. 6 (color online). Muon transverse momentum distribution of candidate W^+ (top panel) and W^- (bottom panel) events. The simulation is normalized to the data. The QCD background shape is taken from simulation and normalized to the number of QCD events measured from data.

measurements, while the total uncertainty is at the 2.5%–3% level. For the Z rapidity measurement the statistical uncertainty is about 2% for $|y_Z| < 1.6$ and grows to 3%–5% in the more forward bins. The total uncertainty on the Z cross sections is 3%–4% in the central region and up to 10% in the most forward bins. It is mainly driven by the uncertainties on the electron reconstruction and identification efficiencies.

B. Muon cross sections

1. Control distributions: A total of 84 514 W^+, 55 234 W^-, and 11 709 Z candidates are selected in the muon channels. A few distributions of these candidate events are compared to the simulation for the signal and the background contributions in the following. Figures 6 and 7 show the distributions of muon transverse momentum and the transverse missing energy of candidate W events for positive and negative charges. The transverse mass distributions are shown in Fig. 8. The invariant mass distribution of muon pairs, selected by the Z analysis, and the

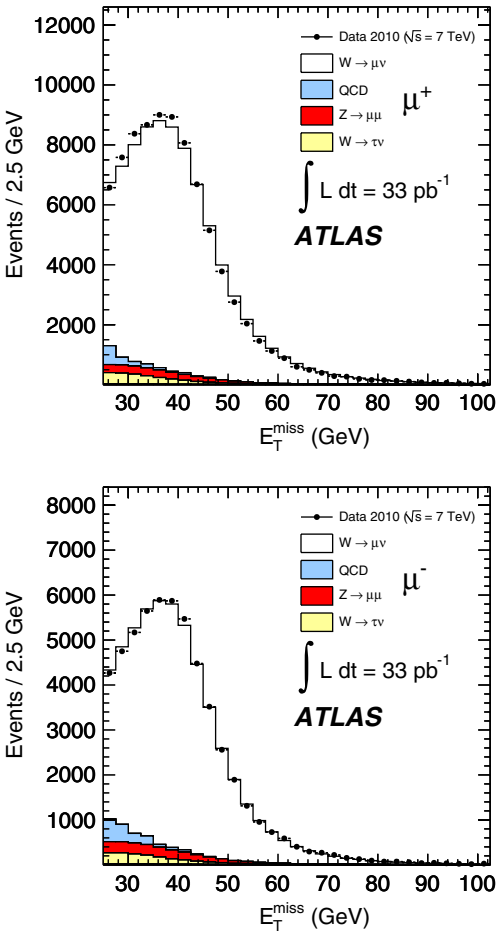

FIG. 7 (color online). Missing transverse energy distribution of candidate W^+ (top panel) and W^- (bottom panel) events. The simulation is normalized to the data. The QCD background shape is taken from simulation and normalized to the number of QCD events measured from data.

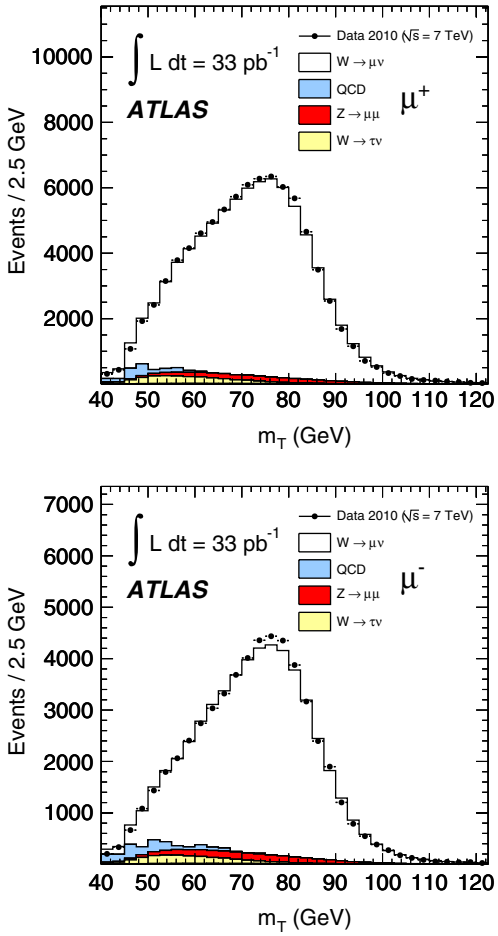

FIG. 8 (color online). Transverse mass distribution of candidate W^+ (top panel) and W^- (bottom panel) events. The simulation is normalized to the data. The QCD background shape is taken from simulation and normalized to the number of QCD events measured from data.

boson rapidity distribution are shown in Fig. 9. The agreement between data and Monte Carlo is good in all cases.

3. Results: Table VII reports the number of candidates, the estimated background events, and the $C_{W/Z}$ and $A_{W/Z}$ correction factors used for the different measurements. The fiducial and total cross sections are reported in Table VIII for all channels, with the uncertainties due to data statistics, luminosity, further experimental systematics, and the acceptance extrapolation in the case of the total cross sections.

The breakdown of the systematic uncertainty in all channels is shown in Table IX. Apart from the luminosity contribution of 3.4%, the $W \to \mu\nu$ cross section is measured with an experimental uncertainty of 1.6%. The largest contribution comes from the muon efficiencies (1.1%), followed by several contributions in the 0.3%–0.8% range such as the QCD background, the transverse missing energy scale and resolution uncertainties, and the uncertainty on the momentum scale correction.

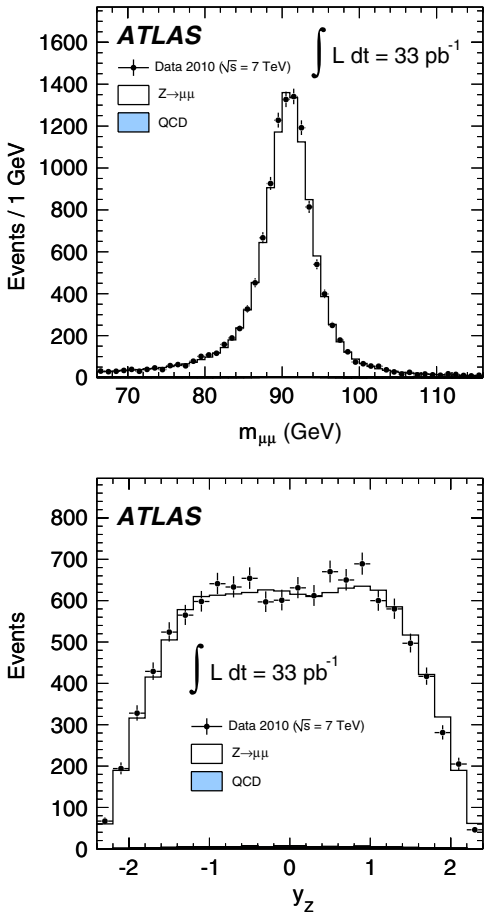

FIG. 9 (color online). Invariant mass (top panel) and rapidity (bottom panel) distributions of candidate Z bosons. The simulation is normalized to the data. The QCD background normalization and shapes are taken from control samples as described in the text.

The $Z \to \mu\mu$ cross section is measured, apart from the luminosity contribution, with an experimental precision of 0.9%. This is dominated by the uncertainty in the muon reconstruction efficiency (0.6%), with about equal systematic and statistical components due to the limited sample of $Z \to \mu\mu$ events. The uncertainty of

TABLE VII. Number of observed candidates N and expected background events B, efficiency and acceptance correction factors for the W and Z muon channels. Efficiency scale factors used to correct the simulation for differences between data and MC are included in the $C_{W/Z}$ factors. The given uncertainties are the quadratic sum of statistical and systematic components. The statistical uncertainties on the $C_{W/Z}$ and $A_{W/Z}$ factors are negligible.

	N	B	$C_{W/Z}$	$A_{W/Z}$
W^+	84 514	6600 ± 600	0.796 ± 0.016	0.495 ± 0.008
W^-	55 234	5700 ± 600	0.779 ± 0.015	0.470 ± 0.010
$W^{\pm}$	139 748	12 300 ± 1100	0.789 ± 0.015	0.485 ± 0.007
Z	11 709	86 ± 32	0.782 ± 0.007	0.487 ± 0.010

TABLE VIII. Fiducial and total cross sections times branching ratios for W^+, W^-, $W^{\pm}$, and Z/γ^* production in the muon decay channel. The muon fiducial regions are defined in Sec. II D. The uncertainties denote the statistical (sta), the experimental systematic (sys), the luminosity (lum), and the extrapolation (acc) uncertainties.

	$\sigma_W^{\text{fid}} \cdot \text{BR}(W \to \mu\nu)$ (nb)		
	sta	sys	lum
W^+	3.002 ± 0.011	± 0.050	± 0.102
W^-	1.948 ± 0.009	± 0.034	± 0.066
$W^{\pm}$	4.949 ± 0.015	± 0.081	± 0.168
	$\sigma_W^{\text{tot}} \cdot \text{BR}(W \to \mu\nu)$ (nb)		
	sta	sys	lum acc
W^+	6.062 ± 0.023	± 0.101	± 0.206 ± 0.099
W^-	4.145 ± 0.020	± 0.072	± 0.141 ± 0.086
$W^{\pm}$	10.210 ± 0.030	± 0.166	± 0.347 ± 0.153
	$\sigma_{Z/\gamma^*}^{\text{fid}} \cdot \text{BR}(Z/\gamma^* \to \mu\mu)$ (nb)		
	sta	sys	lum
Z/γ^*	0.456 ± 0.004	± 0.004	± 0.015
	$\sigma_{Z/\gamma^*}^{\text{tot}} \cdot \text{BR}(Z/\gamma^* \to \mu\mu)$ (nb)		
	sta	sys	lum acc
Z/γ^*	0.935 ± 0.009	± 0.009	± 0.032 ± 0.019

TABLE IX. Summary of relative systematic uncertainties on the measured integrated cross sections in the muon channels in percent. The efficiency systematic uncertainties are partially correlated between the trigger, reconstruction, and isolation terms. This is taken into account in the computation of the total uncertainty quoted in the table. The theoretical uncertainty on $A_{W/Z}$ applies only to the total cross section.

	$\delta\sigma_{W^{\pm}}$	$\delta\sigma_{W^+}$	$\delta\sigma_{W^-}$	$\delta\sigma_Z$
Trigger	0.5	0.5	0.5	0.1
Muon reconstruction	0.3	0.3	0.3	0.6
Muon isolation	0.2	0.2	0.2	0.3
Muon p_T resolution	0.04	0.03	0.05	0.02
Muon p_T scale	0.4	0.6	0.6	0.2
QCD background	0.6	0.5	0.8	0.3
Electroweak + $t\bar{t}$ background	0.4	0.3	0.4	0.02
E_T^{miss} resolution and scale	0.5	0.4	0.6	...
Pile-up modeling	0.3	0.3	0.3	0.3
Vertex position	0.1	0.1	0.1	0.1
$C_{W/Z}$ theoretical uncertainty	0.8	0.8	0.7	0.3
Total experimental uncertainty	1.6	1.7	1.7	0.9
$A_{W/Z}$ theoretical uncertainty	1.5	1.6	2.1	2.0
Total excluding luminosity	2.1	2.3	2.6	2.2
Luminosity		3.4		

the momentum scale correction has an effect of 0.2%, while the uncertainty from momentum resolution is again found to be negligible. The impact of the QCD background uncertainty is at the level of 3 per mille.

The theoretical uncertainties on $C_{W/Z}$ are evaluated as in the electron channels and found to be 0.7%–0.8% for C_W and 0.3% for C_Z.

The uncertainty on the theoretical extrapolation from the fiducial region to the total phase space for W and Z production is between 1.5% and 2.1%.

The cross sections measured as a function of the W muon pseudorapidity, for separated charges, and of the Z rapidity are shown in Tables XX, XXI, and XXII. The statistical, bin-correlated, and uncorrelated systematic and total uncertainties are provided. The uncertainties on the extrapolation to the common fiducial volume, on electroweak and multijet backgrounds, on the momentum scale and resolution are treated as fully correlated between bins for both W and Z measurements. Other uncertainties are considered as uncorrelated.

The statistical uncertainties on the W differential cross sections are in the range 1%–2%, and the total uncertainties are in the range of 2%–3%.

The differential Z cross section is measured with a statistical uncertainty of about 2% up to $|y_Z| < 1.6$, 2.6% for $1.6 < |y_Z| < 2.0$, and 4.4% for $2.0 < |y_Z| < 2.4$. The available number of Z events dominates the total uncertainty, with systematic sources below 1.5% in the whole rapidity range.

VI. COMBINED CROSS SECTIONS AND COMPARISON WITH THEORY

A. Data combination

Assuming lepton universality for the W and Z boson e and μ decays, the measured cross sections in both channels can be combined to decrease the statistical and systematic uncertainties. This combination cannot trivially be applied to the pure fiducial cross sections as somewhat different geometrical acceptances are used for the electron and the muon measurements. This requires the introduction of the common kinematic regions, defined in Sec. II D, where W and Z measurements can be combined.

The method of combination used here is an averaging procedure which has been introduced and described in detail in [60,61]. It distinguishes different sources of systematic errors on the combination of the W and Z cross section measurements, in electron and muon channels.

The sources of uncertainty which are fully correlated between the electron and muon measurements are as follows: the hadronic recoil uncertainty of the E_T^{miss} measurement (for W measurements), electroweak backgrounds, pile-up effects, uncertainties of the z-vertex position, the theoretical uncertainties on the acceptance, and extrapolation correction factors.

The sources of uncertainty considered fully correlated bin-to-bin and across data sets are as follows: the extrapolation into noncovered phase space, normalization of the electroweak background, lepton energy or momentum scale and resolution, and systematic effects on reconstruction efficiencies.

In addition, the QCD background systematics are bin-to-bin correlated but independent for the e and μ data sets. The statistical components of the lepton identification efficiencies are largely bin-to-bin uncorrelated but correlated for the W and Z cross sections, whereas the statistical uncertainties of the background and the electron isolation determinations are fully uncorrelated sources. Finally, some sources are considered as fully anticorrelated for W^+ and W^- production, specifically the PDF uncertainty on C_W and the charge misidentification. The luminosity uncertainty is common to all data points, and it is therefore not used in the combination procedure.

In total there are 59 differential cross section measurements entering the combination with 30 sources of correlated systematic uncertainties. The data are combined using the following χ^2 function [61], which is minimized in the averaging procedure:

$$\chi^2 = \sum_{k,i} w_k^i \frac{[m^i - (\mu_k^i + \sum_j \gamma_{j,k}^i m^i b_j)]^2}{(\delta_{\text{sta},k}^i)^2 \mu_k^i (m^i - \sum_j \gamma_{j,k}^i m^i b_j) + (\delta_{\text{unc},k}^i m^i)^2} + \sum_j b_j^2.$$

The sums run over all measurement sets k and points i considered. In case a specific set k contributes a measurement μ_k^i to point i, one has $w_k^i = 1$; otherwise $w_k^i = 0$. The deviations of the combined measurements m^i from the original measurements μ_k^i are minimized. The correlated error sources j can shift, i.e. $b_j \neq 0$, where b_j is expressed in units of standard deviations, and such shifts incur a χ^2 penalty of b_j^2. The relative statistical and uncorrelated systematic uncertainties of a specific measurement are labeled $\delta_{\text{sta},k}^i$ and $\delta_{\text{unc},k}^i$, respectively. The relative correlated systematic uncertainties are given by the matrix $\gamma_{j,k}^i$, which quantifies the influence of the correlated systematic error source j on the measurement i in the experimental data set k. In addition, total correlated uncertainty $\delta_{\text{corr},k}^i$ can be estimated as a sum in quadrature of $\gamma_{j,k}^i$.

The combined Z, W^-, and W^+ differential cross sections are given in Tables XXIII, XXIV, and XXV. The data can be obtained electronically through the HepData repository [62]. The results are quoted with their statistical, uncorrelated, and correlated uncertainties per bin, where the influence of all correlated sources is quantified individually with the matrix $\gamma_{j,k}^i$.

The data show good compatibility, with the total $\chi^2/\text{dof} = 33.9/29$. A good level of agreement is also seen if combinations are performed separately for the Z ($\chi^2/\text{dof} = 15.5/9$), the W^+ ($\chi^2/\text{dof} = 10.2/10$), and the W^- data ($\chi^2/\text{dof} = 7.0/10$).

B. Theoretical calculations

The precision of the current differential and integrated cross section measurements has reached the percent level. Comparisons with QCD predictions therefore are made at next-to-next-to-leading order in perturbation theory using recent NNLO sets of PDFs. The dependence of the cross section predictions on the renormalization (μ_r) and factorization (μ_f) scales is reduced at NNLO. Varying μ_r and μ_f independently around their central values, taken to be M_W or M_Z, with the constraint $0.5 < \mu_r/\mu_f < 2$, a maximum effect of about 3% is observed on the NLO cross sections, which is reduced to 0.6% at NNLO, using the MSTW08 PDF sets.

The theoretical Z/γ^* and $W^{\pm}$ predictions, used in the following for a comparison with the data, are obtained with the most recent versions of the programs FEWZ [9,51] and DYNNLO [63,64], which provide NNLO cross sections for vector boson production and decays with full spin correlations and finite width effects. Calculations are performed using the G_μ electroweak parameter scheme and those values of the strong coupling constant α_s which belong to the original determinations of the PDFs. The predictions obtained with FEWZ and DYNNLO are found to agree to within 0.5% for the total cross sections and to within 1% for the fiducial cross sections when using the same electroweak parameter settings and the standard model predictions for the total and partial widths of the W and Z vector bosons, which also account for higher order electroweak and QCD corrections [65].

The NNLO QCD predictions do not include corrections due to pure weak and interference effects between initial and final state radiation. Both effects have been estimated using the SANC program [66]. The interference effects are below 0.1% for all considered channels. Pure weak effects may change the predicted cross sections by about 0.5%. Shape modifications due to the pure weak corrections are calculated to be at most 10% of the quoted correction values. Since the size of the pure weak corrections is estimated to be of the same order as the level of agreement of the NNLO QCD predictions for the fiducial cross sections, they are not applied for the subsequent comparison of the theory with the data.

For the following comparisons to data, all integrated cross section values, the y_Z distributions, and the normalization of the η_ℓ distributions are taken from FEWZ. The shapes of the pseudorapidity distributions are taken from DYNNLO which have a higher statistical precision than the differential distributions obtained with FEWZ.

C. Differential cross sections

The differential Z and $W^{\pm}$ cross sections are shown in Figs. 10 and 11. The measurements for different channels are seen to be in good agreement with each other. Excluding the overall luminosity normalization uncertainty, the data accuracy reaches about 2% in the central region of the Z rapidity. In the most forward region of the Z cross section measurement, the accuracy is still limited to 6% (10%) at $y_Z \simeq 2.6\,(3.2)$. For the W cross section measurements, a precision of about 2% is obtained in each bin of η_ℓ.

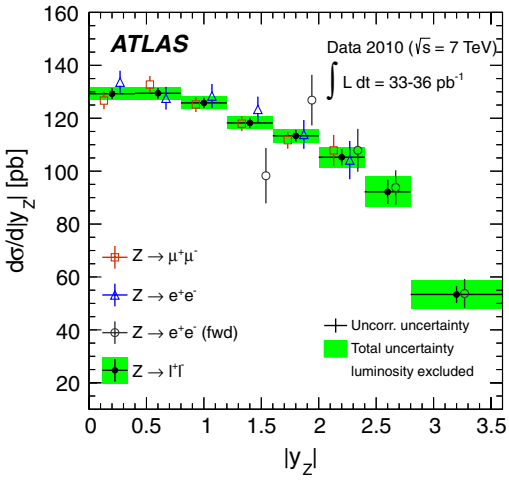

FIG. 10 (color online). The combined $d\sigma/d|y_Z|$ cross section, for $Z/\gamma^* \to \ell^+\ell^-$, compared to measurements obtained separately in the muon and electron (central and forward) channels. The kinematic requirements are $66 < m_{\ell\ell} < 116$ GeV and $p_{T,\ell} > 20$ GeV. For the combined result, the uncorrelated uncertainties are shown as crosses and the total uncertainties as boxes. Only the total uncertainties are shown for uncombined measurements. The luminosity uncertainty is not included. Points are displaced for clarity within each bin.

The combined differential Z and $W^{\pm}$ cross sections are compared in Figs. 12 and 13 with the calculated NNLO predictions using the JR09, ABKM09, HERAPDF1.5, and MSTW08 NNLO PDF sets. The uncertainties of the bin-wise predictions are a convolution of the PDF uncertainties, considered by the authors of the various PDF sets[4] to correspond to 68% C.L., and a residual numerical uncertainty of below 0.5%. One observes that the measured y_Z and η_ℓ dependencies are broadly described by the predictions of the PDF sets considered. Some deviations, however, are visible, for example, the lower Z cross section at central rapidities in the case of the JR09 PDF set, or the tendency of the ABKM09 prediction to overshoot the Z and the W cross sections at larger y_Z and η_ℓ, respectively. It thus can be expected that the differential cross sections presented here will reduce the uncertainties of PDF determinations and also influence the central values.

[4]The HERAPDF analysis considers explicitly uncertainties due to parametrization and fit parameter choices. This leads to somewhat enlarged and asymmetric errors as compared to the genuine experimental uncertainties, which in the HERAPDF analysis correspond to a change of χ^2 by one unit.

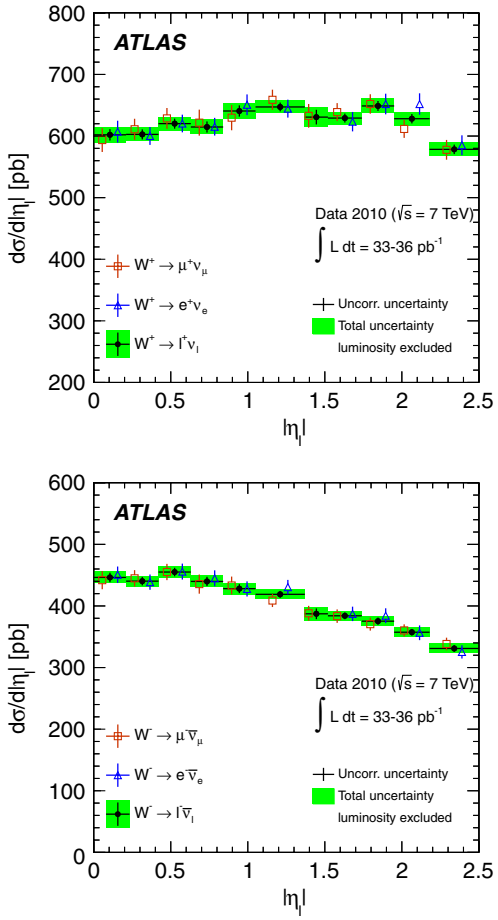

FIG. 11 (color online). The combined $d\sigma/d|\eta_\ell|$ cross sections, for W^+ (top panel) and W^- (bottom panel), compared to measurements obtained separately in the electron and muon channels. The kinematic requirements are $p_{T,\ell} > 20$ GeV, $p_{T,\nu} > 25$ GeV, and $m_T > 40$ GeV. For the combined result, the uncorrelated uncertainties are shown as crosses and the total uncertainties as boxes. Only the total uncertainties are shown for uncombined measurements. The luminosity uncertainty is not included. Points are displaced for clarity within each bin.

The combined electron and muon data allow for an update of the measurement of the W charge asymmetry

$$A_\ell(\eta_\ell) = \frac{d\sigma_{W^+}/d\eta_\ell - d\sigma_{W^-}/d\eta_\ell}{d\sigma_{W^+}/d\eta_\ell + d\sigma_{W^-}/d\eta_\ell}, \tag{5}$$

which was previously published [26] by ATLAS based on initial muon measurements alone. The asymmetry values, obtained in the W fiducial region of this analysis, and their uncertainties are listed in Table XXVI. The measurement accuracy ranges between 4% and 8%. The previous and the new measurements are consistent. Since the present measurement is more precise and relies on the same data-taking period, it supersedes the previous result.

Figure 14 shows the measured W charge asymmetry together with the NNLO predictions obtained from the

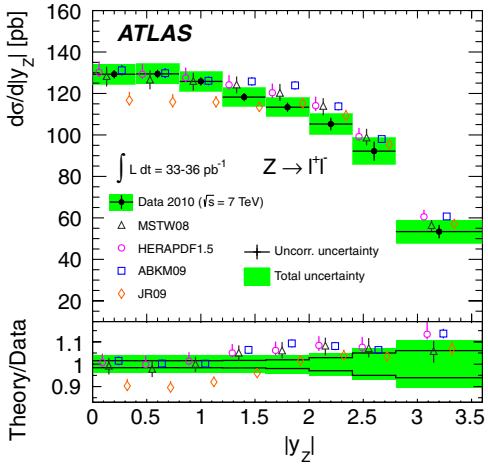

FIG. 12 (color online). Differential $d\sigma/d|y_Z|$ cross section measurement for $Z \to \ell\ell$ compared to NNLO theory predictions using various PDF sets. The kinematic requirements are $66 < m_{\ell\ell} < 116$ GeV and $p_{T,\ell} > 20$ GeV. The ratio of theoretical predictions to data is also shown. Theoretical points are displaced for clarity within each bin.

DYNNLO program. The ABKM09 and the HERAPDF 1.5 predictions give the best agreement with these results. Some deviations from the measured W^+ cross section of ABKM09 (HERAPDF 1.5) observed at larger (smaller) $|\eta_\ell|$, however, illustrate that more sensitive information is inherent in the separate W^+ and W^- cross sections and their correlations rather than in the asymmetry.

D. Integrated cross sections

The combination procedure as outlined above is also used to combine the integrated electron and muon Z and $W^\pm$ cross sections, separately for the common fiducial and the total cross sections.

The integrated fiducial cross sections for the W^+, W^-, $W^\pm$, and Z channels, listed in Table X with their uncertainties, are all measured to about 1% systematic uncertainty, with significantly smaller uncertainties due to statistics and essentially negligible uncertainties due to the extrapolation to the common fiducial phase space. The luminosity uncertainty of 3.4% is fully correlated between the measurements.

It is instructive to compare the measured integrated cross sections with the theoretical predictions, evaluated in the fiducial region of the measurement. The cross sections are calculated, as described above, to NNLO using the FEWZ program and the four NNLO PDF sets as used also for the differential comparisons. Figure 15 shows the W^+ and W^- cross sections (left panel) and the $(W^+ + W^-)$ and Z/γ^* cross sections (right panel). The outer ellipse is obtained using the correlation coefficients for the total uncertainty, while the inner, much shorter ellipse is obtained excluding the luminosity uncertainty. The numerical values of these

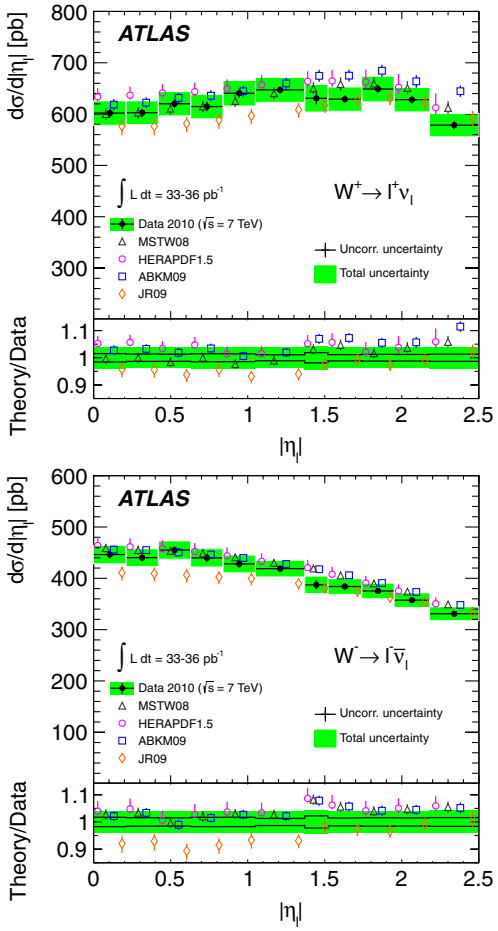

FIG. 13 (color online). Differential $d\sigma/d|\eta_{\ell^+}|$ (top panel) and $d\sigma/d|\eta_{\ell^-}|$ (bottom panel) cross section measurements for $W \to \ell\nu$ compared to the NNLO theory predictions using various PDF sets. The kinematic requirements are $p_{T,\ell} > 20$ GeV, $p_{T,\nu} > 25$ GeV, and $m_T > 40$ GeV. The ratio of theoretical predictions to data is also shown. Theoretical points are displaced for clarity within each bin.

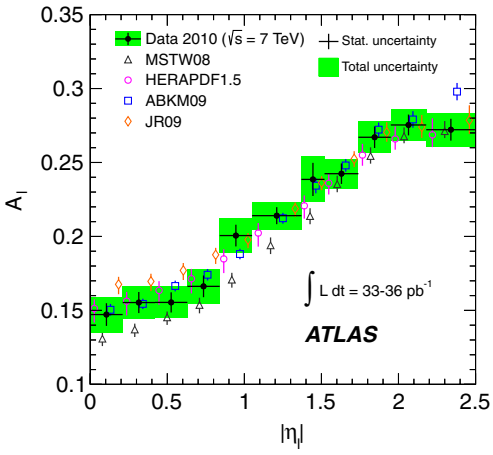

FIG. 14 (color online). Measured W charge asymmetry as a function of lepton pseudorapidity $|\eta_\ell|$ compared with theoretical predictions calculated to NNLO. The kinematic requirements are $p_{T,\ell} > 20$ GeV, $p_{T,\nu} > 25$ GeV, and $m_T > 40$ GeV. Theoretical points are displaced for clarity within each bin.

correlation coefficients are given in Table XI. The theoretical ellipses result from the PDF uncertainties, quoted to correspond to about 68% C.L. in their two-dimensional area,[5] and the cross section correlations are obtained from the different error eigenvector sets. The measurement exhibits a sensitivity to differences in the predicted cross sections, which is hindered, however, by the luminosity uncertainty which dominates the error on the integrated cross section measurement.

[5]All experimental and theoretical ellipses are defined such that their area corresponds to 68% C.L. This implies that the projections onto the axes correspond to 1.52 times the usual one-dimensional uncertainty. Note that this convention differs from the one chosen in [10,12,67], in which the ellipses are narrower to reflect the one-dimensional uncertainties.

The predictions rely on the evolution of the PDFs, determined mainly by deep inelastic scattering data from HERA, into the region of the W and Z mass scales. While possible deviations from the measured cross section values are of interest, it is also remarkable, however, to note the overall agreement between theory and experiment. This is evidence that universality of the PDFs and perturbative QCD at high orders continue to work up to the kinematic range probed in W and Z production at the LHC.

The combination and theory comparisons are also performed with the total integrated cross sections, listed in Table XII. The correlation coefficients are given in Table XIII. The pure experimental precision of the total

TABLE X. Combined cross sections times leptonic branching ratios for W^+, W^-, $W^{\pm}$, and Z/γ^* production within the corresponding fiducial regions of the measurements. The uncertainties denote the statistical (sta), the experimental systematic (sys), the luminosity (lum), and the extrapolation (acc) uncertainties.

	$\sigma_W^{\text{fid}} \cdot \text{BR}(W \to \ell\nu)$ (nb)			
	$\lvert\eta_\ell\rvert < 2.5$, $p_{T,\ell} > 20$ GeV, $p_{T,\nu} > 25$ GeV, and $m_T > 40$ GeV			
	sta	sys	lum	acc
W^+	3.110 ± 0.008	± 0.036	± 0.106	± 0.004
W^-	2.017 ± 0.007	± 0.028	± 0.069	± 0.002
$W^{\pm}$	5.127 ± 0.011	± 0.061	± 0.174	± 0.005
	$\sigma_{Z/\gamma^*}^{\text{fid}} \cdot \text{BR}(Z/\gamma^* \to \ell\ell)$ (nb)			
	$\lvert\eta_\ell\rvert < 2.5$, $p_{T,\ell} > 20$ GeV and $66 < m_{\ell\ell} < 116$ GeV			
	sta	sys	lum	acc
Z/γ^*	0.479 ± 0.003	± 0.005	± 0.016	± 0.001

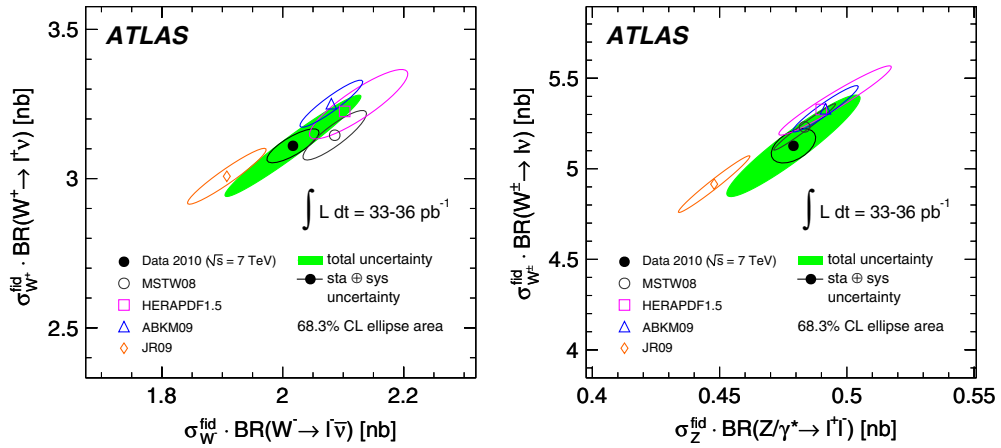

FIG. 15 (color online). Measured and predicted fiducial cross sections times leptonic branching ratios, σ_{W^+} vs σ_{W^-} (left panel) and $(\sigma_{W^+} + \sigma_{W^-})$ vs σ_{Z/γ^*} (right panel). The ellipses illustrate the 68% C.L. coverage for total uncertainties (full) and excluding the luminosity uncertainty (open black). The uncertainties of the theoretical predictions correspond to the PDF uncertainties only.

cross sections is as high as that of the fiducial cross sections. However, the additional extrapolation uncertainty, described in Sec. III, amounts to about 2%, which is larger than the experimental systematic error. The total cross section measurements are thus less able to discriminate details of the PDFs, as may be deduced from comparing Fig. 16 with Fig. 15.

Compared to the first total W, Z cross section measurements by ATLAS [20], the statistical uncertainty is improved by a factor of 10, to 0.2% (0.6%) for W (Z), the systematic uncertainty by a factor of about 5, and the luminosity uncertainty by a factor of 4, to 3.4%.

E. Ratios of cross sections

1. Electron-muon universality

Ratios of electron and muon cross sections can be evaluated in the common kinematic fiducial region. Since the production of the W and Z bosons is independent of the flavor of the decay lepton, the corresponding cross section ratios represent new measurements of the ratios of the e and μ branching fractions, i.e.

TABLE XII. Combined total cross sections times leptonic branching ratios for W^+, W^-, W, and Z/γ^* production. The uncertainties denote the statistical (sta), the experimental systematic (sys), the luminosity (lum), and the extrapolation (acc) uncertainties.

	$\sigma^{tot}_{W} \cdot BR(W \to \ell\nu)$ (nb)			
	sta	sys	lum	acc
W^+	$6.048 \pm 0.016 \pm 0.072 \pm 0.206 \pm 0.096$			
W^-	$4.160 \pm 0.014 \pm 0.057 \pm 0.141 \pm 0.083$			
$W^\pm$	$10.207 \pm 0.021 \pm 0.121 \pm 0.347 \pm 0.164$			
	$\sigma^{tot}_{Z/\gamma^*} \cdot BR(Z/\gamma^* \to \ell\ell)$ (nb)			
	$66 < m_{\ell\ell} < 116$ GeV			
	sta	sys	lum	acc
Z/γ^*	$0.937 \pm 0.006 \pm 0.009 \pm 0.032 \pm 0.016$			

TABLE XI. Correlation matrix for the measurements of the Z, W^+, and W^- cross sections in the fiducial volume, for the full uncertainty (top) and for all but the luminosity uncertainty (bottom).

	Z	W^+	W^-
Z	1.00	0.94	0.93
W^+	0.94	1.00	0.97
W^-	0.93	0.97	1.00

	Z	W^+	W^-
Z	1.00	0.48	0.44
W^+	0.48	1.00	0.79
W^-	0.44	0.79	1.00

TABLE XIII. Correlation matrix for the measurements of the total Z, W^+, and W^- cross sections for the full uncertainty (top) and for all but the luminosity uncertainty (bottom).

	Z	W^+	W^-
Z	1.00	0.91	0.91
W^+	0.91	1.00	0.91
W^-	0.91	0.91	1.00

	Z	W^+	W^-
Z	1.00	0.67	0.71
W^+	0.67	1.00	0.70
W^-	0.71	0.70	1.00

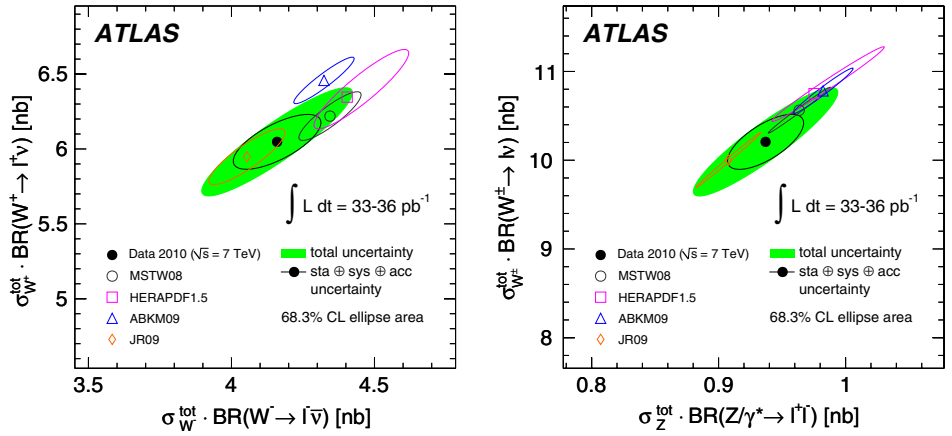

FIG. 16 (color online). Measured and predicted total cross sections times leptonic branching ratios: σ_{W^+} vs σ_{W^-} (left panel) and $(\sigma_{W^+} + \sigma_{W^-})$ vs σ_{Z/γ^*} (right panel). The ellipses illustrate the 68% C.L. coverage for total uncertainties (full) and excluding the luminosity uncertainty (open black). The uncertainties of the theoretical predictions correspond to the PDF uncertainties only.

$$R_W = \frac{\sigma_W^e}{\sigma_W^\mu} = \frac{\mathrm{Br}(W \to e\nu)}{\mathrm{Br}(W \to \mu\nu)}$$
$$= 1.006 \pm 0.004(\mathrm{sta}) \pm 0.006(\mathrm{unc}) \pm 0.022(\mathrm{cor})$$
$$= 1.006 \pm 0.024.$$

This can be compared with the current world average of 1.017 ± 0.019 [65] and a similar measurement performed by CDF giving 1.018 ± 0.025 [24]. Similarly, one obtains for the Z decays into electrons and muons a ratio

$$R_Z = \frac{\sigma_Z^e}{\sigma_Z^\mu} = \frac{\mathrm{Br}(Z \to ee)}{\mathrm{Br}(Z \to \mu\mu)}$$
$$= 1.018 \pm 0.014(\mathrm{sta}) \pm 0.016(\mathrm{unc}) \pm 0.028(\mathrm{cor})$$
$$= 1.018 \pm 0.031.$$

This confirms $e - \mu$ universality in Z decays as well, but the result is much less accurate than the world average

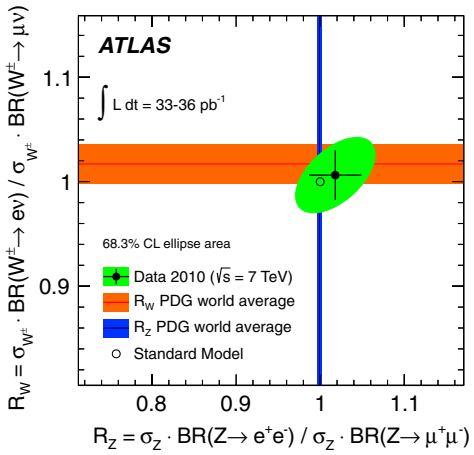

FIG. 17 (color online). The correlated measurement of the electron-to-muon cross section ratios in the W and the Z channels. The vertical (horizontal) band represents the uncertainty of the corresponding Z (W) branching fractions based on the current world average data. The ellipse illustrates the 68% C.L. for the correlated measurement of R_W and R_Z, while the error bars correspond to the one-dimensional uncertainties of either R_W or R_Z, respectively.

TABLE XIV. Measured ratios of the cross sections times leptonic branching ratios for W^+/W^-, W^+/Z, W^-/Z, and $(W^+ + W^-)/Z$, obtained in the fiducial regions and combining the electron and muon final states. The uncertainties denote the statistical (sta), the experimental systematic (sys), and the acceptance (acc) uncertainties.

	sta	sys	acc
W^+/W^-	1.542 ± 0.007	± 0.012	± 0.001
W^+/Z	6.493 ± 0.049	± 0.064	± 0.005
W^-/Z	4.210 ± 0.033	± 0.049	± 0.003
$W^\pm/Z$	10.703 ± 0.078	± 0.110	± 0.008

TABLE XV. Measured ratios of the total cross sections times leptonic branching ratios for W^+/W^-, W^+/Z, W^-/Z, and $(W^+ + W^-)/Z$, combining the electron and muon final states. The uncertainties denote the statistical (sta), the experimental systematic (sys), and the acceptance (acc) uncertainties.

	sta	sys	acc
W^+/W^-	1.454 ± 0.006	± 0.012	± 0.022
W^+/Z	6.454 ± 0.048	± 0.065	± 0.072
W^-/Z	4.439 ± 0.034	± 0.050	± 0.049
$W^\pm/Z$	10.893 ± 0.079	± 0.110	± 0.116

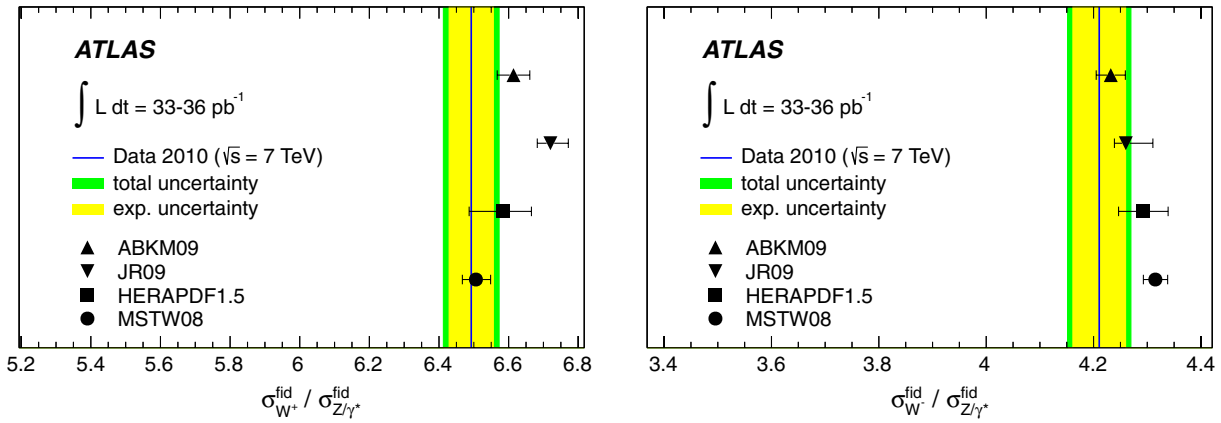

FIG. 19 (color online). Measured and predicted fiducial cross section ratios, $\sigma_{W^+}/\sigma_{Z/\gamma^*}$ (left panel) and $\sigma_{W^-}/\sigma_{Z/\gamma^*}$ (right panel). The experimental uncertainty (inner band) includes the experimental systematic errors. The total uncertainty (outer band) includes the statistical uncertainty and the small contribution from the acceptance correction. The uncertainties of the ABKM, JR, and MSTW predictions are given by the PDF uncertainties considered to correspond to 68% C.L., and their correlations are derived from the eigenvector sets. The results for HERAPDF comprise all three sources of uncertainty of that set.

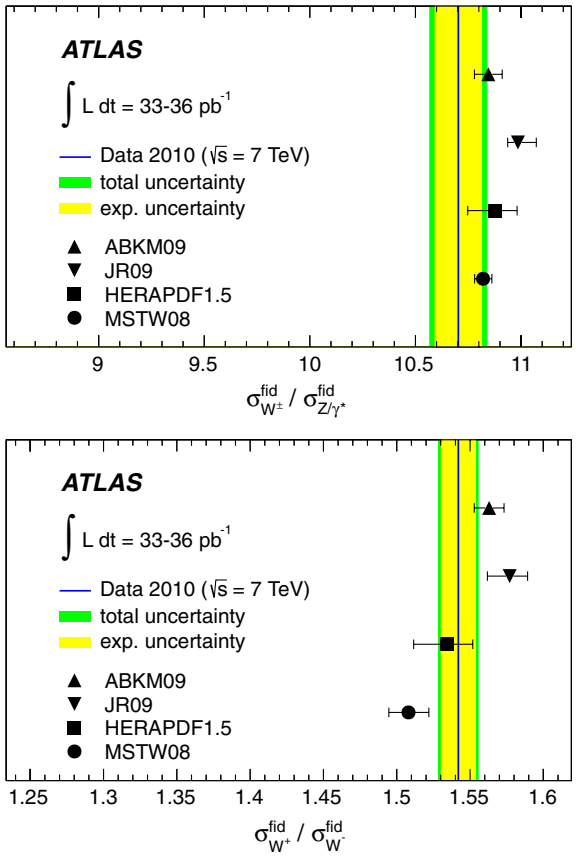

FIG. 18 (color online). Measured and predicted fiducial cross section ratios, $(\sigma_{W^+} + \sigma_{W^-})/\sigma_{Z/\gamma^*}$ (top panel) and $\sigma_{W^+}/\sigma_{W^-}$ (bottom panel). The experimental uncertainty (inner band) includes the experimental systematic errors. The total uncertainty (outer band) includes the statistical uncertainty and the small contribution from the acceptance correction. The uncertainties of the ABKM, JR, and MSTW predictions are given by the PDF uncertainties considered to correspond to 68% C.L., and their correlations are derived from the eigenvector sets. The results for HERAPDF comprise all three sources of uncertainty of that set.

value of 0.9991 ± 0.0024 [65]. If one uses this world average as a constraint on the analysis presented here, the correlated systematic uncertainty on R_W is reduced, and an improved value $R_W = 0.999 \pm 0.020$ is obtained. The correlation of R_W and R_Z and the comparison with the world average values is illustrated in Fig. 17.

2. Combined cross section ratios

Ratios of the $W^{\pm}$ and Z cross sections are calculated accounting for the correlations between uncertainties. The results obtained in the fiducial region are given in Table XIV.

TABLE XVI. Differential cross section for the $W^+ \to e^+\nu$ process, extrapolated to the common fiducial region. The statistical (sta), uncorrelated systematic (δ_{unc}), correlated systematic (δ_{cor}), and total (δ_{tot}) uncertainties are given in percent of the cross section values. The overall 3.4% luminosity uncertainty is not included.

η_{min}	η_{max}	$d\sigma/d\eta$	δ_{sta}	δ_{unc}	δ_{cor}	δ_{tot}
		pb	%	%	%	%
0.00	0.21	607.1	1.29	1.32	2.26	2.92
0.21	0.42	600.2	1.26	1.16	1.71	2.42
0.42	0.63	620.3	1.19	1.15	1.62	2.31
0.63	0.84	615.1	1.21	1.25	1.56	2.34
0.84	1.05	650.8	1.18	1.19	1.96	2.58
1.05	1.37	644.5	0.99	1.00	1.76	2.26
1.52	1.74	623.3	1.26	1.15	1.86	2.52
1.74	1.95	652.0	1.31	1.21	1.85	2.57
1.95	2.18	651.9	1.24	1.23	2.02	2.67
2.18	2.50	585.1	1.31	1.35	2.01	2.75

TABLE XVII. Differential cross section for the $W^- \to e^- \bar{\nu}$ process, extrapolated to the common fiducial region. The statistical (δ_{sta}), uncorrelated systematic (δ_{unc}), correlated systematic (δ_{cor}), and total (δ_{tot}) uncertainties are given in percent of the cross section values. The overall 3.4% luminosity uncertainty is not included.

η_{min}	η_{max}	$d\sigma/d\eta$ pb	δ_{sta} %	δ_{unc} %	δ_{cor} %	δ_{tot} %
0.00	0.21	450.7	1.51	1.52	2.01	2.94
0.21	0.42	438.7	1.48	1.42	1.94	2.83
0.42	0.63	455.8	1.40	1.41	2.03	2.84
0.63	0.84	444.9	1.46	1.53	1.99	2.90
0.84	1.05	427.6	1.47	1.55	1.93	2.88
1.05	1.37	430.5	1.21	1.25	2.10	2.73
1.52	1.74	387.2	1.62	1.62	1.97	3.02
1.74	1.95	384.2	1.70	1.64	2.04	3.13
1.95	2.18	356.5	1.68	1.53	2.47	3.35
2.18	2.50	325.4	1.73	1.67	2.26	3.30

TABLE XVIII. Differential cross section for the central $Z \to e^+e^-$ selection, extrapolated to the common fiducial region. The statistical (δ_{sta}), uncorrelated systematic (δ_{unc}), correlated systematic (δ_{cor}), and total (δ_{tot}) uncertainties are given in percent of the cross section values. The overall 3.4% luminosity uncertainty is not included.

y_{min}	y_{max}	$d\sigma/dy$ pb	δ_{sta} %	δ_{unc} %	δ_{cor} %	δ_{tot} %
0.0	0.4	133.6	2.06	0.68	2.41	3.25
0.4	0.8	127.6	2.17	0.67	2.49	3.37
0.8	1.2	128.4	2.26	0.64	2.66	3.55
1.2	1.6	123.3	2.52	0.65	2.92	3.91
1.6	2.0	113.9	3.30	0.73	3.38	4.78
2.0	2.4	104.2	5.07	0.90	4.65	6.94

TABLE XIX. Differential cross section for the forward $Z \to e^+e^-$ selection, extrapolated to the common fiducial region. The statistical (δ_{sta}), uncorrelated systematic (δ_{unc}), correlated systematic (δ_{cor}), and total (δ_{tot}) uncertainties are given in percent of the cross section values. The overall 3.4% luminosity uncertainty is not included.

y_{min}	y_{max}	$d\sigma/dy$ pb	δ_{sta} %	δ_{unc} %	δ_{cor} %	δ_{tot} %
1.2	1.6	98.3	7.31	4.94	5.94	10.64
1.6	2.0	126.9	3.74	3.16	5.74	7.54
2.0	2.4	107.9	3.28	4.30	5.21	7.51
2.4	2.8	93.8	3.21	3.81	4.80	6.92
2.8	3.6	53.7	4.20	4.37	8.22	10.21

TABLE XX. Differential cross section for the $W^+ \to \mu^+ \nu$ process, extrapolated to the common fiducial region. The statistical (δ_{sta}), uncorrelated systematic (δ_{unc}), correlated systematic (δ_{cor}), and total (δ_{tot}) uncertainties are given in percent of the cross section values. The overall 3.4% luminosity uncertainty is not included.

η_{min}	η_{max}	$d\sigma/d\eta$ pb	δ_{sta} %	δ_{unc} %	δ_{cor} %	δ_{tot} %
0.00	0.21	593.5	1.48	2.32	1.76	3.26
0.21	0.42	611.0	1.31	1.79	1.69	2.79
0.42	0.63	628.7	1.27	1.72	1.62	2.68
0.63	0.84	621.7	1.38	2.34	2.04	3.40
0.84	1.05	629.8	1.37	2.32	1.81	3.24
1.05	1.37	658.8	1.01	1.43	1.78	2.50
1.37	1.52	632.8	1.37	1.30	2.38	3.04
1.52	1.74	638.9	1.13	1.07	1.67	2.28
1.74	1.95	652.1	1.17	1.26	1.70	2.42
1.95	2.18	611.5	1.15	1.22	1.68	2.37
2.18	2.50	577.6	1.21	1.43	2.05	2.78

TABLE XXI. Differential cross section for the $W^- \to \mu^- \nu$ process, extrapolated to the common fiducial region. The statistical (δ_{sta}), uncorrelated systematic (δ_{unc}), correlated systematic (δ_{cor}), and total (δ_{tot}) uncertainties are given in percent of the cross section values. The overall 3.4% luminosity uncertainty is not included.

η_{min}	η_{max}	$d\sigma/d\eta$ pb	δ_{sta} %	δ_{unc} %	δ_{cor} %	δ_{tot} %
0.00	0.21	441.9	1.73	2.34	1.63	3.33
0.21	0.42	444.9	1.56	1.82	1.79	2.99
0.42	0.63	455.1	1.52	1.75	1.75	2.91
0.63	0.84	435.5	1.68	2.39	2.07	3.57
0.84	1.05	433.2	1.67	2.36	1.68	3.34
1.05	1.37	408.8	1.32	1.47	1.66	2.58
1.37	1.52	388.1	1.79	1.35	2.14	3.10
1.52	1.74	383.5	1.50	1.11	2.15	2.85
1.74	1.95	370.5	1.59	1.32	1.94	2.83
1.95	2.18	360.3	1.53	1.26	1.88	2.73
2.18	2.50	338.3	1.60	1.47	2.11	3.03

TABLE XXII. Differential cross section for the $Z \to \mu^+\mu^-$ process, extrapolated to the common fiducial region. The statistical (δ_{sta}), uncorrelated systematic (δ_{unc}), correlated systematic (δ_{cor}), and total (δ_{tot}) uncertainties are given in percent of the cross section values. The overall 3.4% luminosity uncertainty is not included.

y_{min}	y_{max}	$d\sigma/dy$ pb	δ_{sta} %	δ_{unc} %	δ_{cor} %	δ_{tot} %
0.0	0.4	126.7	2.04	0.97	1.22	2.57
0.4	0.8	132.7	1.97	0.73	1.23	2.44
0.8	1.2	125.2	2.01	0.68	0.82	2.27
1.2	1.6	117.9	2.16	0.55	0.82	2.38
1.6	2.0	111.7	2.63	0.65	1.08	2.92
2.0	2.4	107.8	4.43	1.32	2.88	5.45

TABLE XXIII. Combined differential cross section $d\sigma/dy_Z$ for the $Z \to \ell^+\ell^-$ process measured for $66 < m_{\ell\ell} < 116$ GeV and $p_{T,\ell} > 20$ GeV. All uncertainties are quoted in % with respect to the cross section values. $\delta_{\rm sta}$, $\delta_{\rm unc}$, $\delta_{\rm cor}$, and $\delta_{\rm tot}$ represent statistical, uncorrelated systematic, correlated systematic, and total uncertainties. $\gamma_1 - \gamma_{30}$ represent diagonalized correlated systematic uncertainties, which are correlated bin to bin and across the W^+, W^-, and Z measurements. The overall 3.4% luminosity uncertainty is not included.

$y_{\rm min} - y_{\rm max}$	0.0–0.4	0.4–0.8	0.8–1.2	1.2–1.6	1.6–2.0	2.0–2.4	2.4–2.8	2.8–3.6
$d\sigma/dy$ (pb)	129.27	129.44	125.81	118.23	113.37	105.26	92.18	53.38
$\delta_{\rm sta}$, %	1.46	1.47	1.50	1.61	1.84	2.57	3.24	4.21
$\delta_{\rm unc}$, %	0.59	0.50	0.47	0.45	0.63	1.37	3.81	4.37
$\delta_{\rm cor}$, %	1.07	1.08	0.93	0.97	1.26	2.19	3.77	8.06
$\delta_{\rm tot}$, %	1.90	1.89	1.83	1.94	2.32	3.65	6.26	10.09
γ_1, %	0.29	0.29	0.29	0.29	0.29	0.29	0.29	0.29
γ_2, %	0.09	0.09	0.09	0.09	0.09	0.09	0.09	0.09
γ_3, %	0.04	0.04	0.04	0.04	0.04	0.04	0.04	0.04
γ_4, %	0.19	0.19	0.19	0.19	0.19	0.19	0.19	0.18
γ_5, %	0.07	0.07	0.05	0.04	0.01	0.00	0.06	0.18
γ_6, %	−0.13	−0.10	−0.08	−0.05	−0.04	−0.07	−0.06	−0.03
γ_7, %	0.05	0.04	0.05	0.04	0.05	0.09	0.58	1.76
γ_8, %	−0.07	−0.09	−0.07	−0.09	−0.08	−0.19	−0.42	−1.16
γ_9, %	−0.03	−0.02	−0.05	0.01	0.05	0.18	0.61	1.28
γ_{10}, %	0.12	0.13	0.11	0.08	0.03	−0.05	−0.40	−0.93
γ_{11}, %	−0.10	−0.10	−0.10	−0.05	0.01	0.13	0.63	1.87
γ_{12}, %	0.06	0.06	0.06	0.15	0.33	0.76	2.26	4.97
γ_{13}, %	−0.28	−0.29	−0.17	−0.15	0.15	0.18	0.11	−0.39
γ_{14}, %	−0.02	0.01	−0.03	0.05	−0.01	0.23	1.16	3.19
γ_{15}, %	0.07	0.06	0.01	0.03	0.02	0.23	1.18	2.70
γ_{16}, %	−0.10	−0.08	−0.08	−0.03	−0.09	0.04	0.23	1.64
γ_{17}, %	−0.53	−0.55	−0.43	−0.37	−0.37	−0.58	−0.82	−1.95
γ_{18}, %	0.07	0.02	0.03	0.07	0.17	0.17	0.45	0.56
γ_{19}, %	−0.16	−0.16	−0.13	−0.06	−0.07	−0.06	0.03	0.37
γ_{20}, %	0.34	0.32	0.22	0.30	0.41	0.66	−0.03	−0.83
γ_{21}, %	−0.15	−0.17	−0.15	−0.09	0.04	0.13	0.04	−0.03
γ_{22}, %	−0.10	−0.15	0.00	−0.25	−0.45	−1.15	−0.28	1.39
γ_{23}, %	0.05	0.02	0.00	−0.23	−0.49	−0.85	−0.09	0.78
γ_{24}, %	0.22	0.23	0.23	0.16	0.00	0.15	0.49	0.28
γ_{25}, %	0.17	0.16	0.12	0.14	0.08	0.01	0.26	0.26
γ_{26}, %	0.18	0.25	0.28	0.18	0.24	0.69	0.03	−1.13
γ_{27}, %	0.00	−0.01	−0.04	−0.04	−0.06	−0.20	−0.19	−0.04
γ_{28}, %	0.50	0.47	0.45	0.52	0.66	0.62	0.70	0.26
γ_{29}, %	0.17	0.18	0.16	0.13	−0.06	−0.14	−1.68	−0.46
γ_{30}, %	−0.12	−0.11	−0.14	−0.12	−0.11	−0.20	−0.21	−0.21

The precision of these measurements is very high, with a total uncertainty of 0.9% for the W^+/W^- ratio and of 1.3% for the $W^\pm/Z$ ratio.

Ratios for the total cross sections are given in Table XV. The uncertainties of the total cross section ratios are enlarged significantly by the additional acceptance contribution. Compared to the fiducial cross section ratios, the uncertainties are almost doubled, with a value of 1.8% for the W^+/W^- ratio and of 1.6% for the $W^\pm/Z$ ratio.

The cross section ratios, determined in the fiducial regions of the W and Z measurements, are compared in Figs. 18 and 19 with the theoretical predictions, accounting for the correlations inherent in the PDF determinations.

The mean boson rapidity for the data presented here is about zero, and thus on average the Bjorken x values of the incoming partons are equal, $x_1 = x_2 \simeq 0.01$. In a rough leading order calculation, neglecting the heavy-quark and Cabibbo disfavored parts of the cross sections and the γ^* contribution to the Z cross section, and also assuming the light sea and antiquark distributions to all be the same, xs, the $(W^+ + W^-)/Z$ ratio is found to be proportional to $(u_v + d_v + 2s)/[(v_u^2 + a_u^2) \times$

TABLE XXIV. Combined differential cross section $d\sigma/d\eta_{\ell^-}$ for the $W^- \to \ell^- \bar{\nu}$ process measured for $p_{T,\ell} > 20$ GeV, $p_{T,\nu} > 25$ GeV, and $m_T > 40$ GeV. All uncertainties are quoted in % with respect to the cross section values. $\delta_{\rm sta}$, $\delta_{\rm unc}$, $\delta_{\rm cor}$, and $\delta_{\rm tot}$ represent statistical, uncorrelated systematic, correlated systematic, and total uncertainties. $\gamma_1 - \gamma_{30}$ represent diagonalized correlated systematic uncertainties, which are correlated bin to bin and across the W^+, W^-, and Z measurements. The overall 3.4% luminosity uncertainty is not included.

$\eta_{\rm min} - \eta_{\rm max}$	0.00–0.21	0.21–0.42	0.42–0.63	0.63–0.84	0.84–1.05	1.05–1.37	1.37–1.52	1.52–1.74	1.74–1.95	1.95–2.18	2.18–2.50
$d\sigma/d\eta$ (pb)	446.32	440.26	455.06	439.81	428.07	418.89	387.27	384.03	375.29	357.39	330.99
$\delta_{\rm sta}$, %	1.16	1.08	1.04	1.12	1.12	0.90	1.79	1.11	1.17	1.13	1.18
$\delta_{\rm unc}$, %	1.29	1.13	1.10	1.30	1.30	0.95	1.35	0.93	1.03	0.98	1.10
$\delta_{\rm cor}$, %	1.30	1.29	1.31	1.35	1.36	1.37	1.67	1.47	1.48	1.50	1.64
$\delta_{\rm tot}$, %	2.16	2.02	2.00	2.18	2.19	1.90	2.80	2.06	2.15	2.12	2.30
γ_1, %	0.10	0.10	0.10	0.10	0.10	0.10	0.10	0.10	0.10	0.10	0.10
γ_2, %	0.18	0.18	0.18	0.18	0.18	0.18	0.18	0.18	0.18	0.18	0.18
γ_3, %	0.23	0.23	0.23	0.23	0.23	0.23	0.23	0.23	0.23	0.23	0.23
γ_4, %	0.19	0.19	0.19	0.19	0.19	0.19	0.19	0.19	0.19	0.19	0.19
γ_5, %	0.03	0.03	0.04	0.04	0.03	0.04	0.05	0.04	0.05	0.04	0.06
γ_6, %	−0.01	0.00	−0.01	−0.01	−0.01	0.00	−0.02	0.00	0.00	−0.01	0.00
γ_7, %	0.04	0.05	0.06	0.05	0.04	0.05	0.04	0.06	0.04	0.04	0.14
γ_8, %	0.05	0.06	0.03	0.06	0.06	0.03	0.06	0.04	0.03	0.05	0.01
γ_9, %	0.07	0.07	0.07	0.08	0.05	0.11	0.12	0.11	0.10	0.10	0.02
γ_{10}, %	0.11	0.11	0.09	0.10	0.11	0.13	0.19	0.15	0.11	0.10	0.14
γ_{11}, %	0.17	0.18	0.16	0.18	0.21	0.18	0.20	0.20	0.19	0.20	0.35
γ_{12}, %	0.06	0.09	0.06	0.09	0.07	0.13	0.09	0.13	0.13	0.14	0.12
γ_{13}, %	−0.42	−0.42	−0.45	−0.49	−0.46	−0.49	−0.62	−0.53	−0.54	−0.52	−0.49
γ_{14}, %	0.08	0.05	0.05	0.08	0.09	0.11	0.14	0.11	0.13	0.15	0.16
γ_{15}, %	−0.18	−0.20	−0.20	−0.22	−0.23	−0.32	−0.25	−0.36	−0.35	−0.36	−0.36
γ_{16}, %	−0.29	−0.29	−0.31	−0.31	−0.27	−0.34	−0.38	−0.36	−0.37	−0.32	−0.31
γ_{17}, %	−0.57	−0.48	−0.52	−0.49	−0.61	−0.60	−0.81	−0.74	−0.61	−0.64	−0.84
γ_{18}, %	0.39	0.44	0.50	0.56	0.53	0.37	0.52	0.35	0.47	0.36	0.40
γ_{19}, %	0.30	0.37	0.32	0.38	0.26	0.33	0.25	0.23	0.33	0.15	0.08
γ_{20}, %	0.34	0.34	0.32	0.44	0.29	0.45	0.58	0.40	0.48	0.53	0.58
γ_{21}, %	−0.41	−0.38	−0.28	−0.36	−0.47	−0.47	−0.53	−0.43	−0.44	−0.56	−0.55
γ_{22}, %	−0.11	−0.08	−0.08	−0.03	−0.09	−0.02	−0.05	−0.01	−0.01	−0.02	−0.10
γ_{23}, %	0.12	0.17	0.19	0.14	0.07	0.03	0.01	0.01	0.11	0.06	−0.01
γ_{24}, %	−0.11	−0.18	−0.14	−0.09	−0.22	−0.15	0.00	−0.29	−0.23	−0.32	−0.45
γ_{25}, %	−0.02	−0.16	−0.14	−0.07	−0.12	−0.11	0.13	−0.22	−0.10	−0.04	−0.04
γ_{26}, %	0.51	0.41	0.50	0.32	0.36	0.25	0.19	0.26	0.36	0.42	0.24
γ_{27}, %	−0.08	−0.15	−0.18	−0.08	−0.07	−0.02	−0.25	−0.09	−0.08	0.00	0.09
γ_{28}, %	0.11	0.21	0.12	0.21	0.21	0.27	0.34	0.32	0.25	0.25	0.29
γ_{29}, %	0.07	0.07	0.05	0.07	0.06	0.09	0.12	0.08	0.08	0.09	0.09
γ_{30}, %	−0.16	−0.10	−0.10	−0.13	−0.14	−0.10	0.31	0.03	−0.01	−0.04	0.00

$(u_v + s) + (v_d^2 + a_d^2)(d_v + s)]$. Here $xu_v(xd_v)$ is the up (down) valence-quark momentum distribution and $v_{u,d}$ and $a_{u,d}$ are the vector and axial-vector weak neutral current couplings of the light quarks. As the numerical values for the Z coupling to the up and down quarks, $v_{u,d}^2 + a_{u,d}^2$, are of similar size, the $W^{\pm}/Z$ ratio measures a rather PDF insensitive quantity, provided that the sea is flavor symmetric. Since this symmetry assumption, with a small deviation to account for some light sea quark asymmetry near Bjorken $x \simeq 0.1$, is inherent in all major PDF fit determinations, there is indeed not much difference observed between the various $W^{\pm}/Z$ ratio predictions; see Fig. 18 (top panel). The agreement with the present measurement therefore supports the assumption of a flavor independent light quark sea at high scales, and Bjorken x near 0.01. The predictions for the charge dependent W^+/W^-, W^+/Z, and W^-/Z ratios, shown in Figs. 18 (bottom panel) and 19, exhibit more significant deviations as they are more sensitive to up-down quark distribution differences.

TABLE XXV. Combined differential cross section $d\sigma/d\eta_{\ell^+}$ for the $W^+ \to \ell^+\nu$ process measured for $p_{T,\ell} > 20$ GeV, $p_{T,\nu} > 25$ GeV, and $m_T > 40$ GeV. All uncertainties are quoted in % with respect to the cross section values. $\delta_{\rm sta}$, $\delta_{\rm unc}$, $\delta_{\rm cor}$, and $\delta_{\rm tot}$ represent statistical, uncorrelated systematic, correlated systematic, and total uncertainties. $\gamma_1 - \gamma_{30}$ represent diagonalized correlated systematic uncertainties, which are correlated bin to bin and across the W^+, W^-, and Z measurements. The overall 3.4% luminosity uncertainty is not included.

$\eta_{\rm min} - \eta_{\rm max}$	0.00–0.21	0.21–0.42	0.42–0.63	0.63–0.84	0.84–1.05	1.05–1.37	1.37–1.52	1.52–1.74	1.74–1.95	1.95–2.18	2.18–2.50
$d\sigma/d\eta$ (pb)	602.00	602.67	620.15	614.69	640.65	647.21	630.74	629.17	648.85	628.13	578.39
$\delta_{\rm sta}$, %	1.00	0.93	0.89	0.95	0.94	0.72	1.37	0.84	0.88	0.85	0.89
$\delta_{\rm unc}$, %	1.16	0.99	0.97	1.12	1.07	0.83	1.30	0.78	0.88	0.87	0.98
$\delta_{\rm cor}$, %	1.33	1.17	1.17	1.20	1.26	1.19	1.73	1.15	1.29	1.21	1.39
$\delta_{\rm tot}$, %	2.03	1.79	1.76	1.89	1.90	1.62	2.56	1.63	1.79	1.71	1.92
γ_1, %	0.23	0.23	0.23	0.23	0.23	0.23	0.23	0.23	0.23	0.23	0.23
γ_2, %	−0.18	−0.18	−0.18	−0.18	−0.18	−0.18	−0.18	−0.18	−0.18	−0.18	−0.18
γ_3, %	0.09	0.09	0.09	0.09	0.09	0.09	0.09	0.09	0.09	0.09	0.09
γ_4, %	0.20	0.20	0.20	0.20	0.20	0.20	0.20	0.20	0.20	0.20	0.20
γ_5, %	0.03	0.03	0.03	0.04	0.04	0.04	0.06	0.04	0.05	0.03	0.02
γ_6, %	−0.01	−0.01	−0.01	−0.01	0.00	−0.01	−0.02	−0.01	−0.01	0.00	−0.01
γ_7, %	0.03	0.03	0.02	0.04	0.04	0.02	0.02	0.02	0.02	0.03	0.08
γ_8, %	0.03	0.03	0.04	0.02	0.04	0.00	−0.03	0.00	0.00	0.03	−0.03
γ_9, %	0.08	0.08	0.06	0.09	0.07	0.11	0.17	0.11	0.12	0.11	0.05
γ_{10}, %	0.10	0.11	0.14	0.12	0.11	0.15	0.18	0.11	0.12	0.12	0.11
γ_{11}, %	0.13	0.12	0.13	0.12	0.19	0.11	0.12	0.12	0.13	0.13	0.24
γ_{12}, %	0.08	0.08	0.07	0.07	0.10	0.10	0.07	0.11	0.11	0.11	0.01
γ_{13}, %	−0.43	−0.39	−0.40	−0.47	−0.48	−0.46	−0.61	−0.49	−0.51	−0.44	−0.48
γ_{14}, %	0.03	0.01	0.04	0.01	0.05	0.08	0.08	0.06	0.09	0.07	0.05
γ_{15}, %	−0.17	−0.15	−0.16	−0.16	−0.22	−0.23	−0.18	−0.26	−0.26	−0.26	−0.29
γ_{16}, %	−0.22	−0.19	−0.17	−0.23	−0.23	−0.22	−0.26	−0.21	−0.24	−0.17	−0.24
γ_{17}, %	−0.59	−0.60	−0.55	−0.63	−0.46	−0.66	−1.00	−0.64	−0.62	−0.60	−0.82
γ_{18}, %	0.37	0.34	0.47	0.47	0.64	0.36	0.40	0.37	0.46	0.36	0.46
γ_{19}, %	0.21	0.31	0.44	0.35	0.28	0.29	0.10	0.17	0.28	0.21	0.23
γ_{20}, %	0.30	0.20	0.17	0.23	0.28	0.29	0.48	0.27	0.37	0.25	0.19
γ_{21}, %	−0.18	−0.19	−0.28	−0.10	−0.31	−0.17	−0.30	−0.11	−0.16	−0.25	−0.33
γ_{22}, %	−0.05	−0.08	−0.12	−0.01	−0.08	0.00	0.03	0.01	0.11	−0.01	0.08
γ_{23}, %	0.09	0.08	0.06	0.05	0.01	−0.05	−0.19	−0.11	−0.10	−0.10	−0.19
γ_{24}, %	−0.08	−0.14	−0.05	−0.13	0.26	−0.04	−0.07	0.14	−0.12	−0.03	−0.04
γ_{25}, %	−0.24	−0.13	0.06	−0.09	−0.03	0.02	0.02	0.03	−0.02	−0.07	−0.01
γ_{26}, %	0.74	0.45	0.05	0.18	0.04	0.22	0.49	0.13	0.27	0.44	0.27
γ_{27}, %	0.09	0.16	0.23	0.14	0.13	0.18	0.41	0.18	0.22	0.18	0.19
γ_{28}, %	0.12	0.21	0.25	0.26	0.18	0.21	0.46	0.18	0.29	0.24	0.31
γ_{29}, %	0.07	0.06	0.03	0.03	0.05	0.05	0.15	0.05	0.08	0.09	0.06
γ_{30}, %	−0.18	−0.10	−0.07	−0.09	−0.19	−0.09	0.36	−0.03	−0.02	−0.06	−0.02

VII. SUMMARY

New measurements are presented of the inclusive cross sections of Drell-Yan $W^{\pm}$ and Z/γ^* production in the electron and muon decay channels. They are based on the full data sample collected by the ATLAS experiment at the LHC in 2010 at a center-of-mass energy of 7 TeV. With an integrated luminosity of about 35 pb^{-1}, a total of about 270 000 W boson decays into an electron or muon and the associated neutrino and a total of about 24 000 Z/γ^* decays into electron or muon pairs have been observed.

The cross sections are measured in a well-defined kinematic range within the detector acceptance, defined by charged lepton pseudorapidity and charged lepton and neutrino transverse momentum cuts. Integrated cross sections are determined in these fiducial regions and are also extrapolated to the full kinematic range to obtain the total integrated W and Z/γ^* cross sections.

TABLE XXVI. The combined lepton charge asymmetry A_ℓ from W boson decays in bins of absolute lepton pseudorapidity measured for $p_{T,\ell} > 20$ GeV, $p_{T,\nu} > 25$ GeV, and $m_T > 40$ GeV. $\Delta_{\rm sta}$, $\Delta_{\rm unc}$, $\Delta_{\rm cor}$, and $\Delta_{\rm tot}$ represent statistical, uncorrelated systematic, correlated systematic, and total uncertainty.

$\eta_{\rm min}$	$\eta_{\rm max}$	A_ℓ	$\Delta_{\rm sta}$	$\Delta_{\rm unc}$	$\Delta_{\rm cor}$	$\Delta_{\rm tot}$
0.00	0.21	0.149	0.008	0.009	0.003	0.012
0.21	0.42	0.156	0.007	0.008	0.003	0.011
0.42	0.63	0.154	0.007	0.007	0.004	0.011
0.63	0.84	0.166	0.007	0.009	0.003	0.012
0.84	1.05	0.199	0.007	0.008	0.004	0.012
1.05	1.37	0.214	0.006	0.006	0.003	0.009
1.37	1.52	0.239	0.011	0.010	0.005	0.016
1.52	1.74	0.242	0.007	0.006	0.004	0.010
1.74	1.95	0.267	0.007	0.007	0.003	0.011
1.95	2.18	0.275	0.007	0.007	0.003	0.010
2.18	2.50	0.272	0.007	0.008	0.004	0.011

The $W^{\pm}$ cross sections are measured differentially as a function of the lepton pseudorapidity, extending to $|\eta_\ell| \leq 2.5$. The Z/γ^* cross section is measured as a function of the boson rapidity $|y_Z|$ up to a value of 2.4. An extension to $|y_Z| \leq 3.6$ is obtained through the electron channel measurements, which include the forward detector region and $|\eta_e|$ as large as 4.9.

The electron and muon measurements are found to be consistent in the three channels, W^+, W^-, and Z/γ^*. The data sets are therefore combined using a method which accounts for the different systematic error correlations.

This combination provides the most accurate integrated inclusive W and Z/γ^* cross sections so far obtained by the ATLAS Collaboration and the first measurements of rapidity dependent cross sections. An update is also presented of the W charge asymmetry as a function of $|\eta_\ell|$.

The precision of the integrated W and Z/γ^* cross sections in the fiducial region is $\sim$1.2% with an additional uncertainty of 3.4% resulting from the luminosity error. The uncertainties on the total integrated cross sections are about twice as large because of the extrapolation uncertainties in the determination of the acceptance correction. The differential cross sections are determined in the fiducial region with a typical precision of 2%, apart from the most forward part of y_Z.

The results are compared with QCD predictions calculated to NNLO in the fiducial regions of the measurements which allows for maximum sensitivity to details of the parton distributions used in these calculations.

The broad agreement of the theory predictions at the few percent level with the data supports the validity of the QCD evolution equations, as the results rely on lower scale parton distribution functions evolved to the W and Z kinematic regions, at the average value of Bjorken x of about 0.01.

Interesting differences between sets of parton distributions are observed, both in the integrated and the differential fiducial cross sections. The results presented in this paper therefore provide a further basis for sensitive tests of perturbative QCD and determinations of the partonic content of the proton.

ACKNOWLEDGMENTS

We thank CERN for the very successful operation of the LHC, as well as the support staff from our institutions without whom ATLAS could not be operated efficiently. We acknowledge the support of ANPCyT, Argentina; YerPhI, Armenia; ARC, Australia; BMWF, Austria; ANAS, Azerbaijan; SSTC, Belarus; CNPq and FAPESP, Brazil; NSERC, NRC and CFI, Canada; CERN; CONICYT, Chile; CAS, MOST and NSFC, China; COLCIENCIAS, Colombia; MSMT CR, MPO CR and VSC CR, Czech Republic; DNRF, DNSRC and Lundbeck Foundation, Denmark; ARTEMIS, European Union; IN2P3-CNRS, CEA-DSM/IRFU, France; GNAS, Georgia; BMBF, DFG, HGF, MPG and AvH Foundation, Germany; GSRT, Greece; ISF, MINERVA, GIF, DIP and Benoziyo Center, Israel; INFN, Italy; MEXT and JSPS, Japan; CNRST, Morocco; FOM and NWO, Netherlands; RCN, Norway; MNiSW, Poland; GRICES and FCT, Portugal; MERYS (MECTS), Romania; MES of Russia and ROSATOM, Russian Federation; JINR; MSTD, Serbia; MSSR, Slovakia; ARRS and MVZT, Slovenia; DST/NRF, South Africa; MICINN, Spain; SRC and Wallenberg Foundation, Sweden; SER, SNSF and Cantons of Bern and Geneva, Switzerland; NSC, Taiwan; TAEK, Turkey; STFC, the Royal Society and Leverhulme Trust, United Kingdom; DOE and NSF, USA. The crucial computing support from all WLCG partners is acknowledged gratefully, in particular, from CERN and the ATLAS Tier-1 facilities at TRIUMF (Canada), NDGF (Denmark, Norway, Sweden), CC-IN2P3 (France), KIT/GridKA (Germany), INFN-CNAF (Italy), NL-T1 (Netherlands), PIC (Spain), ASGC (Taiwan), RAL (UK) and BNL (USA), and in the Tier-2 facilities worldwide.

[1] S. D. Drell and T.-M. Yan, Phys. Rev. Lett. **25**, 316 (1970).
[2] J. Kubar and F. E. Paige, Phys. Rev. D **19**, 221 (1979).
[3] G. Altarelli, R. K. Ellis, and G. Martinelli, Nucl. Phys. **B157**, 461 (1979).
[4] J. Kubar, M. Le Bellac, J. L. Meunier, and G. Plaut, Nucl. Phys. **B175**, 251 (1980).
[5] P. J. Rijken and W. L. van Neerven, Phys. Rev. D **51**, 44 (1995).
[6] R. Hamberg, W. L. van Neerven, and T. Matsuura, Nucl. Phys. **B359**, 343 (1991).
[7] W. L. van Neerven and E. B. Zijlstra, Nucl. Phys. **B382**, 11 (1992).
[8] R. V. Harlander and W. B. Kilgore, Phys. Rev. Lett. **88**, 201801 (2002).
[9] C. Anastasiou, L. J. Dixon, K. Melnikov, and F. Petriello, Phys. Rev. D **69**, 094008 (2004).
[10] P. M. Nadolsky *et al.*, Phys. Rev. D **78**, 013004 (2008).
[11] L. Hung-Liang *et al.*, Phys. Rev. D **82**, 074024 (2010).
[12] A. D. Martin, W. J. Stirling, R. S. Thorne, and G. Watt, Eur. Phys. J. C **63**, 189 (2009).
[13] S. Alekhin, J. Blumlein, S. Klein, and S. Moch, Phys. Rev. D **81**, 014032 (2010).
[14] S. Alekhin, J. Blumlein, and S.-O. Moch, Proc. Sci., DIS2010 (2010) 021.
[15] F. D. Aaron *et al.* (H1 and ZEUS Collaborations), J. High Energy Phys. 01 (2010) 109.
[16] V. Radescu (H1 and ZEUS Collaborations), Reports No. H1prelim-11-042 and No. ZEUS-prel-11-002, 2011.
[17] P. Jimenez-Delgado and E. Reya, Phys. Rev. D **79**, 074023 (2009).
[18] R. D. Ball, V. Bertone, F. Cerutti, L. Del Deb-bio, S. Forte *et al.*, Nucl. Phys. **B849**, 296 (2011).
[19] R. D. Ball *et al.* (NNPDF Collaboration), Nucl. Phys. **B855**, 153 (2012).
[20] ATLAS Collaboration, J. High Energy Phys. 12 (2010) 060.
[21] ATLAS Collaboration, ATLAS Note No. ATLAS-CONF-2011-034, 2011.
[22] V. Khachatryan *et al.* (CMS Collaboration), J. High Energy Phys. 01 (2011) 080.
[23] S. Chatrchyan *et al.* (CMS Collaboration), J. High Energy Phys. 10 (2011) 132.
[24] A. Abulencia *et al.* (CDF Collaboration), J. Phys. G **34**, 2457 (2007).
[25] B. Abbott *et al.* (D0 Collaboration), Phys. Rev. D **61**, 072001 (2000).
[26] ATLAS Collaboration, Phys. Lett. B **701**, 31 (2011).
[27] S. Chatrchyan *et al.* (CMS Collaboration), Phys. Rev. D **85**, 032002 (2012).
[28] S. Chatrchyan *et al.* (CMS Collaboration), J. High Energy Phys. 04 (2011) 050.
[29] T. A. Aaltonen *et al.* (CDF Collaboration), Phys. Lett. B **692**, 232 (2010).
[30] V. Abazov *et al.* (D0 Collaboration), Phys. Rev. D **76**, 012003 (2007).
[31] T. Aaltonen *et al.* (CDF Collaboration), Phys. Rev. Lett. **102**, 181801 (2009).
[32] D. E. Acosta *et al.* (CDF Collaboration), Phys. Rev. D **71**, 051104 (2005).
[33] V. M. Abazov *et al.* (D0 Collaboration), Phys. Rev. D **77**, 011106 (2008).
[34] V. M. Abazov *et al.* (D0 Collaboration), Phys. Rev. Lett. **101**, 211801 (2008).
[35] ATLAS Collaboration, JINST **3**, S08003 (2008).
[36] ATLAS Collaboration, Eur. Phys. J. C **72**, 1909 (2012).
[37] S. Frixione and B. R. Webber, J. High Energy Phys. 06 (2002) 029.
[38] P. Nason, J. High Energy Phys. 11 (2004) 040.
[39] S. Frixione, P. Nason, and C. Oleari, J. High Energy Phys. 11 (2007) 070.
[40] S. Alioli, P. Nason, C. Oleari, and E. Re, J. High Energy Phys. 06 (2010) 043.
[41] S. Alioli, P. Nason, C. Oleari, and E. Re, J. High Energy Phys. 07 (2008) 060.
[42] T. Sjostrand, S. Mrenna, and P. Z. Skands, J. High Energy Phys. 05 (2006) 026.
[43] G. Corcella *et al.*, J. High Energy Phys. 01 (2001) 010.
[44] P. Golonka and Z. Was, Eur. Phys. J. C **45**, 97 (2006).
[45] G. Aad *et al.* (ATLAS Collaboration), Eur. Phys. J. C **70**, 823 (2010).
[46] S. Agostinelli *et al.* (GEANT4 Collaboration), Nucl. Instrum. Methods Phys. Res., Sect. A **506**, 250 (2003).
[47] A. Sherstnev and R. S. Thorne, Eur. Phys. J. C **55**, 553 (2008).
[48] ATLAS Collaboration, ATLAS Note No. ATLAS-CONF-2010-031, 2010.
[49] ATLAS Collaboration, Phys. Lett. B **705**, 415 (2011).
[50] ATLAS Collaboration, Phys. Rev. D **85**, 012005 (2012).
[51] R. Gavin, Y. Li, F. Petriello, and S. Quackenbush, Comput. Phys. Commun. **182**, 2388 (2011).
[52] S. Moch and P. Uwer, Nucl. Phys. B, Proc. Suppl. **183**, 75 (2008).
[53] U. Langenfeld, S. Moch, and P. Uwer, arXiv:0907.2527.
[54] G. Aad *et al.* (ATLAS Collaboration), Phys. Lett. B **707**, 459 (2012).
[55] ATLAS Collaboration, ATLAS Note No. ATLAS-CONF-2011-063.
[56] D. Bourilkov, R. C. Group, and M. R. Whalley, arXiv:hep-ph/0605240.
[57] ATLAS Collaboration, Eur. Phys. J. C **72**, 1844 (2012).
[58] ATLAS Collaboration, ATLAS Note No. ATLAS-CONF-2010-036.
[59] ATLAS Collaboration, ATLAS Note No. ATLAS-CONF-2011-046.
[60] A. Glazov, AIP Conf. Proc. **792**, 237 (2005).
[61] F. D. Aaron *et al.*, Eur. Phys. J. C **63**, 625 (2009).
[62] HepData, http://hepdata.cedar.ac.uk.
[63] S. Catani and M. Grazzini, Phys. Rev. Lett. **98**, 222002 (2007).
[64] S. Catani, L. Cieri, G. Ferrera, D. de Florian, and M. Grazzini, Phys. Rev. Lett. **103**, 082001 (2009).
[65] K. Nakamura *et al.* (Particle Data Group), J. Phys. G **37**, 075021 (2010).
[66] A. Andonov, A. Arbuzov, D. Bardin, S. Bondarenko, P. Christova *et al.*, Comput. Phys. Commun. **181**, 305 (2010).
[67] G. Watt, J. High Energy Phys. 09 (2011) 069.

G. Aad,[47] B. Abbott,[110] J. Abdallah,[11] A. A. Abdelalim,[48] A. Abdesselam,[117] O. Abdinov,[10] B. Abi,[111] M. Abolins,[87] H. Abramowicz,[152] H. Abreu,[114] E. Acerbi,[88a,88b] B. S. Acharya,[163a,163b] D. L. Adams,[24] T. N. Addy,[55] J. Adelman,[174] M. Aderholz,[98] S. Adomeit,[97] P. Adragna,[74] T. Adye,[128] S. Aefsky,[22] J. A. Aguilar-Saavedra,[123b,b] M. Aharrouche,[80] S. P. Ahlen,[21] F. Ahles,[47] A. Ahmad,[147] M. Ahsan,[40] G. Aielli,[132a,132b] T. Akdogan,[18a] T. P. A. Åkesson,[78] G. Akimoto,[154] A. V. Akimov,[93] A. Akiyama,[66] M. S. Alam,[1] M. A. Alam,[75] J. Albert,[168] S. Albrand,[54] M. Aleksa,[29] I. N. Aleksandrov,[64] F. Alessandria,[88a] C. Alexa,[25a] G. Alexander,[152] G. Alexandre,[48] T. Alexopoulos,[9] M. Alhroob,[20] M. Aliev,[15] G. Alimonti,[88a] J. Alison,[119] M. Aliyev,[10] P. P. Allport,[72] S. E. Allwood-Spiers,[52] J. Almond,[81] A. Aloisio,[101a,101b] R. Alon,[170] A. Alonso,[78] M. G. Alviggi,[101a,101b] K. Amako,[65] P. Amaral,[29] C. Amelung,[22] V. V. Ammosov,[127] A. Amorim,[123a,c] G. Amorós,[166] N. Amram,[152] C. Anastopoulos,[29] L. S. Ancu,[16] N. Andari,[114] T. Andeen,[34] C. F. Anders,[20] G. Anders,[57a] K. J. Anderson,[30] A. Andreazza,[88a,88b] V. Andrei,[57a] M-L. Andrieux,[54] X. S. Anduaga,[69] A. Angerami,[34] F. Anghinolfi,[29] N. Anjos,[123a] A. Annovi,[46] A. Antonaki,[8] M. Antonelli,[46] A. Antonov,[95] J. Antos,[143b] F. Anulli,[131a] S. Aoun,[82] L. Aperio Bella,[4] R. Apolle,[117,d] G. Arabidze,[87] I. Aracena,[142] Y. Arai,[65] A. T. H. Arce,[44] J. P. Archambault,[28] S. Arfaoui,[29,e] J-F. Arguin,[14] E. Arik,[18a,a] M. Arik,[18a] A. J. Armbruster,[86] O. Arnaez,[80] C. Arnault,[114] A. Artamonov,[94] G. Artoni,[131a,131b] D. Arutinov,[20] S. Asai,[154] R. Asfandiyarov,[171] S. Ask,[27] B. Åsman,[145a,145b] L. Asquith,[5] K. Assamagan,[24] A. Astbury,[168] A. Astvatsatourov,[51] G. Atoian,[174] B. Aubert,[4] E. Auge,[114] K. Augsten,[126] M. Aurousseau,[144a] N. Austin,[72] G. Avolio,[162] R. Avramidou,[9] D. Axen,[167] C. Ay,[53] G. Azuelos,[92,f] Y. Azuma,[154] M. A. Baak,[29] G. Baccaglioni,[88a] C. Bacci,[133a,133b] A. M. Bach,[14] H. Bachacou,[135] K. Bachas,[29] G. Bachy,[29] M. Backes,[48] M. Backhaus,[20] E. Badescu,[25a] P. Bagnaia,[131a,131b] S. Bahinipati,[2] Y. Bai,[32a] D. C. Bailey,[157] T. Bain,[157] J. T. Baines,[128] O. K. Baker,[174] M. D. Baker,[24] S. Baker,[76] E. Banas,[38] P. Banerjee,[92] Sw. Banerjee,[171] D. Banfi,[29] A. Bangert,[136] V. Bansal,[168] H. S. Bansil,[17] L. Barak,[170] S. P. Baranov,[93] A. Barashkou,[64] A. Barbaro Galtieri,[14] T. Barber,[27] E. L. Barberio,[85] D. Barberis,[49a,49b] M. Barbero,[20] D. Y. Bardin,[64] T. Barillari,[98] M. Barisonzi,[173] T. Barklow,[142] N. Barlow,[27] B. M. Barnett,[128] R. M. Barnett,[14] A. Baroncelli,[133a] G. Barone,[48] A. J. Barr,[117] F. Barreiro,[79] J. Barreiro Guimarães da Costa,[56] P. Barrillon,[114] R. Bartoldus,[142] A. E. Barton,[70] D. Bartsch,[20] V. Bartsch,[148] R. L. Bates,[52] L. Batkova,[143a] J. R. Batley,[27] A. Battaglia,[16] M. Battistin,[29] G. Battistoni,[88a] F. Bauer,[135] H. S. Bawa,[142,g] B. Beare,[157] T. Beau,[77] P. H. Beauchemin,[117] R. Beccherle,[49a] P. Bechtle,[41] H. P. Beck,[16] M. Beckingham,[47] K. H. Becks,[173] A. J. Beddall,[18c] A. Beddall,[18c] S. Bedikian,[174] V. A. Bednyakov,[64] C. P. Bee,[82] M. Begel,[24] S. Behar Harpaz,[151] P. K. Behera,[62] M. Beimforde,[98] C. Belanger-Champagne,[84] P. J. Bell,[48] W. H. Bell,[48] G. Bella,[152] L. Bellagamba,[19a] F. Bellina,[29] M. Bellomo,[29] A. Belloni,[56] O. Beloborodova,[106] K. Belotskiy,[95] O. Beltramello,[29] S. Ben Ami,[151] O. Benary,[152] D. Benchekroun,[134a] C. Benchouk,[82] M. Bendel,[80] N. Benekos,[164] Y. Benhammou,[152] D. P. Benjamin,[44] M. Benoit,[114] J. R. Bensinger,[22] K. Benslama,[129] S. Bentvelsen,[104] D. Berge,[29] E. Bergeaas Kuutmann,[41] N. Berger,[4] F. Berghaus,[168] E. Berglund,[48] J. Beringer,[14] K. Bernardet,[82] P. Bernat,[76] R. Bernhard,[47] C. Bernius,[24] T. Berry,[75] A. Bertin,[19a,19b] F. Bertinelli,[29] F. Bertolucci,[121a,121b] M. I. Besana,[88a,88b] N. Besson,[135] S. Bethke,[98] W. Bhimji,[45] R. M. Bianchi,[29] M. Bianco,[71a,71b] O. Biebel,[97] S. P. Bieniek,[76] K. Bierwagen,[53] J. Biesiada,[14] M. Biglietti,[133a,133b] H. Bilokon,[46] M. Bindi,[19a,19b] S. Binet,[114] A. Bingul,[18c] C. Bini,[131a,131b] C. Biscarat,[176] U. Bitenc,[47] K. M. Black,[21] R. E. Blair,[5] J.-B. Blanchard,[114] G. Blanchot,[29] T. Blazek,[143a] C. Blocker,[22] J. Blocki,[38] A. Blondel,[48] W. Blum,[80] U. Blumenschein,[53] G. J. Bobbink,[104] V. B. Bobrovnikov,[106] S. S. Bocchetta,[78] A. Bocci,[44] C. R. Boddy,[117] M. Boehler,[41] J. Boek,[173] N. Boelaert,[35] S. Böser,[76] J. A. Bogaerts,[29] A. Bogdanchikov,[106] A. Bogouch,[89,a] C. Bohm,[145a] V. Boisvert,[75] T. Bold,[162,h] V. Boldea,[25a] N. M. Bolnet,[135] M. Bona,[74] V. G. Bondarenko,[95] M. Bondioli,[162] M. Boonekamp,[135] G. Boorman,[75] C. N. Booth,[138] S. Bordoni,[77] C. Borer,[16] A. Borisov,[127] G. Borissov,[70] I. Borjanovic,[12a] S. Borroni,[86] K. Bos,[104] D. Boscherini,[19a] M. Bosman,[11] H. Boterenbrood,[104] D. Botterill,[128] J. Bouchami,[92] J. Boudreau,[122] E. V. Bouhova-Thacker,[70] C. Bourdarios,[114] N. Bousson,[82] A. Boveia,[30] J. Boyd,[29] I. R. Boyko,[64] N. I. Bozhko,[127] I. Bozovic-Jelisavcic,[12b] J. Bracinik,[17] A. Braem,[29] P. Branchini,[133a] G. W. Brandenburg,[56] A. Brandt,[7] G. Brandt,[15] O. Brandt,[53] U. Bratzler,[155] B. Brau,[83] J. E. Brau,[113] H. M. Braun,[173] B. Brelier,[157] J. Bremer,[29] R. Brenner,[165] S. Bressler,[151] D. Breton,[114] D. Britton,[52] F. M. Brochu,[27] I. Brock,[20] R. Brock,[87] T. J. Brodbeck,[70] E. Brodet,[152] F. Broggi,[88a] C. Bromberg,[87] G. Brooijmans,[34] W. K. Brooks,[31b] G. Brown,[81] H. Brown,[7] P. A. Bruckman de Renstrom,[38] D. Bruncko,[143b] R. Bruneliere,[47] S. Brunet,[60] A. Bruni,[19a] G. Bruni,[19a] M. Bruschi,[19a] T. Buanes,[13] F. Bucci,[48] J. Buchanan,[117] N. J. Buchanan,[2] P. Buchholz,[140] R. M. Buckingham,[117]

A. G. Buckley,[45] S. I. Buda,[25a] I. A. Budagov,[64] B. Budick,[107] V. Büscher,[80] L. Bugge,[116] D. Buira-Clark,[117] O. Bulekov,[95] M. Bunse,[42] T. Buran,[116] H. Burckhart,[29] S. Burdin,[72] T. Burgess,[13] S. Burke,[128] E. Busato,[33] P. Bussey,[52] C. P. Buszello,[165] F. Butin,[29] B. Butler,[142] J. M. Butler,[21] C. M. Buttar,[52] J. M. Butterworth,[76] W. Buttinger,[27] T. Byatt,[76] S. Cabrera Urbán,[166] D. Caforio,[19a,19b] O. Cakir,[3a] P. Calafiura,[14] G. Calderini,[77] P. Calfayan,[97] R. Calkins,[105] L. P. Caloba,[23a] R. Caloi,[131a,131b] D. Calvet,[33] S. Calvet,[33] R. Camacho Toro,[33] P. Camarri,[132a,132b] M. Cambiaghi,[118a,118b] D. Cameron,[116] S. Campana,[29] M. Campanelli,[76] V. Canale,[101a,101b] F. Canelli,[30,i] A. Canepa,[158a] J. Cantero,[79] L. Capasso,[101a,101b] M. D. M. Capeans Garrido,[29] I. Caprini,[25a] M. Caprini,[25a] D. Capriotti,[98] M. Capua,[36a,36b] R. Caputo,[147] R. Cardarelli,[132a] T. Carli,[29] G. Carlino,[101a] L. Carminati,[88a,88b] B. Caron,[158a] S. Caron,[47] G. D. Carrillo Montoya,[171] A. A. Carter,[74] J. R. Carter,[27] J. Carvalho,[123a,j] D. Casadei,[107] M. P. Casado,[11] M. Cascella,[121a,121b] C. Caso,[49a,49b,a] A. M. Castaneda Hernandez,[171] E. Castaneda-Miranda,[171] V. Castillo Gimenez,[166] N. F. Castro,[123a] G. Cataldi,[71a] F. Cataneo,[29] A. Catinaccio,[29] J. R. Catmore,[70] A. Cattai,[29] G. Cattani,[132a,132b] S. Caughron,[87] D. Cauz,[163a,163c] P. Cavalleri,[77] D. Cavalli,[88a] M. Cavalli-Sforza,[11] V. Cavasinni,[121a,121b] F. Ceradini,[133a,133b] A. S. Cerqueira,[23a] A. Cerri,[29] L. Cerrito,[74] F. Cerutti,[46] S. A. Cetin,[18b] F. Cevenini,[101a,101b] A. Chafaq,[134a] D. Chakraborty,[105] K. Chan,[2] B. Chapleau,[84] J. D. Chapman,[27] J. W. Chapman,[86] E. Chareyre,[77] D. G. Charlton,[17] V. Chavda,[81] C. A. Chavez Barajas,[29] S. Cheatham,[84] S. Chekanov,[5] S. V. Chekulaev,[158a] G. A. Chelkov,[64] M. A. Chelstowska,[103] C. Chen,[63] H. Chen,[24] S. Chen,[32c] T. Chen,[32c] X. Chen,[171] S. Cheng,[32a] A. Cheplakov,[64] V. F. Chepurnov,[64] R. Cherkaoui El Moursli,[134e] V. Chernyatin,[24] E. Cheu,[6] S. L. Cheung,[157] L. Chevalier,[135] G. Chiefari,[101a,101b] L. Chikovani,[50a] J. T. Childers,[57a] A. Chilingarov,[70] G. Chiodini,[71a] M. V. Chizhov,[64] G. Choudalakis,[30] S. Chouridou,[136] I. A. Christidi,[76] A. Christov,[47] D. Chromek-Burckhart,[29] M. L. Chu,[150] J. Chudoba,[124] G. Ciapetti,[131a,131b] K. Ciba,[37] A. K. Ciftci,[3a] R. Ciftci,[3a] D. Cinca,[33] V. Cindro,[73] M. D. Ciobotaru,[162] C. Ciocca,[19a] A. Ciocio,[14] M. Cirilli,[86] M. Ciubancan,[25a] A. Clark,[48] P. J. Clark,[45] W. Cleland,[122] J. C. Clemens,[82] B. Clement,[54] C. Clement,[145a,145b] R. W. Clifft,[128] Y. Coadou,[82] M. Cobal,[163a,163c] A. Coccaro,[49a,49b] J. Cochran,[63] P. Coe,[117] J. G. Cogan,[142] J. Coggeshall,[164] E. Cogneras,[176] C. D. Cojocaru,[28] J. Colas,[4] A. P. Colijn,[104] C. Collard,[114] N. J. Collins,[17] C. Collins-Tooth,[52] J. Collot,[54] G. Colon,[83] P. Conde Muiño,[123a] E. Coniavitis,[117] M. C. Conidi,[11] M. Consonni,[103] V. Consorti,[47] S. Constantinescu,[25a] C. Conta,[118a,118b] F. Conventi,[101a,k] J. Cook,[29] M. Cooke,[14] B. D. Cooper,[76] A. M. Cooper-Sarkar,[117] N. J. Cooper-Smith,[75] K. Copic,[34] T. Cornelissen,[173] M. Corradi,[19a] F. Corriveau,[84,l] A. Cortes-Gonzalez,[164] G. Cortiana,[98] G. Costa,[88a] M. J. Costa,[166] D. Costanzo,[138] T. Costin,[30] D. Côté,[29] L. Courneyea,[168] G. Cowan,[75] C. Cowden,[27] B. E. Cox,[81] K. Cranmer,[107] F. Crescioli,[121a,121b] M. Cristinziani,[20] G. Crosetti,[36a,36b] R. Crupi,[71a,71b] S. Crépé-Renaudin,[54] C.-M. Cuciuc,[25a] C. Cuenca Almenar,[174] T. Cuhadar Donszelmann,[138] M. Curatolo,[46] C. J. Curtis,[17] P. Cwetanski,[60] H. Czirr,[140] Z. Czyczula,[174] S. D'Auria,[52] M. D'Onofrio,[72] A. D'Orazio,[131a,131b] P. V. M. Da Silva,[23a] C. Da Via,[81] W. Dabrowski,[37] T. Dai,[86] C. Dallapiccola,[83] M. Dam,[35] M. Dameri,[49a,49b] D. S. Damiani,[136] H. O. Danielsson,[29] D. Dannheim,[98] V. Dao,[48] G. Darbo,[49a] G. L. Darlea,[25b] C. Daum,[104] J. P. Dauvergne,[29] W. Davey,[85] T. Davidek,[125] N. Davidson,[85] R. Davidson,[70] E. Davies,[117,d] M. Davies,[92] A. R. Davison,[76] Y. Davygora,[57a] E. Dawe,[141] I. Dawson,[138] J. W. Dawson,[5,a] R. K. Daya,[39] K. De,[7] R. de Asmundis,[101a] S. De Castro,[19a,19b] P. E. De Castro Faria Salgado,[24] S. De Cecco,[77] J. de Graat,[97] N. De Groot,[103] P. de Jong,[104] C. De La Taille,[114] H. De la Torre,[79] B. De Lotto,[163a,163c] L. De Mora,[70] L. De Nooij,[104] D. De Pedis,[131a] A. De Salvo,[131a] U. De Sanctis,[163a,163c] A. De Santo,[148] J. B. De Vivie De Regie,[114] S. Dean,[76] R. Debbe,[24] D. V. Dedovich,[64] J. Degenhardt,[119] M. Dehchar,[117] C. Del Papa,[163a,163c] J. Del Peso,[79] T. Del Prete,[121a,121b] M. Deliyergiyev,[73] A. Dell'Acqua,[29] L. Dell'Asta,[88a,88b] M. Della Pietra,[101a,k] D. della Volpe,[101a,101b] M. Delmastro,[29] P. Delpierre,[82] N. Delruelle,[29] P. A. Delsart,[54] C. Deluca,[147] S. Demers,[174] M. Demichev,[64] B. Demirkoz,[11,m] J. Deng,[162] S. P. Denisov,[127] D. Derendarz,[38] J. E. Derkaoui,[134d] F. Derue,[77] P. Dervan,[72] K. Desch,[20] E. Devetak,[147] P. O. Deviveiros,[157] A. Dewhurst,[128] B. DeWilde,[147] S. Dhaliwal,[157] R. Dhullipudi,[24,n] A. Di Ciaccio,[132a,132b] L. Di Ciaccio,[4] A. Di Girolamo,[29] B. Di Girolamo,[29] S. Di Luise,[133a,133b] A. Di Mattia,[171] B. Di Micco,[29] R. Di Nardo,[132a,132b] A. Di Simone,[132a,132b] R. Di Sipio,[19a,19b] M. A. Diaz,[31a] F. Diblen,[18c] E. B. Diehl,[86] J. Dietrich,[41] T. A. Dietzsch,[57a] S. Diglio,[114] K. Dindar Yagci,[39] J. Dingfelder,[20] C. Dionisi,[131a,131b] P. Dita,[25a] S. Dita,[25a] F. Dittus,[29] F. Djama,[82] T. Djobava,[50b] M. A. B. do Vale,[23a] A. Do Valle Wemans,[123a] T. K. O. Doan,[4] M. Dobbs,[84] R. Dobinson,[29,a] D. Dobos,[29] E. Dobson,[29] M. Dobson,[162] J. Dodd,[34] C. Doglioni,[117] T. Doherty,[52] Y. Doi,[65,a] J. Dolejsi,[125] I. Dolenc,[73] Z. Dolezal,[125] B. A. Dolgoshein,[95,a] T. Dohmae,[154] M. Donadelli,[23d] M. Donega,[119] J. Donini,[54] J. Dopke,[29] A. Doria,[101a] A. Dos Anjos,[171] M. Dosil,[11] A. Dotti,[121a,121b] M. T. Dova,[69] J. D. Dowell,[17] A. D. Doxiadis,[104] A. T. Doyle,[52] Z. Drasal,[125] J. Drees,[173]

N. Dressnandt,[119] H. Drevermann,[29] C. Driouichi,[35] M. Dris,[9] J. Dubbert,[98] T. Dubbs,[136] S. Dube,[14] E. Duchovni,[170] G. Duckeck,[97] A. Dudarev,[29] F. Dudziak,[63] M. Dührssen,[29] I. P. Duerdoth,[81] L. Duflot,[114] M-A. Dufour,[84] M. Dunford,[29] H. Duran Yildiz,[3b] R. Duxfield,[138] M. Dwuznik,[37] F. Dydak,[29] M. Düren,[51] W. L. Ebenstein,[44] J. Ebke,[97] S. Eckert,[47] S. Eckweiler,[80] K. Edmonds,[80] C. A. Edwards,[75] N. C. Edwards,[52] W. Ehrenfeld,[41] T. Ehrich,[98] T. Eifert,[29] G. Eigen,[13] K. Einsweiler,[14] E. Eisenhandler,[74] T. Ekelof,[165] M. El Kacimi,[134c] M. Ellert,[165] S. Elles,[4] F. Ellinghaus,[80] K. Ellis,[74] N. Ellis,[29] J. Elmsheuser,[97] M. Elsing,[29] D. Emeliyanov,[128] R. Engelmann,[147] A. Engl,[97] B. Epp,[61] A. Eppig,[86] J. Erdmann,[53] A. Ereditato,[16] D. Eriksson,[145a] J. Ernst,[1] M. Ernst,[24] J. Ernwein,[135] D. Errede,[164] S. Errede,[164] E. Ertel,[80] M. Escalier,[114] C. Escobar,[122] X. Espinal Curull,[11] B. Esposito,[46] F. Etienne,[82] A. I. Etienvre,[135] E. Etzion,[152] D. Evangelakou,[53] H. Evans,[60] L. Fabbri,[19a,19b] C. Fabre,[29] R. M. Fakhrutdinov,[127] S. Falciano,[131a] Y. Fang,[171] M. Fanti,[88a,88b] A. Farbin,[7] A. Farilla,[133a] J. Farley,[147] T. Farooque,[157] S. M. Farrington,[117] P. Farthouat,[29] P. Fassnacht,[29] D. Fassouliotis,[8] B. Fatholahzadeh,[157] A. Favareto,[88a,88b] L. Fayard,[114] S. Fazio,[36a,36b] R. Febbraro,[33] P. Federic,[143a] O. L. Fedin,[120] W. Fedorko,[87] M. Fehling-Kaschek,[47] L. Feligioni,[82] D. Fellmann,[5] C. U. Felzmann,[85] C. Feng,[32d] E. J. Feng,[30] A. B. Fenyuk,[127] J. Ferencei,[143b] J. Ferland,[92] W. Fernando,[108] S. Ferrag,[52] J. Ferrando,[52] V. Ferrara,[41] A. Ferrari,[165] P. Ferrari,[104] R. Ferrari,[118a] A. Ferrer,[166] M. L. Ferrer,[46] D. Ferrere,[48] C. Ferretti,[86] A. Ferretto Parodi,[49a,49b] M. Fiascaris,[30] F. Fiedler,[80] A. Filipčič,[73] A. Filippas,[9] F. Filthaut,[103] M. Fincke-Keeler,[168] M. C. N. Fiolhais,[123a,j] L. Fiorini,[166] A. Firan,[39] G. Fischer,[41] P. Fischer,[20] M. J. Fisher,[108] S. M. Fisher,[128] M. Flechl,[47] I. Fleck,[140] J. Fleckner,[80] P. Fleischmann,[172] S. Fleischmann,[173] T. Flick,[173] L. R. Flores Castillo,[171] M. J. Flowerdew,[98] M. Fokitis,[9] T. Fonseca Martin,[16] D. A. Forbush,[137] A. Formica,[135] A. Forti,[81] D. Fortin,[158a] J. M. Foster,[81] D. Fournier,[114] A. Foussat,[29] A. J. Fowler,[44] K. Fowler,[136] H. Fox,[70] P. Francavilla,[121a,121b] S. Franchino,[118a,118b] D. Francis,[29] T. Frank,[170] M. Franklin,[56] S. Franz,[29] M. Fraternali,[118a,118b] S. Fratina,[119] S. T. French,[27] F. Friedrich,[43] R. Froeschl,[29] D. Froidevaux,[29] J. A. Frost,[27] C. Fukunaga,[155] E. Fullana Torregrosa,[29] J. Fuster,[166] C. Gabaldon,[29] O. Gabizon,[170] T. Gadfort,[24] S. Gadomski,[48] G. Gagliardi,[49a,49b] P. Gagnon,[60] C. Galea,[97] E. J. Gallas,[117] M. V. Gallas,[29] V. Gallo,[16] B. J. Gallop,[128] P. Gallus,[124] E. Galyaev,[40] K. K. Gan,[108] Y. S. Gao,[142,g] V. A. Gapienko,[127] A. Gaponenko,[14] F. Garberson,[174] M. Garcia-Sciveres,[14] C. García,[166] J. E. García Navarro,[48] R. W. Gardner,[30] N. Garelli,[29] H. Garitaonandia,[104] V. Garonne,[29] J. Garvey,[17] C. Gatti,[46] G. Gaudio,[118a] O. Gaumer,[48] B. Gaur,[140] L. Gauthier,[135] I. L. Gavrilenko,[93] C. Gay,[167] G. Gaycken,[20] J-C. Gayde,[29] E. N. Gazis,[9] P. Ge,[32d] C. N. P. Gee,[128] D. A. A. Geerts,[104] Ch. Geich-Gimbel,[20] K. Gellerstedt,[145a,145b] C. Gemme,[49a] A. Gemmell,[52] M. H. Genest,[97] S. Gentile,[131a,131b] M. George,[53] S. George,[75] P. Gerlach,[173] A. Gershon,[152] C. Geweniger,[57a] H. Ghazlane,[134b] P. Ghez,[4] N. Ghodbane,[33] B. Giacobbe,[19a] S. Giagu,[131a,131b] V. Giakoumopoulou,[8] V. Giangiobbe,[121a,121b] F. Gianotti,[29] B. Gibbard,[24] A. Gibson,[157] S. M. Gibson,[29] L. M. Gilbert,[117] V. Gilewsky,[90] D. Gillberg,[28] A. R. Gillman,[128] D. M. Gingrich,[2,f] J. Ginzburg,[152] N. Giokaris,[8] M. P. Giordani,[163c] R. Giordano,[101a,101b] F. M. Giorgi,[15] P. Giovannini,[98] P. F. Giraud,[135] D. Giugni,[88a] M. Giunta,[92] P. Giusti,[19a] B. K. Gjelsten,[116] L. K. Gladilin,[96] C. Glasman,[79] J. Glatzer,[47] A. Glazov,[41] K. W. Glitza,[173] G. L. Glonti,[64] J. Godfrey,[141] J. Godlewski,[29] M. Goebel,[41] T. Göpfert,[43] C. Goeringer,[80] C. Gössling,[42] T. Göttfert,[98] S. Goldfarb,[86] T. Golling,[174] S. N. Golovnia,[127] A. Gomes,[123a,c] L. S. Gomez Fajardo,[41] R. Gonçalo,[75] J. Goncalves Pinto Firmino Da Costa,[41] L. Gonella,[20] A. Gonidec,[29] S. Gonzalez,[171] S. González de la Hoz,[166] M. L. Gonzalez Silva,[26] S. Gonzalez-Sevilla,[48] J. J. Goodson,[147] L. Goossens,[29] P. A. Gorbounov,[94] H. A. Gordon,[24] I. Gorelov,[102] G. Gorfine,[173] B. Gorini,[29] E. Gorini,[71a,71b] A. Gorišek,[73] E. Gornicki,[38] S. A. Gorokhov,[127] V. N. Goryachev,[127] B. Gosdzik,[41] M. Gosselink,[104] M. I. Gostkin,[64] I. Gough Eschrich,[162] M. Gouighri,[134a] D. Goujdami,[134c] M. P. Goulette,[48] A. G. Goussiou,[137] C. Goy,[4] I. Grabowska-Bold,[162,h] V. Grabski,[175] P. Grafström,[29] C. Grah,[173] K-J. Grahn,[41] F. Grancagnolo,[71a] S. Grancagnolo,[15] V. Grassi,[147] V. Gratchev,[120] N. Grau,[34] H. M. Gray,[29] J. A. Gray,[147] E. Graziani,[133a] O. G. Grebenyuk,[120] D. Greenfield,[128] T. Greenshaw,[72] Z. D. Greenwood,[24,n] K. Gregersen,[35] I. M. Gregor,[41] P. Grenier,[142] J. Griffiths,[137] N. Grigalashvili,[64] A. A. Grillo,[136] S. Grinstein,[11] Y. V. Grishkevich,[96] J.-F. Grivaz,[114] J. Grognuz,[29] M. Groh,[98] E. Gross,[170] J. Grosse-Knetter,[53] J. Groth-Jensen,[170] K. Grybel,[140] V. J. Guarino,[5] D. Guest,[174] C. Guicheney,[33] A. Guida,[71a,71b] T. Guillemin,[4] S. Guindon,[53] H. Guler,[84,o] J. Gunther,[124] B. Guo,[157] J. Guo,[34] A. Gupta,[30] Y. Gusakov,[64] V. N. Gushchin,[127] A. Gutierrez,[92] P. Gutierrez,[110] N. Guttman,[152] O. Gutzwiller,[171] C. Guyot,[135] C. Gwenlan,[117] C. B. Gwilliam,[72] A. Haas,[142] S. Haas,[29] C. Haber,[14] R. Hackenburg,[24] H. K. Hadavand,[39] D. R. Hadley,[17] P. Haefner,[98] F. Hahn,[29] S. Haider,[29] Z. Hajduk,[38] H. Hakobyan,[175] J. Haller,[53] K. Hamacher,[173] P. Hamal,[112] A. Hamilton,[48] S. Hamilton,[160] H. Han,[32a] L. Han,[32b] K. Hanagaki,[115] M. Hance,[119] C. Handel,[80] P. Hanke,[57a] J. R. Hansen,[35] J. B. Hansen,[35] J. D. Hansen,[35] P. H. Hansen,[35] P. Hansson,[142] K. Hara,[159]

G. A. Hare,[136] T. Harenberg,[173] S. Harkusha,[89] D. Harper,[86] R. D. Harrington,[45] O. M. Harris,[137] K. Harrison,[17] J. Hartert,[47] F. Hartjes,[104] T. Haruyama,[65] A. Harvey,[55] S. Hasegawa,[100] Y. Hasegawa,[139] S. Hassani,[135] M. Hatch,[29] D. Hauff,[98] S. Haug,[16] M. Hauschild,[29] R. Hauser,[87] M. Havranek,[20] B. M. Hawes,[117] C. M. Hawkes,[17] R. J. Hawkings,[29] D. Hawkins,[162] T. Hayakawa,[66] D. Hayden,[75] H. S. Hayward,[72] S. J. Haywood,[128] E. Hazen,[21] M. He,[32d] S. J. Head,[17] V. Hedberg,[78] L. Heelan,[7] S. Heim,[87] B. Heinemann,[14] S. Heisterkamp,[35] L. Helary,[4] S. Hellman,[145a,145b] D. Hellmich,[20] C. Helsens,[11] R. C. W. Henderson,[70] M. Henke,[57a] A. Henrichs,[53] A. M. Henriques Correia,[29] S. Henrot-Versille,[114] F. Henry-Couannier,[82] C. Hensel,[53] T. Henß,[173] C. M. Hernandez,[7] Y. Hernández Jiménez,[166] R. Herrberg,[15] A. D. Hershenhorn,[151] G. Herten,[47] R. Hertenberger,[97] L. Hervas,[29] N. P. Hessey,[104] A. Hidvegi,[145a] E. Higón-Rodriguez,[166] D. Hill,[5,a] J. C. Hill,[27] N. Hill,[5] K. H. Hiller,[41] S. Hillert,[20] S. J. Hillier,[17] I. Hinchliffe,[14] E. Hines,[119] M. Hirose,[115] F. Hirsch,[42] D. Hirschbuehl,[173] J. Hobbs,[147] N. Hod,[152] M. C. Hodgkinson,[138] P. Hodgson,[138] A. Hoecker,[29] M. R. Hoeferkamp,[102] J. Hoffman,[39] D. Hoffmann,[82] M. Hohlfeld,[80] M. Holder,[140] S. O. Holmgren,[145a] T. Holy,[126] J. L. Holzbauer,[87] Y. Homma,[66] T. M. Hong,[119] L. Hooft van Huysduynen,[107] T. Horazdovsky,[126] C. Horn,[142] S. Horner,[47] K. Horton,[117] J-Y. Hostachy,[54] S. Hou,[150] M. A. Houlden,[72] A. Hoummada,[134a] J. Howarth,[81] D. F. Howell,[117] I. Hristova,[15] J. Hrivnac,[114] I. Hruska,[124] T. Hryn'ova,[4] P. J. Hsu,[174] S.-C. Hsu,[14] G. S. Huang,[110] Z. Hubacek,[126] F. Hubaut,[82] F. Huegging,[20] T. B. Huffman,[117] E. W. Hughes,[34] G. Hughes,[70] R. E. Hughes-Jones,[81] M. Huhtinen,[29] P. Hurst,[56] M. Hurwitz,[14] U. Husemann,[41] N. Huseynov,[64,p] J. Huston,[87] J. Huth,[56] G. Iacobucci,[48] G. Iakovidis,[9] M. Ibbotson,[81] I. Ibragimov,[140] R. Ichimiya,[66] L. Iconomidou-Fayard,[114] J. Idarraga,[114] M. Idzik,[37] P. Iengo,[101a,101b] O. Igonkina,[104] Y. Ikegami,[65] M. Ikeno,[65] Y. Ilchenko,[39] D. Iliadis,[153] D. Imbault,[77] M. Imhaeuser,[173] M. Imori,[154] T. Ince,[20] J. Inigo-Golfin,[29] P. Ioannou,[8] M. Iodice,[133a] G. Ionescu,[4] A. Irles Quiles,[166] K. Ishii,[65] A. Ishikawa,[66] M. Ishino,[67] R. Ishmukhametov,[39] C. Issever,[117] S. Istin,[18a] A. V. Ivashin,[127] W. Iwanski,[38] H. Iwasaki,[65] J. M. Izen,[40] V. Izzo,[101a] B. Jackson,[119] J. N. Jackson,[72] P. Jackson,[142] M. R. Jaekel,[29] V. Jain,[60] K. Jakobs,[47] S. Jakobsen,[35] J. Jakubek,[126] D. K. Jana,[110] E. Jankowski,[157] E. Jansen,[76] A. Jantsch,[98] M. Janus,[20] G. Jarlskog,[78] L. Jeanty,[56] K. Jelen,[37] I. Jen-La Plante,[30] P. Jenni,[29] A. Jeremie,[4] P. Ježˇ,[35] S. Jézéquel,[4] M. K. Jha,[19a] H. Ji,[171] W. Ji,[80] J. Jia,[147] Y. Jiang,[32b] M. Jimenez Belenguer,[41] G. Jin,[32b] S. Jin,[32a] O. Jinnouchi,[156] M. D. Joergensen,[35] D. Joffe,[39] L. G. Johansen,[13] M. Johansen,[145a,145b] K. E. Johansson,[145a] P. Johansson,[138] S. Johnert,[41] K. A. Johns,[6] K. Jon-And,[145a,145b] G. Jones,[81] R. W. L. Jones,[70] T. W. Jones,[76] T. J. Jones,[72] O. Jonsson,[29] C. Joram,[29] P. M. Jorge,[123a,c] J. Joseph,[14] T. Jovin,[12b] X. Ju,[129] V. Juranek,[124] P. Jussel,[61] A. Juste Rozas,[11] V. V. Kabachenko,[127] S. Kabana,[16] M. Kaci,[166] A. Kaczmarska,[38] P. Kadlecik,[35] M. Kado,[114] H. Kagan,[108] M. Kagan,[56] S. Kaiser,[98] E. Kajomovitz,[151] S. Kalinin,[173] L. V. Kalinovskaya,[64] S. Kama,[39] N. Kanaya,[154] M. Kaneda,[29] T. Kanno,[156] V. A. Kantserov,[95] J. Kanzaki,[65] B. Kaplan,[174] A. Kapliy,[30] J. Kaplon,[29] D. Kar,[43] M. Karagoz,[117] M. Karnevskiy,[41] K. Karr,[5] V. Kartvelishvili,[70] A. N. Karyukhin,[127] L. Kashif,[171] A. Kasmi,[39] R. D. Kass,[108] A. Kastanas,[13] M. Kataoka,[4] Y. Kataoka,[154] E. Katsoufis,[9] J. Katzy,[41] V. Kaushik,[6] K. Kawagoe,[66] T. Kawamoto,[154] G. Kawamura,[80] M. S. Kayl,[104] V. A. Kazanin,[106] M. Y. Kazarinov,[64] J. R. Keates,[81] R. Keeler,[168] R. Kehoe,[39] M. Keil,[53] G. D. Kekelidze,[64] M. Kelly,[81] J. Kennedy,[97] C. J. Kenney,[142] M. Kenyon,[52] O. Kepka,[124] N. Kerschen,[29] B. P. Kerševan,[73] S. Kersten,[173] K. Kessoku,[154] C. Ketterer,[47] J. Keung,[157] M. Khakzad,[28] F. Khalil-zada,[10] H. Khandanyan,[164] A. Khanov,[111] D. Kharchenko,[64] A. Khodinov,[95] A. G. Kholodenko,[127] A. Khomich,[57a] T. J. Khoo,[27] G. Khoriauli,[20] A. Khoroshilov,[173] N. Khovanskiy,[64] V. Khovanskiy,[94] E. Khramov,[64] J. Khubua,[50b] H. Kim,[7] M. S. Kim,[2] P. C. Kim,[142] S. H. Kim,[159] N. Kimura,[169] O. Kind,[15] B. T. King,[72] M. King,[66] R. S. B. King,[117] J. Kirk,[128] L. E. Kirsch,[22] A. E. Kiryunin,[98] T. Kishimoto,[66] D. Kisielewska,[37] T. Kittelmann,[122] A. M. Kiver,[127] E. Kladiva,[143b] J. Klaiber-Lodewigs,[42] M. Klein,[72] U. Klein,[72] K. Kleinknecht,[80] M. Klemetti,[84] A. Klier,[170] A. Klimentov,[24] R. Klingenberg,[42] E. B. Klinkby,[35] T. Klioutchnikova,[29] P. F. Klok,[103] S. Klous,[104] E.-E. Kluge,[57a] T. Kluge,[72] P. Kluit,[104] S. Kluth,[98] N. S. Knecht,[157] E. Kneringer,[61] J. Knobloch,[29] E.B.F.G. Knoops,[82] A. Knue,[53] B. R. Ko,[44] T. Kobayashi,[154] M. Kobel,[43] M. Kocian,[142] A. Kocnar,[112] P. Kodys,[125] K. Köneke,[29] A. C. König,[103] S. Koenig,[80] L. Köpke,[80] F. Koetsveld,[103] P. Koevesarki,[20] T. Koffas,[28] E. Koffeman,[104] F. Kohn,[53] Z. Kohout,[126] T. Kohriki,[65] T. Koi,[142] T. Kokott,[20] G. M. Kolachev,[106] H. Kolanoski,[15] V. Kolesnikov,[64] I. Koletsou,[88a] J. Koll,[87] D. Kollar,[29] M. Kollefrath,[47] S. D. Kolya,[81] A. A. Komar,[93] Y. Komori,[154] T. Kondo,[65] T. Kono,[41,q] A. I. Kononov,[47] R. Konoplich,[107,r] N. Konstantinidis,[76] A. Kootz,[173] S. Koperny,[37] S. V. Kopikov,[127] K. Korcyl,[38] K. Kordas,[153] V. Koreshev,[127] A. Korn,[117] A. Korol,[106] I. Korolkov,[11] E. V. Korolkova,[138] V. A. Korotkov,[127] O. Kortner,[98] S. Kortner,[98] V. V. Kostyukhin,[20] M. J. Kotamäki,[29] S. Kotov,[98] V. M. Kotov,[64] A. Kotwal,[44] C. Kourkoumelis,[8] V. Kouskoura,[153] A. Koutsman,[104] R. Kowalewski,[168] T. Z. Kowalski,[37] W. Kozanecki,[135] A. S. Kozhin,[127]

V. Kral,[126] V. A. Kramarenko,[96] G. Kramberger,[73] M. W. Krasny,[77] A. Krasznahorkay,[107] J. Kraus,[87] A. Kreisel,[152] F. Krejci,[126] J. Kretzschmar,[72] N. Krieger,[53] P. Krieger,[157] K. Kroeninger,[53] H. Kroha,[98] J. Kroll,[119] J. Kroseberg,[20] J. Krstic,[12a] U. Kruchonak,[64] H. Krüger,[20] T. Kruker,[16] Z. V. Krumshteyn,[64] A. Kruth,[20] T. Kubota,[85] S. Kuehn,[47] A. Kugel,[57c] T. Kuhl,[41] D. Kuhn,[61] V. Kukhtin,[64] Y. Kulchitsky,[89] S. Kuleshov,[31b] C. Kummer,[97] M. Kuna,[77] N. Kundu,[117] J. Kunkle,[119] A. Kupco,[124] H. Kurashige,[66] M. Kurata,[159] Y. A. Kurochkin,[89] V. Kus,[124] W. Kuykendall,[137] M. Kuze,[156] P. Kuzhir,[90] J. Kvita,[29] R. Kwee,[15] A. La Rosa,[171] L. La Rotonda,[36a,36b] L. Labarga,[79] J. Labbe,[4] S. Lablak,[134a] C. Lacasta,[166] F. Lacava,[131a,131b] H. Lacker,[15] D. Lacour,[77] V. R. Lacuesta,[166] E. Ladygin,[64] R. Lafaye,[4] B. Laforge,[77] T. Lagouri,[79] S. Lai,[47] E. Laisne,[54] M. Lamanna,[29] C. L. Lampen,[6] W. Lampl,[6] E. Lancon,[135] U. Landgraf,[47] M. P. J. Landon,[74] H. Landsman,[151] J. L. Lane,[81] C. Lange,[41] A. J. Lankford,[162] F. Lanni,[24] K. Lantzsch,[173] S. Laplace,[77] C. Lapoire,[20] J. F. Laporte,[135] T. Lari,[88a] A. V. Larionov,[127] A. Larner,[117] C. Lasseur,[29] M. Lassnig,[29] P. Laurelli,[46] A. Lavorato,[117] W. Lavrijsen,[14] P. Laycock,[72] A. B. Lazarev,[64] O. Le Dortz,[77] E. Le Guirriec,[82] C. Le Maner,[157] E. Le Menedeu,[135] C. Lebel,[92] T. LeCompte,[5] F. Ledroit-Guillon,[54] H. Lee,[104] J. S. H. Lee,[149] S. C. Lee,[150] L. Lee,[174] M. Lefebvre,[168] M. Legendre,[135] A. Leger,[48] B. C. LeGeyt,[119] F. Legger,[97] C. Leggett,[14] M. Lehmacher,[20] G. Lehmann Miotto,[29] X. Lei,[6] M. A. L. Leite,[23d] R. Leitner,[125] D. Lellouch,[170] M. Leltchouk,[34] B. Lemmer,[53] V. Lendermann,[57a] K. J. C. Leney,[144b] T. Lenz,[104] G. Lenzen,[173] B. Lenzi,[29] K. Leonhardt,[43] S. Leontsinis,[9] C. Leroy,[92] J-R. Lessard,[168] J. Lesser,[145a] C. G. Lester,[27] A. Leung Fook Cheong,[171] J. Levêque,[4] D. Levin,[86] L. J. Levinson,[170] M. S. Levitski,[127] M. Lewandowska,[21] A. Lewis,[117] G. H. Lewis,[107] A. M. Leyko,[20] M. Leyton,[15] B. Li,[82] H. Li,[171] S. Li,[32b,e] X. Li,[86] Z. Liang,[39] Z. Liang,[117,s] H. Liao,[33] B. Liberti,[132a] P. Lichard,[29] M. Lichtnecker,[97] K. Lie,[164] W. Liebig,[13] R. Lifshitz,[151] J. N. Lilley,[17] C. Limbach,[20] A. Limosani,[85] M. Limper,[62] S. C. Lin,[150,t] F. Linde,[104] J. T. Linnemann,[87] E. Lipeles,[119] L. Lipinsky,[124] A. Lipniacka,[13] T. M. Liss,[164] D. Lissauer,[24] A. Lister,[48] A. M. Litke,[136] C. Liu,[28] D. Liu,[150,u] H. Liu,[86] J. B. Liu,[86] M. Liu,[32b] S. Liu,[2] Y. Liu,[32b] M. Livan,[118a,118b] S. S. A. Livermore,[117] A. Lleres,[54] J. Llorente Merino,[79] S. L. Lloyd,[74] E. Lobodzinska,[41] P. Loch,[6] W. S. Lockman,[136] T. Loddenkoetter,[20] F. K. Loebinger,[81] A. Loginov,[174] C. W. Loh,[167] T. Lohse,[15] K. Lohwasser,[47] M. Lokajicek,[124] J. Loken,[117] V. P. Lombardo,[4] R. E. Long,[70] L. Lopes,[123a,c] D. Lopez Mateos,[56] M. Losada,[161] P. Loscutoff,[14] F. Lo Sterzo,[131a,131b] M. J. Losty,[158a] X. Lou,[40] A. Lounis,[114] K. F. Loureiro,[161] J. Love,[21] P. A. Love,[70] A. J. Lowe,[142,g] F. Lu,[32a] H. J. Lubatti,[137] C. Luci,[131a,131b] A. Lucotte,[54] A. Ludwig,[43] D. Ludwig,[41] I. Ludwig,[47] J. Ludwig,[47] F. Luehring,[60] G. Luijckx,[104] D. Lumb,[47] L. Luminari,[131a] E. Lund,[116] B. Lund-Jensen,[146] B. Lundberg,[78] J. Lundberg,[145a,145b] J. Lundquist,[35] M. Lungwitz,[80] A. Lupi,[121a,121b] G. Lutz,[98] D. Lynn,[24] J. Lys,[14] E. Lytken,[78] H. Ma,[24] L. L. Ma,[171] J. A. Macana Goia,[92] G. Maccarrone,[46] A. Macchiolo,[98] B. Maček,[73] J. Machado Miguens,[123a] R. Mackeprang,[35] R. J. Madaras,[14] W. F. Mader,[43] R. Maenner,[57c] T. Maeno,[24] P. Mättig,[173] S. Mättig,[41] L. Magnoni,[29] E. Magradze,[53] Y. Mahalalel,[152] K. Mahboubi,[47] G. Mahout,[17] C. Maiani,[131a,131b] C. Maidantchik,[23a] A. Maio,[123a,c] S. Majewski,[24] Y. Makida,[65] N. Makovec,[114] P. Mal,[6] Pa. Malecki,[38] P. Malecki,[38] V. P. Maleev,[120] F. Malek,[54] U. Mallik,[62] D. Malon,[5] C. Malone,[142] S. Maltezos,[9] V. Malyshev,[106] S. Malyukov,[29] R. Mameghani,[97] J. Mamuzic,[12b] A. Manabe,[65] L. Mandelli,[88a] I. Mandić,[73] R. Mandrysch,[15] J. Maneira,[123a] P. S. Mangeard,[87] I. D. Manjavidze,[64] A. Mann,[53] P. M. Manning,[136] A. Manousakis-Katsikakis,[8] B. Mansoulie,[135] A. Manz,[98] A. Mapelli,[29] L. Mapelli,[29] L. March,[79] J. F. Marchand,[29] F. Marchese,[132a,132b] G. Marchiori,[77] M. Marcisovsky,[124] A. Marin,[21,a] C. P. Marino,[60] F. Marroquim,[23a] R. Marshall,[81] Z. Marshall,[29] F. K. Martens,[157] S. Marti-Garcia,[166] A. J. Martin,[174] B. Martin,[29] B. Martin,[87] F. F. Martin,[119] J. P. Martin,[92] Ph. Martin,[54] T. A. Martin,[17] V. J. Martin,[45] B. Martin dit Latour,[48] S. Martin-Haugh,[148] M. Martinez,[11] V. Martinez Outschoorn,[56] A. C. Martyniuk,[81] M. Marx,[81] F. Marzano,[131a] A. Marzin,[110] L. Masetti,[80] T. Mashimo,[154] R. Mashinistov,[93] J. Masik,[81] A. L. Maslennikov,[106] I. Massa,[19a,19b] G. Massaro,[104] N. Massol,[4] P. Mastrandrea,[131a,131b] A. Mastroberardino,[36a,36b] T. Masubuchi,[154] M. Mathes,[20] P. Matricon,[114] H. Matsumoto,[154] H. Matsunaga,[154] T. Matsushita,[66] C. Mattravers,[117,d] J. M. Maugain,[29] S. J. Maxfield,[72] D. A. Maximov,[106] E. N. May,[5] A. Mayne,[138] R. Mazini,[150] M. Mazur,[20] M. Mazzanti,[88a] E. Mazzoni,[121a,121b] S. P. Mc Kee,[86] A. McCarn,[164] R. L. McCarthy,[147] T. G. McCarthy,[28] N. A. McCubbin,[128] K. W. McFarlane,[55] J. A. Mcfayden,[138] H. McGlone,[52] G. Mchedlidze,[50b] R. A. McLaren,[29] T. Mclaughlan,[17] S. J. McMahon,[128] R. A. McPherson,[168,l] A. Meade,[83] J. Mechnich,[104] M. Mechtel,[173] M. Medinnis,[41] R. Meera-Lebbai,[110] T. Meguro,[115] R. Mehdiyev,[92] S. Mehlhase,[35] A. Mehta,[72] K. Meier,[57a] J. Meinhardt,[47] B. Meirose,[78] C. Melachrinos,[30] B. R. Mellado Garcia,[171] L. Mendoza Navas,[161] Z. Meng,[150,u] A. Mengarelli,[19a,19b] S. Menke,[98] C. Menot,[29] E. Meoni,[11] K. M. Mercurio,[56] P. Mermod,[117] L. Merola,[101a,101b] C. Meroni,[88a] F. S. Merritt,[30] A. Messina,[29] J. Metcalfe,[102] A. S. Mete,[63] S. Meuser,[20] C. Meyer,[80] J-P. Meyer,[135] J. Meyer,[172]

J. Meyer,[53] T. C. Meyer,[29] W. T. Meyer,[63] J. Miao,[32d] S. Michal,[29] L. Micu,[25a] R. P. Middleton,[128] P. Miele,[29] S. Migas,[72] L. Mijović,[41] G. Mikenberg,[170] M. Mikestikova,[124] M. Mikuž,[73] D. W. Miller,[30] R. J. Miller,[87] W. J. Mills,[167] C. Mills,[56] A. Milov,[170] D. A. Milstead,[145a,145b] D. Milstein,[170] A. A. Minaenko,[127] M. Miñano,[166] I. A. Minashvili,[64] A. I. Mincer,[107] B. Mindur,[37] M. Mineev,[64] Y. Ming,[129] L. M. Mir,[11] G. Mirabelli,[131a] L. Miralles Verge,[11] A. Misiejuk,[75] J. Mitrevski,[136] G. Y. Mitrofanov,[127] V. A. Mitsou,[166] S. Mitsui,[65] P. S. Miyagawa,[138] K. Miyazaki,[66] J. U. Mjörnmark,[78] T. Moa,[145a,145b] P. Mockett,[137] S. Moed,[56] V. Moeller,[27] K. Mönig,[41] N. Möser,[20] S. Mohapatra,[147] W. Mohr,[47] S. Mohrdieck-Möck,[98] A. M. Moisseev,[127,a] R. Moles-Valls,[166] J. Molina-Perez,[29] J. Monk,[76] E. Monnier,[82] S. Montesano,[88a,88b] F. Monticelli,[69] S. Monzani,[19a,19b] R. W. Moore,[2] G. F. Moorhead,[85] C. Mora Herrera,[48] A. Moraes,[52] N. Morange,[135] J. Morel,[53] G. Morello,[36a,36b] D. Moreno,[80] M. Moreno Llácer,[166] P. Morettini,[49a] M. Morii,[56] J. Morin,[74] Y. Morita,[65] A. K. Morley,[29] G. Mornacchi,[29] S. V. Morozov,[95] J. D. Morris,[74] L. Morvaj,[100] H. G. Moser,[98] M. Mosidze,[50b] J. Moss,[108] R. Mount,[142] E. Mountricha,[135] S. V. Mouraviev,[93] E. J. W. Moyse,[83] M. Mudrinic,[12b] F. Mueller,[57a] J. Mueller,[122] K. Mueller,[20] T. A. Müller,[97] D. Muenstermann,[29] A. Muir,[167] Y. Munwes,[152] W. J. Murray,[128] I. Mussche,[104] E. Musto,[101a,101b] A. G. Myagkov,[127] M. Myska,[124] J. Nadal,[11] K. Nagai,[159] K. Nagano,[65] Y. Nagasaka,[59] A. M. Nairz,[29] Y. Nakahama,[29] K. Nakamura,[154] I. Nakano,[109] G. Nanava,[20] A. Napier,[160] M. Nash,[76,d] N. R. Nation,[21] T. Nattermann,[20] T. Naumann,[41] G. Navarro,[161] H. A. Neal,[86] E. Nebot,[79] P.Yu. Nechaeva,[93] A. Negri,[118a,118b] G. Negri,[29] S. Nektarijevic,[48] A. Nelson,[63] S. Nelson,[142] T. K. Nelson,[142] S. Nemecek,[124] P. Nemethy,[107] A. A. Nepomuceno,[23a] M. Nessi,[29,v] S. Y. Nesterov,[120] M. S. Neubauer,[164] A. Neusiedl,[80] R. M. Neves,[107] P. Nevski,[24] P. R. Newman,[17] V. Nguyen Thi Hong,[135] R. B. Nickerson,[117] R. Nicolaidou,[135] L. Nicolas,[138] B. Nicquevert,[29] F. Niedercorn,[114] J. Nielsen,[136] T. Niinikoski,[29] N. Nikiforou,[34] A. Nikiforov,[15] V. Nikolaenko,[127] K. Nikolaev,[64] I. Nikolic-Audit,[77] K. Nikolics,[48] K. Nikolopoulos,[24] H. Nilsen,[47] P. Nilsson,[7] Y. Ninomiya,[154] A. Nisati,[131a] T. Nishiyama,[66] R. Nisius,[98] L. Nodulman,[5] M. Nomachi,[115] I. Nomidis,[153] M. Nordberg,[29] B. Nordkvist,[145a,145b] P. R. Norton,[128] J. Novakova,[125] M. Nozaki,[65] M. Nožička,[41] L. Nozka,[112] I. M. Nugent,[158a] A.-E. Nuncio-Quiroz,[20] G. Nunes Hanninger,[85] T. Nunnemann,[97] E. Nurse,[76] T. Nyman,[29] B. J. O'Brien,[45] S. W. O'Neale,[17,a] D. C. O'Neil,[141] V. O'Shea,[52] F. G. Oakham,[28,f] H. Oberlack,[98] J. Ocariz,[77] A. Ochi,[66] S. Oda,[154] S. Odaka,[65] J. Odier,[82] H. Ogren,[60] A. Oh,[81] S. H. Oh,[44] C. C. Ohm,[145a,145b] T. Ohshima,[100] H. Ohshita,[139] T. K. Ohska,[65] T. Ohsugi,[58] S. Okada,[66] H. Okawa,[162] Y. Okumura,[100] T. Okuyama,[154] M. Olcese,[49a] A. G. Olchevski,[64] M. Oliveira,[123a,j] D. Oliveira Damazio,[24] E. Oliver Garcia,[166] D. Olivito,[119] A. Olszewski,[38] J. Olszowska,[38] C. Omachi,[66] A. Onofre,[123a,w] P. U. E. Onyisi,[30] C. J. Oram,[158a] M. J. Oreglia,[30] Y. Oren,[152] D. Orestano,[133a,133b] I. Orlov,[106] C. Oropeza Barrera,[52] R. S. Orr,[157] B. Osculati,[49a,49b] R. Ospanov,[119] C. Osuna,[11] G. Otero y Garzon,[26] J.P Ottersbach,[104] M. Ouchrif,[134d] F. Ould-Saada,[116] A. Ouraou,[135] Q. Ouyang,[32a] M. Owen,[81] S. Owen,[138] V. E. Ozcan,[18a] N. Ozturk,[7] A. Pacheco Pages,[11] C. Padilla Aranda,[11] S. Pagan Griso,[14] E. Paganis,[138] F. Paige,[24] K. Pajchel,[116] G. Palacino,[158b] C. P. Paleari,[6] S. Palestini,[29] D. Pallin,[33] A. Palma,[123a,c] J. D. Palmer,[17] Y. B. Pan,[171] E. Panagiotopoulou,[9] B. Panes,[31a] N. Panikashvili,[86] S. Panitkin,[24] D. Pantea,[25a] M. Panuskova,[124] V. Paolone,[122] A. Papadelis,[145a] Th.D. Papadopoulou,[9] A. Paramonov,[5] W. Park,[24,x] M. A. Parker,[27] F. Parodi,[49a,49b] J. A. Parsons,[34] U. Parzefall,[47] E. Pasqualucci,[131a] A. Passeri,[133a] F. Pastore,[133a,133b] Fr. Pastore,[75] G. Pásztor,[48,y] S. Pataraia,[173] N. Patel,[149] J. R. Pater,[81] S. Patricelli,[101a,101b] T. Pauly,[29] M. Pecsy,[143a] M. I. Pedraza Morales,[171] S. V. Peleganchuk,[106] H. Peng,[32b] R. Pengo,[29] A. Penson,[34] J. Penwell,[60] M. Perantoni,[23a] K. Perez,[34,z] T. Perez Cavalcanti,[41] E. Perez Codina,[11] M. T. Pérez García-Estañ,[166] V. Perez Reale,[34] L. Perini,[88a,88b] H. Pernegger,[29] R. Perrino,[71a] P. Perrodo,[4] S. Persembe,[3a] V. D. Peshekhonov,[64] B. A. Petersen,[29] J. Petersen,[29] T. C. Petersen,[35] E. Petit,[82] A. Petridis,[153] C. Petridou,[153] E. Petrolo,[131a] F. Petrucci,[133a,133b] D. Petschull,[41] M. Petteni,[141] R. Pezoa,[31b] A. Phan,[85] A. W. Phillips,[27] P. W. Phillips,[128] G. Piacquadio,[29] E. Piccaro,[74] M. Piccinini,[19a,19b] A. Pickford,[52] S. M. Piec,[41] R. Piegaia,[26] J. E. Pilcher,[30] A. D. Pilkington,[81] J. Pina,[123a,c] M. Pinamonti,[163a,163c] A. Pinder,[117] J. L. Pinfold,[2] J. Ping,[32c] B. Pinto,[123a,c] O. Pirotte,[29] C. Pizio,[88a,88b] R. Placakyte,[41] M. Plamondon,[168] W. G. Plano,[81] M.-A. Pleier,[24] A. V. Pleskach,[127] A. Poblaguev,[24] S. Poddar,[57a] F. Podlyski,[33] R. Poettgen,[80] L. Poggioli,[114] T. Poghosyan,[20] M. Pohl,[48] F. Polci,[54] G. Polesello,[118a] A. Policicchio,[137] A. Polini,[19a] J. Poll,[74] V. Polychronakos,[24] D. M. Pomarede,[135] D. Pomeroy,[22] K. Pommès,[29] L. Pontecorvo,[131a] B. G. Pope,[87] G. A. Popeneciu,[25a] D. S. Popovic,[12a] A. Poppleton,[29] X. Portell Bueso,[29] R. Porter,[162] C. Posch,[21] G. E. Pospelov,[98] S. Pospisil,[126] I. N. Potrap,[98] C. J. Potter,[148] C. T. Potter,[113] G. Poulard,[29] J. Poveda,[171] R. Prabhu,[76] P. Pralavorio,[82] S. Prasad,[56] R. Pravahan,[7] S. Prell,[63] K. Pretzl,[16] L. Pribyl,[29] D. Price,[60] L. E. Price,[5] M. J. Price,[29] P. M. Prichard,[72] D. Prieur,[122] M. Primavera,[71a] K. Prokofiev,[107] F. Prokoshin,[31b]

S. Protopopescu,[24] J. Proudfoot,[5] X. Prudent,[43] H. Przysiezniak,[4] S. Psoroulas,[20] E. Ptacek,[113] E. Pueschel,[83] J. Purdham,[86] M. Purohit,[24,x] P. Puzo,[114] Y. Pylypchenko,[116] J. Qian,[86] Z. Qian,[82] Z. Qin,[41] A. Quadt,[53] D. R. Quarrie,[14] W. B. Quayle,[171] F. Quinonez,[31a] M. Raas,[103] V. Radescu,[57b] B. Radics,[20] T. Rador,[18a] F. Ragusa,[88a,88b] G. Rahal,[176] A. M. Rahimi,[108] D. Rahm,[24] S. Rajagopalan,[24] M. Rammensee,[47] M. Rammes,[140] M. Ramstedt,[145a,145b] A. S. Randle-Conde,[39] K. Randrianarivony,[28] P. N. Ratoff,[70] F. Rauscher,[97] E. Rauter,[98] M. Raymond,[29] A. L. Read,[116] D. M. Rebuzzi,[118a,118b] A. Redelbach,[172] G. Redlinger,[24] R. Reece,[119] K. Reeves,[40] A. Reichold,[104] E. Reinherz-Aronis,[152] A. Reinsch,[113] I. Reisinger,[42] D. Reljic,[12a] C. Rembser,[29] Z. L. Ren,[150] A. Renaud,[114] P. Renkel,[39] M. Rescigno,[131a] S. Resconi,[88a] B. Resende,[135] P. Reznicek,[97] R. Rezvani,[157] A. Richards,[76] R. Richter,[98] E. Richter-Was,[4,aa] M. Ridel,[77] S. Rieke,[80] M. Rijpstra,[104] M. Rijssenbeek,[147] A. Rimoldi,[118a,118b] L. Rinaldi,[19a] R. R. Rios,[39] I. Riu,[11] G. Rivoltella,[88a,88b] F. Rizatdinova,[111] E. Rizvi,[74] S. H. Robertson,[84,l] A. Robichaud-Veronneau,[117] D. Robinson,[27] J. E. M. Robinson,[76] M. Robinson,[113] A. Robson,[52] J. G. Rocha de Lima,[105] C. Roda,[121a,121b] D. Roda Dos Santos,[29] S. Rodier,[79] D. Rodriguez,[161] A. Roe,[53] S. Roe,[29] O. Røhne,[116] V. Rojo,[1] S. Rolli,[160] A. Romaniouk,[95] V. M. Romanov,[64] G. Romeo,[26] L. Roos,[77] E. Ros,[166] S. Rosati,[131a,131b] K. Rosbach,[48] A. Rose,[148] M. Rose,[75] G. A. Rosenbaum,[157] E. I. Rosenberg,[63] P. L. Rosendahl,[13] O. Rosenthal,[140] L. Rosselet,[48] V. Rossetti,[11] E. Rossi,[131a,131b] L. P. Rossi,[49a] L. Rossi,[88a,88b] M. Rotaru,[25a] I. Roth,[170] J. Rothberg,[137] D. Rousseau,[114] C. R. Royon,[135] A. Rozanov,[82] Y. Rozen,[151] X. Ruan,[114] I. Rubinskiy,[41] B. Ruckert,[97] N. Ruckstuhl,[104] V. I. Rud,[96] C. Rudolph,[43] G. Rudolph,[61] F. Rühr,[6] F. Ruggieri,[133a,133b] A. Ruiz-Martinez,[63] E. Rulikowska-Zarebska,[37] V. Rumiantsev,[90,a] L. Rumyantsev,[64] K. Runge,[47] O. Runolfsson,[20] Z. Rurikova,[47] N. A. Rusakovich,[64] D. R. Rust,[60] J. P. Rutherfoord,[6] C. Ruwiedel,[14] P. Ruzicka,[124] Y. F. Ryabov,[120] V. Ryadovikov,[127] P. Ryan,[87] M. Rybar,[125] G. Rybkin,[114] N. C. Ryder,[117] S. Rzaeva,[10] A. F. Saavedra,[149] I. Sadeh,[152] H.F-W. Sadrozinski,[136] R. Sadykov,[64] F. Safai Tehrani,[131a,131b] H. Sakamoto,[154] G. Salamanna,[74] A. Salamon,[132a] M. Saleem,[110] D. Salihagic,[98] A. Salnikov,[142] J. Salt,[166] B. M. Salvachua Ferrando,[5] D. Salvatore,[36a,36b] F. Salvatore,[148] A. Salvucci,[103] A. Salzburger,[29] D. Sampsonidis,[153] B. H. Samset,[116] A. Sanchez,[101a,101b] H. Sandaker,[13] H. G. Sander,[80] M. P. Sanders,[97] M. Sandhoff,[173] T. Sandoval,[27] C. Sandoval,[161] R. Sandstroem,[98] S. Sandvoss,[173] D. P. C. Sankey,[128] A. Sansoni,[46] C. Santamarina Rios,[84] C. Santoni,[33] R. Santonico,[132a,132b] H. Santos,[123a] A. Sapronov,[64] J. G. Saraiva,[123a,c] T. Sarangi,[171] E. Sarkisyan-Grinbaum,[7] F. Sarri,[121a,121b] G. Sartisohn,[173] O. Sasaki,[65] T. Sasaki,[65] N. Sasao,[67] I. Satsounkevitch,[89] G. Sauvage,[4] E. Sauvan,[4] J. B. Sauvan,[114] P. Savard,[157,f] V. Savinov,[122] D. O. Savu,[29] P. Savva,[9] L. Sawyer,[24,n] D. H. Saxon,[52] L. P. Says,[33] C. Sbarra,[19a] A. Sbrizzi,[19a,19b] O. Scallon,[92] D. A. Scannicchio,[162] J. Schaarschmidt,[114] P. Schacht,[98] U. Schäfer,[80] S. Schaepe,[20] S. Schaetzel,[57b] A. C. Schaffer,[114] D. Schaile,[97] R. D. Schamberger,[147] A. G. Schamov,[106] V. Scharf,[57a] V. A. Schegelsky,[120] D. Scheirich,[86] M. Schernau,[162] M. I. Scherzer,[14] C. Schiavi,[49a,49b] J. Schieck,[97] M. Schioppa,[36a,36b] S. Schlenker,[29] J. L. Schlereth,[5] E. Schmidt,[47] K. Schmieden,[20] C. Schmitt,[80] S. Schmitt,[57b] M. Schmitz,[20] A. Schöning,[57b] M. Schott,[29] D. Schouten,[158a] J. Schovancova,[124] M. Schram,[84] C. Schroeder,[80] N. Schroer,[57c] S. Schuh,[29] G. Schuler,[29] J. Schultes,[173] H.-C. Schultz-Coulon,[57a] H. Schulz,[15] J. W. Schumacher,[20] M. Schumacher,[47] B. A. Schumm,[136] Ph. Schune,[135] C. Schwanenberger,[81] A. Schwartzman,[142] Ph. Schwemling,[77] R. Schwienhorst,[87] R. Schwierz,[43] J. Schwindling,[135] T. Schwindt,[20] W. G. Scott,[128] J. Searcy,[113] E. Sedykh,[120] E. Segura,[11] S. C. Seidel,[102] A. Seiden,[136] F. Seifert,[43] J. M. Seixas,[23a] G. Sekhniaidze,[101a] D. M. Seliverstov,[120] B. Sellden,[145a] G. Sellers,[72] M. Seman,[143b] N. Semprini-Cesari,[19a,19b] C. Serfon,[97] L. Serin,[114] R. Seuster,[98] H. Severini,[110] M. E. Sevior,[85] A. Sfyrla,[29] E. Shabalina,[53] M. Shamim,[113] L. Y. Shan,[32a] J. T. Shank,[21] Q. T. Shao,[85] M. Shapiro,[14] P. B. Shatalov,[94] L. Shaver,[6] K. Shaw,[163a,163c] D. Sherman,[174] P. Sherwood,[76] A. Shibata,[107] H. Shichi,[100] S. Shimizu,[29] M. Shimojima,[99] T. Shin,[55] A. Shmeleva,[93] M. J. Shochet,[30] D. Short,[117] M. A. Shupe,[6] P. Sicho,[124] A. Sidoti,[131a,131b] A. Siebel,[173] F. Siegert,[47] Dj. Sijacki,[12a] O. Silbert,[170] J. Silva,[123a,c] Y. Silver,[152] D. Silverstein,[142] S. B. Silverstein,[145a] V. Simak,[126] O. Simard,[135] Lj. Simic,[12a] S. Simion,[114] B. Simmons,[76] M. Simonyan,[35] P. Sinervo,[157] N. B. Sinev,[113] V. Sipica,[140] G. Siragusa,[172] A. Sircar,[24] A. N. Sisakyan,[64] S.Yu. Sivoklokov,[96] J. Sjölin,[145a,145b] T. B. Sjursen,[13] L. A. Skinnari,[14] H. P. Skottowe,[56] K. Skovpen,[106] P. Skubic,[110] N. Skvorodnev,[22] M. Slater,[17] T. Slavicek,[126] K. Sliwa,[160] T. J. Sloan,[70] J. Sloper,[29] V. Smakhtin,[170] S.Yu. Smirnov,[95] L. N. Smirnova,[96] O. Smirnova,[78] B. C. Smith,[56] D. Smith,[142] K. M. Smith,[52] M. Smizanska,[70] K. Smolek,[126] A. A. Snesarev,[93] S. W. Snow,[81] J. Snow,[110] J. Snuverink,[104] S. Snyder,[24] M. Soares,[123a] R. Sobie,[168,l] J. Sodomka,[126] A. Soffer,[152] C. A. Solans,[166] M. Solar,[126] J. Solc,[126] E. Soldatov,[95] U. Soldevila,[166] E. Solfaroli Camillocci,[131a,131b] A. A. Solodkov,[127] O. V. Solovyanov,[127] J. Sondericker,[24] N. Soni,[2] V. Sopko,[126] B. Sopko,[126] M. Sorbi,[88a,88b] M. Sosebee,[7] A. Soukharev,[106] S. Spagnolo,[71a,71b] F. Spanò,[75] R. Spighi,[19a] G. Spigo,[29] F. Spila,[131a,131b]

E. Spiriti,[133a] R. Spiwoks,[29] M. Spousta,[125] T. Spreitzer,[157] B. Spurlock,[7] R. D. St. Denis,[52] T. Stahl,[140] J. Stahlman,[119] R. Stamen,[57a] E. Stanecka,[29] R. W. Stanek,[5] C. Stanescu,[133a] S. Stapnes,[116] E. A. Starchenko,[127] J. Stark,[54] P. Staroba,[124] P. Starovoitov,[90] A. Staude,[97] P. Stavina,[143a] G. Stavropoulos,[14] G. Steele,[52] P. Steinbach,[43] P. Steinberg,[24] I. Stekl,[126] B. Stelzer,[141] H. J. Stelzer,[87] O. Stelzer-Chilton,[158a] H. Stenzel,[51] K. Stevenson,[74] G. A. Stewart,[29] J. A. Stillings,[20] T. Stockmanns,[20] M. C. Stockton,[29] K. Stoerig,[47] G. Stoicea,[25a] S. Stonjek,[98] P. Strachota,[125] A. R. Stradling,[7] A. Straessner,[43] J. Strandberg,[146] S. Strandberg,[145a,145b] A. Strandlie,[116] M. Strang,[108] E. Strauss,[142] M. Strauss,[110] P. Strizenec,[143b] R. Ströhmer,[172] D. M. Strom,[113] J. A. Strong,[75,a] R. Stroynowski,[39] J. Strube,[128] B. Stugu,[13] I. Stumer,[24,a] J. Stupak,[147] P. Sturm,[173] D. A. Soh,[150,s] D. Su,[142] HS. Subramania,[2] A. Succurro,[11] Y. Sugaya,[115] T. Sugimoto,[100] C. Suhr,[105] K. Suita,[66] M. Suk,[125] V. V. Sulin,[93] S. Sultansoy,[3d] T. Sumida,[29] X. Sun,[54] J. E. Sundermann,[47] K. Suruliz,[138] S. Sushkov,[11] G. Susinno,[36a,36b] M. R. Sutton,[148] Y. Suzuki,[65] Y. Suzuki,[66] M. Svatos,[124] Yu.M. Sviridov,[127] S. Swedish,[167] I. Sykora,[143a] T. Sykora,[125] B. Szeless,[29] J. Sánchez,[166] D. Ta,[104] K. Tackmann,[41] A. Taffard,[162] R. Tafirout,[158a] N. Taiblum,[152] Y. Takahashi,[100] H. Takai,[24] R. Takashima,[68] H. Takeda,[66] T. Takeshita,[139] M. Talby,[82] A. Talyshev,[106] M. C. Tamsett,[24] J. Tanaka,[154] R. Tanaka,[114] S. Tanaka,[130] S. Tanaka,[65] Y. Tanaka,[99] K. Tani,[66] N. Tannoury,[82] G. P. Tappern,[29] S. Tapprogge,[80] D. Tardif,[157] S. Tarem,[151] F. Tarrade,[28] G. F. Tartarelli,[88a] P. Tas,[125] M. Tasevsky,[124] E. Tassi,[36a,36b] M. Tatarkhanov,[14] Y. Tayalati,[134d] C. Taylor,[76] F. E. Taylor,[91] G. N. Taylor,[85] W. Taylor,[158b] M. Teinturier,[114] M. Teixeira Dias Castanheira,[74] P. Teixeira-Dias,[75] K. K. Temming,[47] H. Ten Kate,[29] P. K. Teng,[150] S. Terada,[65] K. Terashi,[154] J. Terron,[79] M. Terwort,[41,q] M. Testa,[46] R. J. Teuscher,[157,l] J. Thadome,[173] J. Therhaag,[20] T. Theveneaux-Pelzer,[77] M. Thioye,[174] S. Thoma,[47] J. P. Thomas,[17] E. N. Thompson,[83] P. D. Thompson,[17] P. D. Thompson,[157] A. S. Thompson,[52] E. Thomson,[119] M. Thomson,[27] R. P. Thun,[86] F. Tian,[34] T. Tic,[124] V. O. Tikhomirov,[93] Y. A. Tikhonov,[106] C.J.W.P. Timmermans,[103] P. Tipton,[174] F. J. Tique Aires Viegas,[29] S. Tisserant,[82] J. Tobias,[47] B. Toczek,[37] T. Todorov,[4] S. Todorova-Nova,[160] B. Toggerson,[162] J. Tojo,[65] S. Tokár,[143a] K. Tokunaga,[66] K. Tokushuku,[65] K. Tollefson,[87] M. Tomoto,[100] L. Tompkins,[14] K. Toms,[102] G. Tong,[32a] A. Tonoyan,[13] C. Topfel,[16] N. D. Topilin,[64] I. Torchiani,[29] E. Torrence,[113] H. Torres,[77] E. Torró Pastor,[166] J. Toth,[82,y] F. Touchard,[82] D. R. Tovey,[138] D. Traynor,[74] T. Trefzger,[172] L. Tremblet,[29] A. Tricoli,[29] I. M. Trigger,[158a] S. Trincaz-Duvoid,[77] T. N. Trinh,[77] M. F. Tripiana,[69] W. Trischuk,[157] A. Trivedi,[24,x] B. Trocmé,[54] C. Troncon,[88a] M. Trottier-McDonald,[141] A. Trzupek,[38] C. Tsarouchas,[29] J.C-L. Tseng,[117] M. Tsiakiris,[104] P. V. Tsiareshka,[89] D. Tsionou,[4] G. Tsipolitis,[9] V. Tsiskaridze,[47] E. G. Tskhadadze,[50a] I. I. Tsukerman,[94] V. Tsulaia,[14] J.-W. Tsung,[20] S. Tsuno,[65] D. Tsybychev,[147] A. Tua,[138] J. M. Tuggle,[30] M. Turala,[38] D. Turecek,[126] I. Turk Cakir,[3e] E. Turlay,[104] R. Turra,[88a,88b] P. M. Tuts,[34] A. Tykhonov,[73] M. Tylmad,[145a,145b] M. Tyndel,[128] H. Tyrvainen,[29] G. Tzanakos,[8] K. Uchida,[20] I. Ueda,[154] R. Ueno,[28] M. Ugland,[13] M. Uhlenbrock,[20] M. Uhrmacher,[53] F. Ukegawa,[159] G. Unal,[29] D. G. Underwood,[5] A. Undrus,[24] G. Unel,[162] Y. Unno,[65] D. Urbaniec,[34] E. Urkovsky,[152] P. Urrejola,[31a] G. Usai,[7] M. Uslenghi,[118a,118b] L. Vacavant,[82] V. Vacek,[126] B. Vachon,[84] S. Vahsen,[14] J. Valenta,[124] P. Valente,[131a] S. Valentinetti,[19a,19b] S. Valkar,[125] E. Valladolid Gallego,[166] S. Vallecorsa,[151] J. A. Valls Ferrer,[166] H. van der Graaf,[104] E. van der Kraaij,[104] R. Van Der Leeuw,[104] E. van der Poel,[104] D. van der Ster,[29] B. Van Eijk,[104] N. van Eldik,[83] P. van Gemmeren,[5] Z. van Kesteren,[104] I. van Vulpen,[104] M. Vanadia,[98] W. Vandelli,[29] G. Vandoni,[29] A. Vaniachine,[5] P. Vankov,[41] F. Vannucci,[77] F. Varela Rodriguez,[29] R. Vari,[131a] D. Varouchas,[14] A. Vartapetian,[7] K. E. Varvell,[149] V. I. Vassilakopoulos,[55] F. Vazeille,[33] G. Vegni,[88a,88b] J. J. Veillet,[114] C. Vellidis,[8] F. Veloso,[123a] R. Veness,[29] S. Veneziano,[131a] A. Ventura,[71a,71b] D. Ventura,[137] M. Venturi,[47] N. Venturi,[16] V. Vercesi,[118a] M. Verducci,[137] W. Verkerke,[104] J. C. Vermeulen,[104] A. Vest,[43] M. C. Vetterli,[141,f] I. Vichou,[164] T. Vickey,[144b,aa] O. E. Vickey Boeriu,[144b] G. H. A. Viehhauser,[117] S. Viel,[167] M. Villa,[19a,19b] M. Villaplana Perez,[166] E. Vilucchi,[46] M. G. Vincter,[28] E. Vinek,[29] V. B. Vinogradov,[64] M. Virchaux,[135,a] J. Virzi,[14] O. Vitells,[170] M. Viti,[41] I. Vivarelli,[47] F. Vives Vaque,[2] S. Vlachos,[9] M. Vlasak,[126] N. Vlasov,[20] A. Vogel,[20] P. Vokac,[126] G. Volpi,[46] M. Volpi,[85] G. Volpini,[88a] H. von der Schmitt,[98] J. von Loeben,[98] H. von Radziewski,[47] E. von Toerne,[20] V. Vorobel,[125] A. P. Vorobiev,[127] V. Vorwerk,[11] M. Vos,[166] R. Voss,[29] T. T. Voss,[173] J. H. Vossebeld,[72] N. Vranjes,[12a] M. Vranjes Milosavljevic,[104] V. Vrba,[124] M. Vreeswijk,[104] T. Vu Anh,[80] R. Vuillermet,[29] I. Vukotic,[114] W. Wagner,[173] P. Wagner,[119] H. Wahlen,[173] J. Wakabayashi,[100] J. Walbersloh,[42] S. Walch,[86] J. Walder,[70] R. Walker,[97] W. Walkowiak,[140] R. Wall,[174] P. Waller,[72] C. Wang,[44] H. Wang,[171] H. Wang,[32b,bb] J. Wang,[150] J. Wang,[32d] J. C. Wang,[137] R. Wang,[102] S. M. Wang,[150] A. Warburton,[84] C. P. Ward,[27] M. Warsinsky,[47] P. M. Watkins,[17] A. T. Watson,[17] M. F. Watson,[17] G. Watts,[137] S. Watts,[81] A. T. Waugh,[149] B. M. Waugh,[76] J. Weber,[42] M. Weber,[128] M. S. Weber,[16] P. Weber,[53] A. R. Weidberg,[117] P. Weigell,[98] J. Weingarten,[53] C. Weiser,[47] H. Wellenstein,[22]

P. S. Wells,[29] M. Wen,[46] T. Wenaus,[24] S. Wendler,[122] Z. Weng,[150,s] T. Wengler,[29] S. Wenig,[29] N. Wermes,[20] M. Werner,[47] P. Werner,[29] M. Werth,[162] M. Wessels,[57a] C. Weydert,[54] K. Whalen,[28] S. J. Wheeler-Ellis,[162] S. P. Whitaker,[21] A. White,[7] M. J. White,[85] S. R. Whitehead,[117] D. Whiteson,[162] D. Whittington,[60] F. Wicek,[114] D. Wicke,[173] F. J. Wickens,[128] W. Wiedenmann,[171] M. Wielers,[128] P. Wienemann,[20] C. Wiglesworth,[74] L. A. M. Wiik,[47] P. A. Wijeratne,[76] A. Wildauer,[166] M. A. Wildt,[41,q] I. Wilhelm,[125] H. G. Wilkens,[29] J. Z. Will,[97] E. Williams,[34] H. H. Williams,[119] W. Willis,[34] S. Willocq,[83] J. A. Wilson,[17] M. G. Wilson,[142] A. Wilson,[86] I. Wingerter-Seez,[4] S. Winkelmann,[47] F. Winklmeier,[29] M. Wittgen,[142] M. W. Wolter,[38] H. Wolters,[123a,j] W. C. Wong,[40] G. Wooden,[86] B. K. Wosiek,[38] J. Wotschack,[29] M. J. Woudstra,[83] K. Wraight,[52] C. Wright,[52] B. Wrona,[72] S. L. Wu,[171] X. Wu,[48] Y. Wu,[32b,cc] E. Wulf,[34] R. Wunstorf,[42] B. M. Wynne,[45] L. Xaplanteris,[9] S. Xella,[35] S. Xie,[47] Y. Xie,[32a] C. Xu,[32b,dd] D. Xu,[138] G. Xu,[32a] B. Yabsley,[149] S. Yacoob,[144b] M. Yamada,[65] H. Yamaguchi,[154] A. Yamamoto,[65] K. Yamamoto,[63] S. Yamamoto,[154] T. Yamamura,[154] T. Yamanaka,[154] J. Yamaoka,[44] T. Yamazaki,[154] Y. Yamazaki,[66] Z. Yan,[21] H. Yang,[86] U. K. Yang,[81] Y. Yang,[60] Y. Yang,[32a] Z. Yang,[145a,145b] S. Yanush,[90] Y. Yao,[14] Y. Yasu,[65] G. V. Ybeles Smit,[129] J. Ye,[39] S. Ye,[24] M. Yilmaz,[3c] R. Yoosoofmiya,[122] K. Yorita,[169] R. Yoshida,[5] C. Young,[142] S. Youssef,[21] D. Yu,[24] J. Yu,[7] J. Yu,[32c,dd] L. Yuan,[32a,ee] A. Yurkewicz,[147] V. G. Zaets,[127] R. Zaidan,[62] A. M. Zaitsev,[127] Z. Zajacova,[29] Yo.K. Zalite,[120] L. Zanello,[131a,131b] P. Zarzhitsky,[39] A. Zaytsev,[106] C. Zeitnitz,[173] M. Zeller,[174] M. Zeman,[124] A. Zemla,[38] C. Zendler,[20] O. Zenin,[127] T. Ženiš,[143a] Z. Zenonos,[121a,121b] S. Zenz,[14] D. Zerwas,[114] G. Zevi della Porta,[56] Z. Zhan,[32d] D. Zhang,[32b,bb] H. Zhang,[87] J. Zhang,[5] X. Zhang,[32d] Z. Zhang,[114] L. Zhao,[107] T. Zhao,[137] Z. Zhao,[32b] A. Zhemchugov,[64] S. Zheng,[32a] J. Zhong,[150,ff] B. Zhou,[86] N. Zhou,[162] Y. Zhou,[150] C. G. Zhu,[32d] H. Zhu,[41] J. Zhu,[86] Y. Zhu,[171] X. Zhuang,[97] V. Zhuravlov,[98] D. Zieminska,[60] R. Zimmermann,[20] S. Zimmermann,[20] S. Zimmermann,[47] M. Ziolkowski,[140] R. Zitoun,[4] L. Živković,[34] V. V. Zmouchko,[127,a] G. Zobernig,[171] A. Zoccoli,[19a,19b] Y. Zolnierowski,[4] A. Zsenei,[29] M. zur Nedden,[15] V. Zutshi,[105] and L. Zwalinski[29]

(ATLAS Collaboration)

[1]*University at Albany, Albany, New York, USA*
[2]*Department of Physics, University of Alberta, Edmonton, Alberta, Canada*
[3a]*Department of Physics, Ankara University, Ankara, Turkey*
[3b]*Department of Physics, Dumlupinar University, Kutahya, Turkey*
[3c]*Department of Physics, Gazi University, Ankara, Turkey*
[3d]*Division of Physics, TOBB University of Economics and Technology, Ankara, Turkey*
[3e]*Turkish Atomic Energy Authority, Ankara, Turkey*
[4]*LAPP, CNRS/IN2P3, and Université de Savoie, Annecy-le-Vieux, France*
[5]*High Energy Physics Division, Argonne National Laboratory, Argonne, Illinois, USA*
[6]*Department of Physics, University of Arizona, Tucson, Arizona, USA*
[7]*Department of Physics, The University of Texas at Arlington, Arlington, Texas, USA*
[8]*Physics Department, University of Athens, Athens, Greece*
[9]*Physics Department, National Technical University of Athens, Zografou, Greece*
[10]*Institute of Physics, Azerbaijan Academy of Sciences, Baku, Azerbaijan*
[11]*Institut de Física d'Altes Energies and Departament de Física de la Universitat Autònoma de Barcelona and ICREA, Barcelona, Spain*
[12a]*Institute of Physics, University of Belgrade, Belgrade, Serbia*
[12b]*Vinca Institute of Nuclear Sciences, Belgrade, Serbia*
[13]*Department for Physics and Technology, University of Bergen, Bergen, Norway*
[14]*Physics Division, Lawrence Berkeley National Laboratory and University of California, Berkeley, California, USA*
[15]*Department of Physics, Humboldt University, Berlin, Germany*
[16]*Albert Einstein Center for Fundamental Physics and Laboratory for High Energy Physics, University of Bern, Bern, Switzerland*
[17]*School of Physics and Astronomy, University of Birmingham, Birmingham, United Kingdom*
[18a]*Department of Physics, Bogazici University, Istanbul, Turkey*
[18b]*Division of Physics, Dogus University, Istanbul, Turkey*
[18c]*Department of Physics Engineering, Gaziantep University, Gaziantep, Turkey*
[18d]*Department of Physics, Istanbul Technical University, Istanbul, Turkey*
[19a]*INFN Sezione di Bologna, Italy*
[19b]*Dipartimento di Fisica, Università di Bologna, Bologna, Italy*
[20]*Physikalisches Institut, University of Bonn, Bonn, Germany*
[21]*Department of Physics, Boston University, Boston, Massachusetts, USA*
[22]*Department of Physics, Brandeis University, Waltham, Massachusetts, USA*

[23a]*Universidade Federal do Rio De Janeiro COPPE/EE/IF, Rio de Janeiro, Brazil*
[23b]*Federal University of Juiz de Fora, Juiz de Fora, Brazil*
[23c]*Federal University of Sao Joao del Rei , Sao Joao del Rei, Brazil*
[23d]*Instituto de Fisica, Universidade de Sao Paulo, Sao Paulo, Brazil*
[24]*Physics Department, Brookhaven National Laboratory, Upton, New York, USA*
[25a]*National Institute of Physics and Nuclear Engineering, Bucharest, Romania*
[25b]*University Politehnica Bucharest, Bucharest, Romania*
[25c]*West University in Timisoara, Timisoara, Romania*
[26]*Departamento de Física, Universidad de Buenos Aires, Buenos Aires, Argentina*
[27]*Cavendish Laboratory, University of Cambridge, Cambridge, United Kingdom*
[28]*Department of Physics, Carleton University, Ottawa, Ontario, Canada*
[29]*CERN, Geneva, Switzerland*
[30]*Enrico Fermi Institute, University of Chicago, Chicago, Illinois, USA*
[31a]*Departamento de Fisica, Pontificia Universidad Católica de Chile, Santiago, Chile*
[31b]*Departamento de Física, Universidad Técnica Federico Santa María, Valparaíso, Chile*
[32a]*Institute of High Energy Physics, Chinese Academy of Sciences, Beijing, China*
[32b]*Department of Modern Physics, University of Science and Technology of China, Anhui, China*
[32c]*Department of Physics, Nanjing University, Jiangsu, China*
[32d]*High Energy Physics Group, Shandong University, Shandong, China*
[33]*Laboratoire de Physique Corpusculaire, Clermont Université and Université Blaise Pascal and CNRS/IN2P3, Aubiere Cedex, France*
[34]*Nevis Laboratory, Columbia University, Irvington, New York, USA*
[35]*Niels Bohr Institute, University of Copenhagen, Kobenhavn, Denmark*
[36a]*INFN Gruppo Collegato di Cosenza, Italy*
[36b]*Dipartimento di Fisica, Università della Calabria, Arcavata di Rende, Italy*
[37]*Faculty of Physics and Applied Computer Science, AGH-University of Science and Technology, Krakow, Poland*
[38]*The Henryk Niewodniczanski Institute of Nuclear Physics, Polish Academy of Sciences, Krakow, Poland*
[39]*Physics Department, Southern Methodist University, Dallas, Texas, USA*
[40]*Physics Department, University of Texas at Dallas, Richardson, Texas, USA*
[41]*DESY, Hamburg and Zeuthen, Germany*
[42]*Institut für Experimentelle Physik IV, Technische Universität Dortmund, Dortmund, Germany*
[43]*Institut für Kern- und Teilchenphysik, Technical University Dresden, Dresden, Germany*
[44]*Department of Physics, Duke University, Durham, North Carolina, USA*
[45]*SUPA-School of Physics and Astronomy, University of Edinburgh, Edinburgh, United Kingdom*
[46]*INFN Laboratori Nazionali di Frascati, Frascati, Italy*
[47]*Fakultät für Mathematik und Physik, Albert-Ludwigs-Universität, Freiburg i.Br., Germany*
[48]*Section de Physique, Université de Genève, Geneva, Switzerland*
[49a]*INFN Sezione di Genova, Italy*
[49b]*Dipartimento di Fisica, Università di Genova, Genova, Italy*
[50a]*E.Andronikashvili Institute of Physics, Georgian Academy of Sciences, Tbilisi, Georgia*
[50b]*High Energy Physics Institute, Tbilisi State University, Tbilisi, Georgia*
[51]*II Physikalisches Institut, Justus-Liebig-Universität Giessen, Giessen, Germany*
[52]*SUPA-School of Physics and Astronomy, University of Glasgow, Glasgow, United Kingdom*
[53]*II Physikalisches Institut, Georg-August-Universität, Göttingen, Germany*
[54]*Laboratoire de Physique Subatomique et de Cosmologie, Université Joseph Fourier and CNRS/IN2P3 and Institut National Polytechnique de Grenoble, Grenoble, France*
[55]*Department of Physics, Hampton University, Hampton, Virginia, USA*
[56]*Laboratory for Particle Physics and Cosmology, Harvard University, Cambridge, Massachusetts, USA*
[57a]*Kirchhoff-Institut für Physik, Ruprecht-Karls-Universität Heidelberg, Heidelberg, Germany*
[57b]*Physikalisches Institut, Ruprecht-Karls-Universität Heidelberg, Heidelberg, Germany*
[57c]*ZITI Institut für technische Informatik, Ruprecht-Karls-Universität Heidelberg, Mannheim, Germany*
[58]*Faculty of Science, Hiroshima University, Hiroshima, Japan*
[59]*Faculty of Applied Information Science, Hiroshima Institute of Technology, Hiroshima, Japan*
[60]*Department of Physics, Indiana University, Bloomington, Indiana, USA*
[61]*Institut für Astro- und Teilchenphysik, Leopold-Franzens-Universität, Innsbruck, Austria*
[62]*University of Iowa, Iowa City, Iowa, USA*
[63]*Department of Physics and Astronomy, Iowa State University, Ames, Iowa, USA*
[64]*Joint Institute for Nuclear Research, JINR Dubna, Dubna, Russia*
[65]*KEK, High Energy Accelerator Research Organization, Tsukuba, Japan*
[66]*Graduate School of Science, Kobe University, Kobe, Japan*
[67]*Faculty of Science, Kyoto University, Kyoto, Japan*

[68]*Kyoto University of Education, Kyoto, Japan*
[69]*Instituto de Física La Plata, Universidad Nacional de La Plata and CONICET, La Plata, Argentina*
[70]*Physics Department, Lancaster University, Lancaster, United Kingdom*
[71a]*INFN Sezione di Lecce, Italy*
[71b]*Dipartimento di Fisica, Università del Salento, Lecce, Italy*
[72]*Oliver Lodge Laboratory, University of Liverpool, Liverpool, United Kingdom*
[73]*Department of Physics, Jožef Stefan Institute and University of Ljubljana, Ljubljana, Slovenia*
[74]*Department of Physics, Queen Mary University of London, London, United Kingdom*
[75]*Department of Physics, Royal Holloway University of London, Surrey, United Kingdom*
[76]*Department of Physics and Astronomy, University College London, London, United Kingdom*
[77]*Laboratoire de Physique Nucléaire et de Hautes Energies, UPMC and Université Paris-Diderot and CNRS/IN2P3, Paris, France*
[78]*Fysiska institutionen, Lunds universitet, Lund, Sweden*
[79]*Departamento de Fisica Teorica C-15, Universidad Autonoma de Madrid, Madrid, Spain*
[80]*Institut für Physik, Universität Mainz, Mainz, Germany*
[81]*School of Physics and Astronomy, University of Manchester, Manchester, United Kingdom*
[82]*CPPM, Aix-Marseille Université and CNRS/IN2P3, Marseille, France*
[83]*Department of Physics, University of Massachusetts, Amherst, Massachusetts, USA*
[84]*Department of Physics, McGill University, Montreal, Quebec, Canada*
[85]*School of Physics, University of Melbourne, Victoria, Australia*
[86]*Department of Physics, The University of Michigan, Ann Arbor, Michigan, USA*
[87]*Department of Physics and Astronomy, Michigan State University, East Lansing, Michigan, USA*
[88a]*INFN Sezione di Milano, Italy*
[88b]*Dipartimento di Fisica, Università di Milano, Milano, Italy*
[89]*B.I. Stepanov Institute of Physics, National Academy of Sciences of Belarus, Minsk, Republic of Belarus*
[90]*National Scientific and Educational Centre for Particle and High Energy Physics, Minsk, Republic of Belarus*
[91]*Department of Physics, Massachusetts Institute of Technology, Cambridge, Massachusetts, USA*
[92]*Group of Particle Physics, University of Montreal, Montreal, Quebec, Canada*
[93]*P.N. Lebedev Institute of Physics, Academy of Sciences, Moscow, Russia*
[94]*Institute for Theoretical and Experimental Physics (ITEP), Moscow, Russia*
[95]*Moscow Engineering and Physics Institute (MEPhI), Moscow, Russia*
[96]*Skobeltsyn Institute of Nuclear Physics, Lomonosov Moscow State University, Moscow, Russia*
[97]*Fakultät für Physik, Ludwig-Maximilians-Universität München, München, Germany*
[98]*Max-Planck-Institut für Physik (Werner-Heisenberg-Institut), München, Germany*
[99]*Nagasaki Institute of Applied Science, Nagasaki, Japan*
[100]*Graduate School of Science, Nagoya University, Nagoya, Japan*
[101a]*INFN Sezione di Napoli, Italy*
[101b]*Dipartimento di Scienze Fisiche, Università di Napoli, Napoli, Italy*
[102]*Department of Physics and Astronomy, University of New Mexico, Albuquerque, New Mexico, USA*
[103]*Institute for Mathematics, Astrophysics and Particle Physics, Radboud University Nijmegen/Nikhef, Nijmegen, Netherlands*
[104]*Nikhef National Institute for Subatomic Physics and University of Amsterdam, Amsterdam, Netherlands*
[105]*Department of Physics, Northern Illinois University, DeKalb, Illinois, USA*
[106]*Budker Institute of Nuclear Physics (BINP), Novosibirsk, Russia*
[107]*Department of Physics, New York University, New York, New York, USA*
[108]*Ohio State University, Columbus, Ohio, USA*
[109]*Faculty of Science, Okayama University, Okayama, Japan*
[110]*Homer L. Dodge Department of Physics and Astronomy, University of Oklahoma, Norman, Oklahoma, USA*
[111]*Department of Physics, Oklahoma State University, Stillwater, Oklahoma, USA*
[112]*Palacký University, RCPTM, Olomouc, Czech Republic*
[113]*Center for High Energy Physics, University of Oregon, Eugene, Oregon, USA*
[114]*LAL, Université Paris-Sud and CNRS/IN2P3, Orsay, France*
[115]*Graduate School of Science, Osaka University, Osaka, Japan*
[116]*Department of Physics, University of Oslo, Oslo, Norway*
[117]*Department of Physics, Oxford University, Oxford, United Kingdom*
[118a]*INFN Sezione di Pavia, Italy*
[118b]*Dipartimento di Fisica Nucleare e Teorica, Università di Pavia, Pavia, Italy*
[119]*Department of Physics, University of Pennsylvania, Philadelphia, Pennsylvania, USA*
[120]*Petersburg Nuclear Physics Institute, Gatchina, Russia*
[121a]*INFN Sezione di Pisa, Italy*
[121b]*Dipartimento di Fisica E. Fermi, Università di Pisa, Pisa, Italy*
[122]*Department of Physics and Astronomy, University of Pittsburgh, Pittsburgh, Pennsylvania, USA*
[123a]*Laboratorio de Instrumentacao e Fisica Experimental de Particulas-LIP, Lisboa, Portugal*

[123b]*Departamento de Fisica Teorica y del Cosmos and CAFPE, Universidad de Granada, Granada, Portugal*
[124]*Institute of Physics, Academy of Sciences of the Czech Republic, Praha, Czech Republic*
[125]*Faculty of Mathematics and Physics, Charles University in Prague, Praha, Czech Republic*
[126]*Czech Technical University in Prague, Praha, Czech Republic*
[127]*State Research Center Institute for High Energy Physics, Protvino, Russia*
[128]*Particle Physics Department, Rutherford Appleton Laboratory, Didcot, United Kingdom*
[129]*Physics Department, University of Regina, Regina, Saskatchewan, Canada*
[130]*Ritsumeikan University, Kusatsu, Shiga, Japan*
[131a]*INFN Sezione di Roma I, Italy*
[131b]*Dipartimento di Fisica, Università La Sapienza, Roma, Italy*
[132a]*INFN Sezione di Roma Tor Vergata, Italy*
[132b]*Dipartimento di Fisica, Università di Roma Tor Vergata, Roma, Italy*
[133a]*INFN Sezione di Roma Tre, Italy*
[133b]*Dipartimento di Fisica, Università Roma Tre, Roma, Italy*
[134a]*Faculté des Sciences Ain Chock, Réseau Universitaire de Physique des Hautes Energies-Université Hassan II, Casablanca, Morocco*
[134b]*Centre National de l'Energie des Sciences Techniques Nucleaires, Rabat, Morocco*
[134c]*Université Cadi Ayyad, Faculté des sciences Semlalia Département de Physique, B.P. 2390 Marrakech 40000, Morocco*
[134d]*Faculté des Sciences, Université Mohamed Premier and LPTPM, Oujda, Morocco*
[134e]*Faculté des Sciences, Université Mohammed V, Rabat, Morocco*
[135]*DSM/IRFU (Institut de Recherches sur les Lois Fondamentales de l'Univers), CEA Saclay (Commissariat a l'Energie Atomique), Gif-sur-Yvette, France*
[136]*Santa Cruz Institute for Particle Physics, University of California Santa Cruz, Santa Cruz, California, USA*
[137]*Department of Physics, University of Washington, Seattle, Washington, USA*
[138]*Department of Physics and Astronomy, University of Sheffield, Sheffield, United Kingdom*
[139]*Department of Physics, Shinshu University, Nagano, Japan*
[140]*Fachbereich Physik, Universität Siegen, Siegen, Germany*
[141]*Department of Physics, Simon Fraser University, Burnaby, British Columbia, Canada*
[142]*SLAC National Accelerator Laboratory, Stanford, California, USA*
[143a]*Faculty of Mathematics, Physics and Informatics, Comenius University, Bratislava, Slovak Republic*
[143b]*Department of Subnuclear Physics, Institute of Experimental Physics of the Slovak Academy of Sciences, Kosice, Slovak Republic*
[144a]*Department of Physics, University of Johannesburg, Johannesburg, South Africa*
[144b]*School of Physics, University of the Witwatersrand, Johannesburg, South Africa*
[145a]*Department of Physics, Stockholm University, Sweden*
[145b]*The Oskar Klein Centre, Stockholm, Sweden*
[146]*Physics Department, Royal Institute of Technology, Stockholm, Sweden*
[147]*Department of Physics and Astronomy, Stony Brook University, Stony Brook, New York, USA*
[148]*Department of Physics and Astronomy, University of Sussex, Brighton, United Kingdom*
[149]*School of Physics, University of Sydney, Sydney, Australia*
[150]*Institute of Physics, Academia Sinica, Taipei, Taiwan*
[151]*Department of Physics, Technion: Israel Institute of Technology, Haifa, Israel*
[152]*Raymond and Beverly Sackler School of Physics and Astronomy, Tel Aviv University, Tel Aviv, Israel*
[153]*Department of Physics, Aristotle University of Thessaloniki, Thessaloniki, Greece*
[154]*International Center for Elementary Particle Physics and Department of Physics, The University of Tokyo, Tokyo, Japan*
[155]*Graduate School of Science and Technology, Tokyo Metropolitan University, Tokyo, Japan*
[156]*Department of Physics, Tokyo Institute of Technology, Tokyo, Japan*
[157]*Department of Physics, University of Toronto, Toronto, Ontario, Canada*
[158a]*TRIUMF, Vancouver, British Columbia, Canada*
[158b]*Department of Physics and Astronomy, York University, Toronto, Ontario, Canada*
[159]*Institute of Pure and Applied Sciences, University of Tsukuba, Ibaraki, Japan*
[160]*Science and Technology Center, Tufts University, Medford, Massachusetts, USA*
[161]*Centro de Investigaciones, Universidad Antonio Narino, Bogota, Colombia*
[162]*Department of Physics and Astronomy, University of California Irvine, Irvine, California, USA*
[163a]*INFN Gruppo Collegato di Udine, Italy*
[163b]*ICTP, Trieste, Italy*
[163c]*Dipartimento di Fisica, Università di Udine, Udine, Italy*
[164]*Department of Physics, University of Illinois, Urbana, Illinois, USA*
[165]*Department of Physics and Astronomy, University of Uppsala, Uppsala, Sweden*
[166]*Instituto de Física Corpuscular (IFIC) and Departamento de Física Atómica, Molecular y Nuclear and Departamento de Ingeniería Electrónica and Instituto de Microelectrónica de Barcelona (IMB-CNM), University of Valencia and CSIC, Valencia, Spain*
[167]*Department of Physics, University of British Columbia, Vancouver, British Columbia, Canada*

[168]*Department of Physics and Astronomy, University of Victoria, Victoria, British Columbia, Canada*
[169]*Waseda University, Tokyo, Japan*
[170]*Department of Particle Physics, The Weizmann Institute of Science, Rehovot, Israel*
[171]*Department of Physics, University of Wisconsin, Madison, Wisconsin, USA*
[172]*Fakultät für Physik und Astronomie, Julius-Maximilians-Universität, Würzburg, Germany*
[173]*Fachbereich C Physik, Bergische Universität Wuppertal, Wuppertal, Germany*
[174]*Department of Physics, Yale University, New Haven, Connecticut, USA*
[175]*Yerevan Physics Institute, Yerevan, Armenia*
[176]*Domaine scientifique de la Doua, Centre de Calcul CNRS/IN2P3, Villeurbanne Cedex, France*

[a]Deceased.
[b]Also at Laboratorio de Instrumentacao e Fisica Experimental de Particulas-LIP, Lisboa, Portugal.
[c]Also at Faculdade de Ciencias and CFNUL, Universidade de Lisboa, Lisboa, Portugal.
[d]Also at Particle Physics Department, Rutherford Appleton Laboratory, Didcot, United Kingdom.
[e]Also at CPPM, Aix-Marseille Université and CNRS/IN2P3, Marseille, France.
[f]Also at TRIUMF, Vancouver, BC, Canada.
[g]Also at Department of Physics, California State University, Fresno, CA, USA.
[h]Also at Faculty of Physics and Applied Computer Science, AGH-University of Science and Technology, Krakow, Poland.
[i]Also at Fermilab, Batavia, IL, USA.
[j]Also at Department of Physics, University of Coimbra, Coimbra, Portugal.
[k]Also at Università di Napoli Parthenope, Napoli, Italy.
[l]Also at Institute of Particle Physics (IPP), Canada.
[m]Also at Department of Physics, Middle East Technical University, Ankara, Turkey.
[n]Also at Louisiana Tech University, Ruston, LA, USA.
[o]Also at Group of Particle Physics, University of Montreal, Montreal, QC, Canada.
[p]Also at Institute of Physics, Azerbaijan Academy of Sciences, Baku, Azerbaijan.
[q]Also at Institut für Experimentalphysik, Universität Hamburg, Hamburg, Germany.
[r]Also at Manhattan College, New York, NY, USA.
[s]Also at School of Physics and Engineering, Sun Yat-sen University, Guanzhou, China.
[t]Also at Academia Sinica Grid Computing, Institute of Physics, Academia Sinica, Taipei, Taiwan.
[u]Also at High Energy Physics Group, Shandong University, Shandong, China.
[v]Also at Section de Physique, Université de Genève, Geneva, Switzerland.
[w]Also at Departamento de Fisica, Universidade de Minho, Braga, Portugal.
[x]Also at Department of Physics and Astronomy, University of South Carolina, Columbia, SC, USA.
[y]Also at KFKI Research Institute for Particle and Nuclear Physics, Budapest, Hungary.
[z]Also at California Institute of Technology, Pasadena, CA, USA.
[aa]Also at Department of Physics, Oxford University, Oxford, United Kingdom.
[bb]Also at Institute of Physics, Academia Sinica, Taipei, Taiwan.
[cc]Also at Department of Physics, The University of Michigan, Ann Arbor, MI, USA.
[dd]Also at DSM/IRFU (Institut de Recherches sur les Lois Fondamentales de l'Univers), CEA Saclay (Commissariat a l'Energie Atomique), Gif-sur-Yvette, France.
[ee]Also at Laboratoire de Physique Nucléaire et de Hautes Energies, UPMC and Université Paris-Diderot and CNRS/IN2P3, Paris, France.
[ff]Also at Department of Physics, Nanjing University, Jiangsu, China.